

INFORMATION TO USERS

The most advanced technology has been used to photograph and reproduce this manuscript from the microfilm master. UMI films the text directly from the original or copy submitted. Thus, some thesis and dissertation copies are in typewriter face, while others may be from any type of computer printer.

The quality of this reproduction is dependent upon the quality of the copy submitted. Broken or indistinct print, colored or poor quality illustrations and photographs, print bleedthrough, substandard margins, and improper alignment can adversely affect reproduction.

In the unlikely event that the author did not send UMI a complete manuscript and there are missing pages, these will be noted. Also, if unauthorized copyright material had to be removed, a note will indicate the deletion.

Oversize materials (e.g., maps, drawings, charts) are reproduced by sectioning the original, beginning at the upper left-hand corner and continuing from left to right in equal sections with small overlaps. Each original is also photographed in one exposure and is included in reduced form at the back of the book.

Photographs included in the original manuscript have been reproduced xerographically in this copy. Higher quality 6" x 9" black and white photographic prints are available for any photographs or illustrations appearing in this copy for an additional charge. Contact UMI directly to order.

U·M·I

University Microfilms International
A Bell & Howell Information Company
300 North Zeeb Road, Ann Arbor, MI 48106-1346 USA
313/761-4700 800/521-0600

Order Number 9022114

**Stabilization of electron deficient sulfur by neighboring sulfur
and oxygen groups**

Steffen, Lawrence Kraig, Ph.D.

The University of Arizona, 1989

U·M·I
300 N. Zeeb Rd.
Ann Arbor, MI 48106

STABILIZATION OF ELECTRON DEFICIENT SULFUR BY
NEIGHBORING SULFUR AND OXYGEN GROUPS

by
Lawrence Kraig Steffen

A Dissertation Submitted to the Faculty of the
CHEMISTRY DEPARTMENT
In Partial Fulfillment of the Requirements
For the Degree of
DOCTOR OF PHILOSOPHY
In the Graduate College
THE UNIVERSITY OF ARIZONA

1 9 9 0

THE UNIVERSITY OF ARIZONA
GRADUATE COLLEGE

2

As members of the Final Examination Committee, we certify that we have read
the dissertation prepared by Lawrence Kraig Steffen

entitled STABILIZATION OF ELECTRON DEFICIENT SULFUR BY
NEIGHBORING SULFUR AND OXYGEN GROUPS

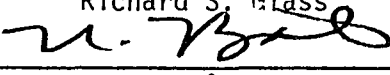
and recommend that it be accepted as fulfilling the dissertation requirement
for the Degree of Doctor of Philosophy.



Richard S. Glass

12/15/89

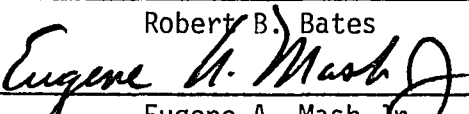
Date



Robert B. Bates

12-15-89

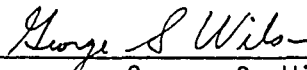
Date



Eugene A. Mash Jr.

12-15-89

Date



George S. Wilson

12-15-89

Date




Walter B. Miller

12-15-89

Date

Final approval and acceptance of this dissertation is contingent upon the
candidate's submission of the final copy of the dissertation to the Graduate
College.

I hereby certify that I have read this dissertation prepared under my
direction and recommend that it be accepted as fulfilling the dissertation
requirement.



Dissertation Director Richard S. Glass

12/20/89

Date

STATEMENT BY AUTHOR

This dissertation has been submitted in partial fulfillment of requirements for an advanced degree at The University of Arizona and is deposited in the University Library to be made available to borrowers under rules of the library.

Brief quotations from this dissertation are allowable without special permission, provided that accurate acknowledgement of source is made. Requests for permission for extended quotation from or reproduction of this manuscript in whole or in part may be granted by the head of the major department or the Dean of the Graduate College when in his or her judgement the proposed use of the material is in the interests of scholarship. In all other instances, however, permission must be obtained from the author.

SIGNED



Acknowledgements

This thesis is dedicated to all the people who have participated in my education. Dr. Richard S. Glass has been an insightful, thorough and helpful research director throughout this research. Dr. George S. Wilson, whose electrochemical expertise was indispensable, has always encouraged me with his cheerful approach to science. I would like to thank all the members of the Glass group past and present, especially Dr. Mahmood Sabahi, Jeff Broeker, Amorn Petsom, and Steve Andruski for their helpful discussions and for being good friends. I acknowledge the National Institute of Health for financial support of this work.

In view of the momentous events occurring in Berlin in November 1989, I would also like to dedicate this thesis to all the people of Berlin (East and West!) and especially Dieter K. Asmus, director of the research done in Berlin at the Hahn-Meitner Institute. Maria Bonifacic was most helpful in teaching me the technique of pulse radiolysis.

I also thank my Father, Mother and the rest of my family for allowing me the freedom to grow and believing in me. Finally, I thank my wife Cathy for tolerating me over the years and being a good friend.

TABLE OF CONTENTS

	Page
LIST OF TABLES	8
LIST OF FIGURES	9
ABSTRACT	12
CHAPTER	
1. INTRODUCTION	14
Sulfur in biological electron transfer ..	14
Neighboring group participation in sulfur oxidation	14
Description of Techniques Used	20
2. ELECTROCHEMICAL AND PULSE RADIOLYTIC OXIDATION OF THE MESOCYCLIC POLYTHIOETHERS 1,4,7-TRITHIACYCLONONANE AND NAPHTHO [1,8- <u>b,c</u>]-1,5-DITHIOCIN	28
Introduction	28
Results and Discussion	29
Electrochemistry of 1,4,7-Trithia- cyclononane	29
Pulse Radiolysis of 1,4,7-Trithia- cyclononane.....	35
Electrochemistry of Naphtho[1,8- <u>b,c</u>]- -1,5-Dithiocin	39
Experimental	44
Cyclic Voltammetry	44
Controlled Potential Electrolysis .	46
Pulse Radiolysis	47

3. ELECTROCHEMISTRY OF (\pm)-2-EXO-AMINO-6-ENDO METHYLTHIOBICYCLO[2.2.1] HEPTANE-2-ENDO- CARBOXYLIC ACID	49
Introduction	49
Results and Discussion	51
Cyclic Voltammetry and Related Electrochemical Studies.....	51
FTIR spectroscopy	70
Controlled Potential Electrolysis .	89
Synthesis of Derivatives	90
Experimental	
Cyclic Voltammetry and Related Electrochemical Studies	93
Chemical oxidation	94
Controlled Potential Electrolysis .	95
Synthesis of Derivatives	101
4. PULSE RADIOLYSIS OF (\pm) -2-EXO-AMINO-6-ENDO- METHYLTHIOBICYCLO[2.2.1] HEPTANE-2-ENDO- CARBOXYLIC ACID	105
Introduction	105
Results and Discussion	107
Absorption Spectrum	107
Conductivity Signal	110
Dependence on pH	110
Gamma radiolysis	118
Experimental	128

	Pulse Radiolysis	128
	Gamma radiolysis	129
5.	ELECTROCHEMICAL AND CHEMICAL OXIDATION OF (±)- ENDO-2-HYDROXY-6-ENDO-METHYLTHIO-BICYCLO [2.2.1] HEPTANE	130
	Introduction	130
	Results and Discussion	131
	Cyclic Voltammetry	131
	FTIR	143
	Controlled Potential Electrolysis .	147
	Chemical Oxidation	149
	Experimental	149
	Cyclic Voltammetry and Related Techniques	149
	Controlled Potential Electrolysis .	150
	Chemical Oxidation	151
APPENDIX I:	REVERSIBLE ELECTROCHEMISTRY OF NAPHTHO-[1,8- <u>b</u> , <u>c</u>]-1,5-DITHIOCIN ...	153
APPENDIX II:	$\text{Cd}(\text{TTCN})_2^{2+}$ and $\text{Cd}(\text{Cu})(\text{TTCN})_2^{2+}$ METAL COMPLEXES	159
REFERENCES	177

LIST OF TABLES

TABLE	Page
2.1 Oxidation of thioethers	32
3.1 Cyclic voltammetry of <u>3.06</u>	71
3.2 FTIR data for <u>3.06</u>	73
4.1 Pulse radiolysis data for <u>3.06b</u>	116
4.2 Conductivity data for <u>3.06b</u>	122
5.1 Cyclic and rotating disk voltammetry data for <u>5.03</u>	136
5.2 FTIR data for <u>5.03</u> and <u>5.04</u>	144
II.1 X-ray crystal data for $\text{Cd(II)(TTCN)}_2(\text{BF}_4)_2$ • CH_3NO_2	164
II.2 X-ray crystal data for $\text{Cu(II)(TTCN)}_2(\text{BF}_4)_2$ • CH_3NO_2	171

LIST OF FIGURES

FIGURE	Page
1.1 Sulfur-sulfur interaction	17
1.2 Sulfur-X interaction	18
1.3 Pulse radiolysis	23
2.1 Cyclic voltammogram of TTCN	30
2.2 Pulse radiolysis of TTCN	36
2.3 Plot of transient absorption decay for TTCN ...	37
2.4 Plot of the conductivity signal observed for TTCN	38
2.5 Cyclic voltammogram of Naphthodithiocin <u>1.02</u> ..	41
2.6 Plot of the square root of the sweep rate versus peak current for <u>1.02</u>	42
3.1 Cyclic voltammogram of amino acid <u>3.06</u>	53
3.2 Plot of the square root of the sweep rate versus peak current for <u>3.06</u>	54
3.3 Rotating disk electrode voltammogram of <u>3.06</u> ..	56
3.4 Levich plot of <u>3.06</u>	57
3.5 Cyclic voltammogram of <u>3.06</u> in the presence of 2,6-di-t-butylpyridine	58
3.6 Rotating disk electrode voltammogram of <u>3.06</u> in the presence of 2,6-di-t-butylpyridine	59
3.7 Cyclic voltammogram of <u>3.06</u> in the presence of trifluoroacetic acid	61
3.8 Rotating disk electrode voltammogram of <u>3.06</u> in the presence of trifluoroacetic acid	62
3.9 Differential pulse voltammogram of <u>3.06</u>	63

3.10	Cyclic voltammogram of the sodium salt of <u>3.06</u>	65
3.11	Cyclic voltammogram of <u>3.06</u> in pH 2.3 aqueous perchloric acid	67
3.12	Cyclic voltammogram of <u>3.06</u> in pH 8.4 aqueous borate buffer	68
3.13	Cyclic voltammogram of <u>3.06</u> in pH 7.5 aqueous acetate buffer	69
3.14	Acid/base equilibria of <u>3.06</u>	79
3.15	Effect of addition of bromide	83
3.16	Effect of addition of bromide continued	84
4.1	Pulse radiolysis of <u>3.06b</u> at pH 2.6	108
4.2	Plot of the transient absorption decay for <u>3.06b</u>	109
4.3	Plot of the conductivity signal observed for <u>3.06b</u>	111
4.4	Pulse radiolysis of <u>3.06b</u> at pH 3.1	113
4.5	Pulse radiolysis of <u>3.06b</u> at pH 5.5	114
4.6	Pulse radiolysis of <u>3.06b</u> at pH 6.9	115
4.7	Plot of the yield of the transient species observed at 355 nm upon pulse radiolysis of <u>3.06b</u> versus pH	117
4.8	Plot of the radiation chemical yield of decarboxylation upon gamma radiolysis of <u>3.06b</u> versus pH	119
4.9	Comparison of yields for pulse radiolysis and gamma radiolysis of <u>3.06b</u> at various pHs	121
4.10	Outline of the possible pulse radiolysis products formed upon radiolysis of <u>3.06b</u>	123
5.1	Cyclic voltammogram of <u>5.03</u>	132

5.2	Plot of the square root of the sweep rate versus peak current for <u>5.03</u>	133
5.3	Cyclic voltammogram of <u>5.03</u> in the presence of LiBr	135
5.4	Differential pulse voltammogram of <u>5.03</u>	137
5.5	Rotating disk electrode voltammogram of <u>5.03</u> ..	138
5.6	Levich plot for <u>5.03</u>	139
5.7	Cyclic voltammogram of <u>5.04</u>	141
5.8	Cyclic voltammogram of <u>5.03</u> and <u>5.04</u> in the same solution	142
I.1	Cyclic voltammogram of <u>1.02</u> in methylene chloride/TFA/TFAA	156
I.2	Rotating disk electrode voltammogram of <u>1.02</u> in methylene chloride/TFA/TFAA	157
I.3	EPR spectrum of <u>1.02</u> in methylene chloride/ TFA/TFAA	158
II.1	Ortep of $\text{Cd(II) (TTCN)}_2(\text{BF}_4)_2 \cdot 2\text{CH}_3\text{NO}_2$	164
II.2	Ortep of $\text{Cu(II) (TTCN)}_2(\text{BF}_4)_2 \cdot 2\text{CH}_3\text{NO}_2$	171

ABSTRACT

The mesocyclic trithioether 1,4,7-trithiacyclononane shows neighboring group participation upon oxidation as evidenced by the peak potential for oxidation in cyclic voltammetry, 0.9 V versus Ag/0.1 M AgNO₃, and by the formation of its monosulfoxide by controlled potential electrolysis in an overall two electron process. Pulse radiolysis of 1,4,7-trithiacyclononane leads to the formation of a two-center three-electron bond of moderate stability. Naptho[1,8-b,c]-1,5-dithiocin shows neighboring group participation upon electrochemical oxidation. A low peak potential is observed, 0.47 V versus Ag/0.1 M AgNO₃, in the cyclic voltammetry. Controlled potential electrolysis leads to formation of the monosulfoxide in a two electron process.

The rigid methionine analog (±)-2-exo-amino-6-endo methylthiobicyclo[2.2.1] heptane-2-endo carboxylic acid exhibits neighboring group participation upon electrochemical oxidation. The degree of participation depends on the acid/base chemistry of the α-amino acid. The zwitterion shows the strongest neighboring group participation. Controlled potential electrolysis led to the formation of two diastereomeric sulfoxides in a two electron process. The diastereomer ratio was suggestive of

participation by the carboxylate in the oxidation. The structures of the sulfoxides were confirmed by comparison with chemically prepared sulfoxides and sulfoxide amino acid derivatives. The stereochemistry was assigned by comparison with related compounds upon which x-ray crystallographic analysis had been performed. Single-electron pulse radiolytic oxidation of the amino acid led to the formation of an absorbing transient which was assigned to a two-center three-electron sulfur-carboxylate oxygen species. The yield of the species formed was pH dependent. At a pH above 3.5 decarboxylation becomes a major decomposition pathway in contrast to the electrochemical experiments where no decarboxylation was seen.

The alcohol (\pm)-endo-2-hydroxy-6-endo-methylthiobicyclo [2.2.1] heptane shows significant neighboring group participation upon electrochemical oxidation in comparison with its exo-hydroxy isomer as indicated by a 350 mV difference in the peak potentials. Controlled potential electrolysis in a two electron process leads to formation of a mixture of diastereomeric alkoxysulfonium salts.

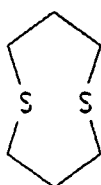
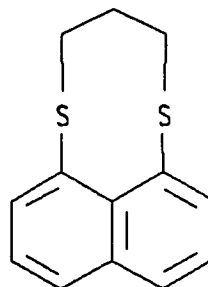
CHAPTER 1

INTRODUCTION

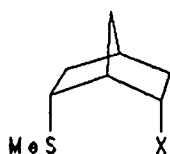
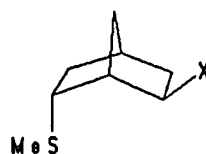
Thioethers are suspected to be involved in electron transfer in biological systems. Methionine, the most ubiquitous thioether in biological systems, is a ligand to the heme moiety of cytochrome c, an electron transfer protein found in mitochondria. Also, the heme group in cytochrome c is covalently attached to the rest of the protein through an alkylated cysteine. Iterative Extended Hückel calculations¹ indicate that this alkylated cysteine sulfur may be involved in electron transfer from the heme. Thioethers may be involved in oxidative phosphorylation.²

Most simple thioethers have oxidation potentials greater than biological oxidants involved in electron transfer. However, the three dimensional structure of proteins may allow the electron rich functional groups of redox proteins to orient themselves in such a way as to allow neighboring group participation in the oxidation of thioethers, thus lowering the potential into the range accessible by biological oxidants. Neighboring group participation has been defined as follows³: When a substituent stabilizes a transition state or intermediate by becoming bonded to the reaction center this effect is called neighboring group participation. The idea that

neighboring group participation plays a role in biological electron transfer is a key postulate of this research.⁴ The approach used has been the synthesis of small molecules designed so as to provide an opportunity for neighboring group participation and subsequent detailed characterization of the redox properties of these target molecules by a variety of methods. Cyclic structures such as 1,5-dithiocane and 1,8-naphtho dithiocin, compounds 1.01 and 1.02, represent one class of compounds that have been

1.011.02

investigated. A second class of compounds is the endo norbornyl derivatives represented by the general structure 1.03. In the case of the norbornyl derivatives excellent controls, the exo derivatives 1.04, are usually available. Compound 1.01 has proven to be a spectacular example of neighboring group participation as exhibited by its reversible electrochemical oxidation to its cation radical and dication.⁵

1.031.04

Sulfur has been shown to be involved in neighboring group participation in numerous situations the majority of which involve the formation of sulfonium salts where the sulfur is bonded to three carbon atoms.⁶ This work looks in detail at another important type of neighboring group participation involving sulfur, that of stabilization of an incipient positive charge on sulfur by an adjacent heteroatom. The important features are outlined in Figure 1.1.⁷ If there is a heteroatom X held proximate in space to a sulfur atom it is reasonable to assume that their lone pair electrons would interact in a destabilizing way. The magnitude of the interaction will depend on the distance between the atoms and the angle of the lone pairs with respect to the internuclear axis. This interaction has been investigated by photoelectron spectroscopy in some detail⁸ and is exemplified in compounds such as 1,5-dithiocane, 1.01, by a 0.43 eV splitting in the HOMO formed by interaction of the two sulfur atoms. Since the HOMO is completely filled as shown in Figure 1.1 the interaction is

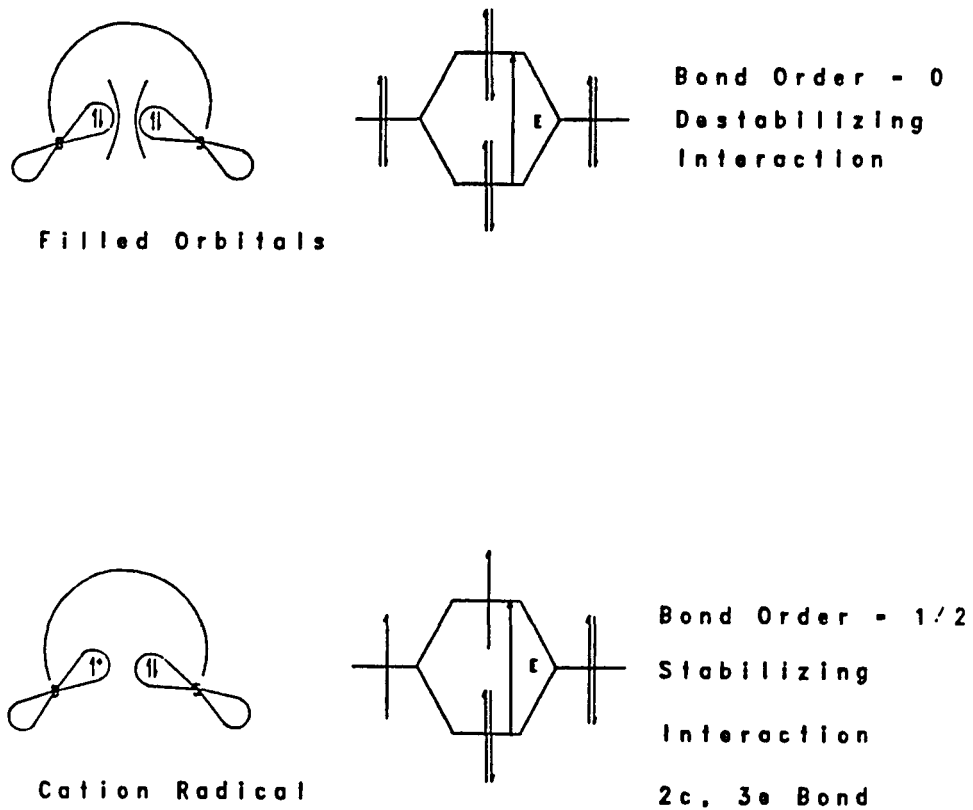


Figure 1.1. Sulfur-Sulfur Interaction.

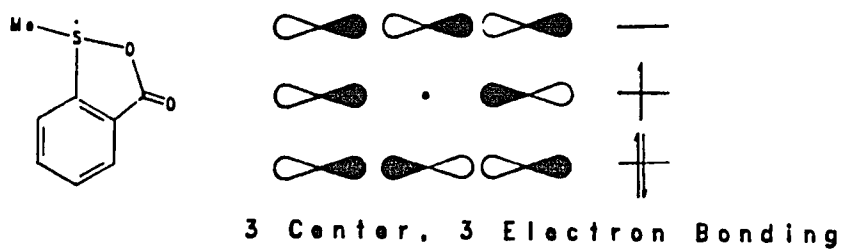
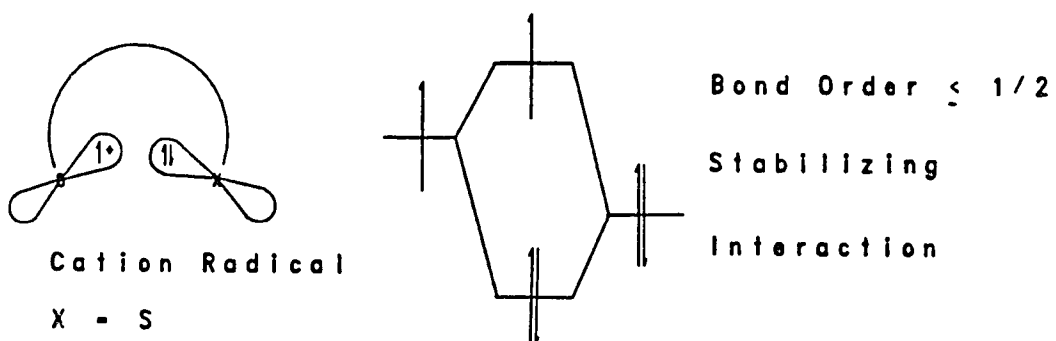


Figure 1.2. Sulfur-X Interaction ($X \neq S$)

repulsive. A more interesting case arises when an electron has been removed from one of the sulfur atoms. In this case the cation radical formed by the interaction of the other sulfur leads to bonding in which the HOMO (σ^*) is only half filled as shown in Figure 1.1. The bond order in this case is theoretically $1/2$ and this is a stabilizing interaction with two electrons in the bonding orbital and one in the antibonding orbital between the two sulfurs. The electron density from the lone electron is spread evenly over the two sulfur atoms. Considerable theoretical work has been done on calculating the strength of such two-center three-electron (2c,3e) bonds.⁹ The magnitude of the stabilization will depend both on the distance between the two centers and angle between the component atomic orbitals used in forming the σ -molecular orbitals. It is important to note that since one electron is in an antibonding orbital, it may be as easy or easier to remove this second electron than it was to remove the first electron resulting in the formation of a dication. Indeed, dithiocane 2.01 exhibits such behavior upon electrochemical oxidation with the E^0 of the second oxidation estimated to be 20 mV cathodic of the E^0 for the first oxidation. If the other heteroatom is not a sulfur, the difference in energy between the atomic orbitals before they interact must be considered as shown in Figure 1.2.

With a non-sulfur heteroatom one would expect the electron density of the antibonding orbital to be shifted towards the most electronegative heteroatom. Alternative bonding schemes to the one just presented have been proposed. Martin¹⁰ has gathered experimental results which are best explained by a three center three electron bonding interaction involving an adjacent oxygen and one of the sulfur carbon sigma bonds in compound 1.05 as illustrated in Figure 1.2. Regardless of the exact structure of the stabilized species the important point is that neighboring heteroatoms can stabilize oxidized sulfur species. This dissertation presents evidence for sulfur-sulfur, sulfur-carboxylate oxygen and sulfur-hydroxyl oxygen interactions.

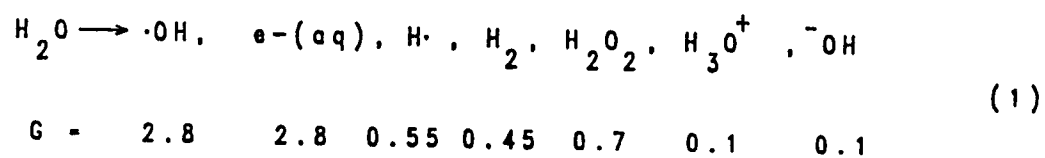
Three general methods have been used to investigate the oxidation of thioethers. The first of these methods is electrochemical oxidation. The most significant attribute of electrochemical techniques is that the oxidation takes place at an electrode surface and is therefore a heterogeneous process. The ability to vary the applied potential over a continuum, versus the addition or formation of species of set oxidizing power, is an advantage of electrochemical techniques. What information about sulfur oxidation can be obtained via electrochemistry? Linear sweep methods can provide both thermodynamic and kinetic

information.¹¹ All of the compounds reported in this work showed irreversible electron transfer under the conditions used as indicated by the lack of a cathodic current upon sweep reversal and the dependence of E_p on the sweep rate.¹² The peak potential of an irreversible process yields no direct thermodynamic information, however, if a series of closely related compounds is being investigated, generalizations about relative thermodynamic stability can be made. As shown by Kochi¹³ if the electron transfer is outer sphere one can get very good correlations between ionization potentials and oxidation potentials even for totally irreversible systems. Thioethers which do not exhibit neighboring group participation show essentially no correlation between their peak potentials and their ionization potentials but when neighboring group participation is present the correlation is much better. The important assumption made is that when a good correlation exists the rate of electron transfer is similar for the series of compounds under investigation. Electrochemical methods also allow the determination of the number of electrons, or "n" value, which are transferred upon oxidation via analysis of the shape of the waves in various sweep methods. Exhaustive controlled potential electrolysis yields complimentary information.

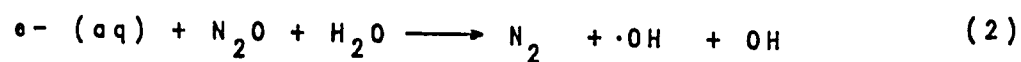
Determination of an "n" value can help to establish the mechanism of oxidation. Controlled potential electrolysis permits the analysis of products of oxidation which in many cases can be used to verify neighboring group participation.

The second general method used to study thioether oxidation was pulse radiolysis. Pulse radiolysis involves irradiation of aqueous solutions with high energy electrons, usually about 1-5 MeV. The electrons transfer energy into the system through a complex set of interactions which have been the subject of many investigations.¹⁴ The important result is that a homogeneous solution is generated consisting primarily of hydroxyl radicals and solvated electrons¹⁵ along with much smaller amounts of molecular products, such as hydrogen and hydrogen peroxide, as shown in reaction 1, Figure 1.3.

The species shown are all formed within 0.1 nanoseconds. The yields shown are expressed in "G" values where G is defined as the number of a particular molecular species formed per 100 eV of energy supplied. Solvated electrons, which are strong reductants, can be easily converted into hydroxyl radicals by allowing them to react with nitrous oxide in a diffusion controlled reaction as shown in reaction 2 of Figure 1.3. The total G value for hydroxyl radicals is therefore about 5.6 which for a normal



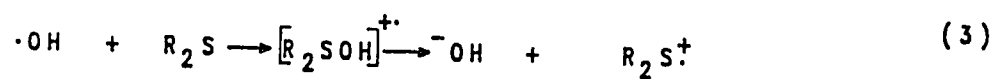
(G is the chemical yield of the species shown
expressed as the number of species formed per 100 eV
absorbed energy)



Diffusion controlled

Overall Yield of $> 90 \times \cdot\text{OH}$

Figure 1.3. Pulse radiolysis part a: Formation of hydroxyl radicals.



Diffusion controlled

Reactions 1-3 usually

complete within 1 microsecond

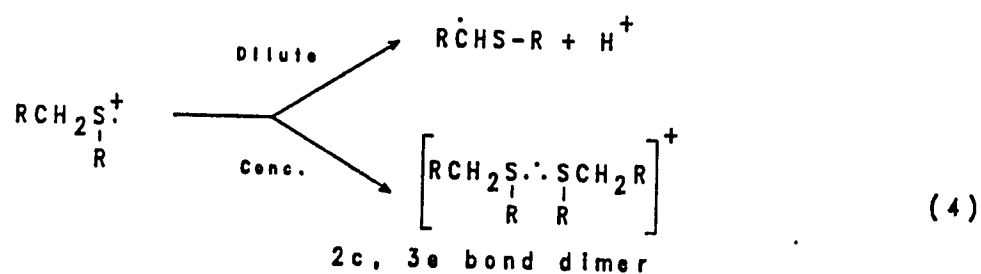


Figure 1.3 Continued. Pulse radiolysis part b: reaction of hydroxyl radicals with thioethers.

pulse of 2-10 Gy (J kg^{-1}) corresponds to the production of $1-2 \times 10^{-6}$ M solutions. Hydroxyl radicals can react in a number of ways including addition, hydrogen abstraction, radical interaction and electron transfer.¹⁶ Thioethers have been shown to react primarily by formation of a hydroxyl radical adduct (addition) in a diffusion controlled reaction followed by rapid loss of hydroxide anion leaving behind a sulfur cation radical¹⁷ as shown in reaction 3 of Figure 1.3. The cation radicals formed can deprotonate to form α -alkylthio radicals or, if the solution is sufficiently concentrated, they can be stabilized by formation of dimer 2c,3e bonds. If another sulfur or other heteroatom is present in the molecule and capable of interacting with the oxidized sulfur an intramolecular 2c,3e bond can form. Because the concentration of thioethers used is generally greater than 0.01 mM and the concentration of hydroxyl radicals formed is uniform and around 0.001 mM the oxidations observed are one electron oxidations only. This occurs even though, as discussed earlier, the second electron may be easier to remove because no single thioether molecule is likely to encounter more than one hydroxyl radical. This is in contrast to the multiple electron oxidations possible in the electrochemical and chemical oxidations.

Since the hydroxyl radical oxidation of thioethers leads to the formation of charged species conductivity measurements can be used to monitor their formation and decay.¹⁸ Conductivity measurements are very sensitive but subject to considerable interpretive difficulty because of the problems encountered in determining which species are contributing to the total conductivity signal since the signal measured is the arithmetic sum of all charged species formed.

The 2c,3e species formed exhibit characteristic absorptions in the UV/vis region. Generally, as the strength of the bonding interaction increases one sees a blue shift in the absorption maxima observed. The absorption observed is assigned to a σ - σ^* transition as a first approximation. This blue shift can be attributed to the increase in the difference between the bonding and antibonding orbital energies as the strength of the interaction increases. Absorption changes can be easily monitored in the UV/vis region on the microsecond or faster time scale, allowing for monitoring of the kinetics related to the formation or decay of absorbing species. The combination of conductivity and absorption data has proven to be very effective in the investigation of the one electron oxidation of thioethers.¹⁹

Chemical oxidation by a variety of oxidants was the third method used. Thioethers can be oxidized by numerous oxidants usually resulting in formation of sulfoxides or sulfones. The cation radical and dication species of mesocyclic thioethers can be formed chemically using nitrosonium or copper(II) salts.²⁰ Decomposition of beta sulfonium peresters can also lead to thioether cation radicals.²¹ Chemical oxidation of thioethers can be stereospecific and proceeds in very high yield. Chemical oxidation was used primarily as a way of generating authentic compounds formed from electrochemical oxidation conveniently and in large amounts in an independent method to provide for determination and confirmation of the structure of the compounds formed. Neighboring group participation is clearly a factor in many of the chemical oxidations as determined by stereochemical effects.

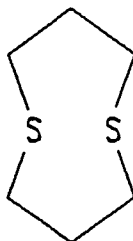
Using the techniques outlined, this dissertation presents evidence for neighboring group participation in thioether oxidation when the neighboring group is another thioether, carboxylate, or hydroxyl group. The techniques described are shown to be useful and complementary techniques for studying the oxidation of thioethers.

CHAPTER 2
ELECTROCHEMICAL AND PULSE RADIOLYTIC OXIDATION OF
THE MESOCYCLIC POLYTHIOETHERS 1,5-DITHIOCANE
AND NAPHTHO[1,8-B,C]-1,5-DITHIOCIN

Introduction

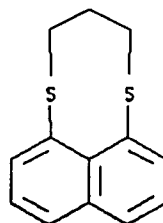
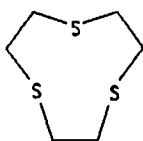
Stabilization of electron deficient sulfur by another sulfur through intramolecular interaction has been studied by electrochemical and pulse radiolysis methods. The extent of neighboring group participation has been shown to be dependent upon the size of the ring formed and the geometry of the sulfur lone pairs of the compounds being studied as can be seen by looking at the peak potentials shown in Table 2.1. The potentials observed for a few aliphatic thioethers are included to illustrate the magnitude of the neighboring group effect. The absorption maxima reported are for the 2c,3e bond formed upon pulse radiolysis and it is clear that there is a correlation between a lower oxidation potential and a stronger 2c,3e bond as evidenced by a shorter wavelength absorption.

The remarkably easy and reversible oxidation of 1,5-dithiocane, 1.01, which occurs at 0.34 V in acetonitrile versus a Ag/0.1 M AgNO₃ reference electrode, provides a dramatic example of neighboring sulfur group participation

2.01

in sulfur oxidation. A combination of steric and electronic factors contributes to this facile oxidation.²² Transannular lone-pair lone-pair repulsion destabilizes the parent compound but the same orbital overlap stabilizes the cation radical as discussed in Chapter 1.

This chapter presents the electrochemical and pulse radiolysis investigation of two cyclic thioethers, 1,4,7-trithiacyclononane (2.01) and naphtho-[1,8-b,c]-1,5-dithiocin (1.02).

2.011.02

Results and Discussion

Cyclic voltammetry of TTCN (2.01) in acetonitrile 0.1 M in LiClO_4 at a platinum electrode exhibits one irreversible oxidation wave at 0.9 V versus a $\text{Ag}/0.1 \text{ M AgNO}_3$ in acetonitrile reference electrode as shown in Figure 2.1.

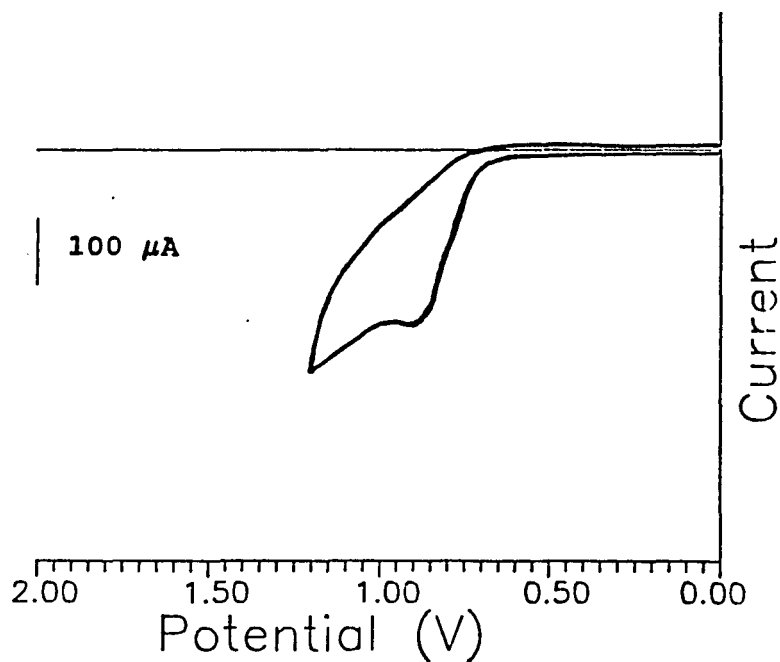
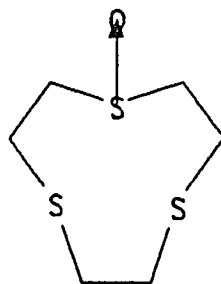


Figure 2.1. Cyclic Voltammogram of 1.5 mM 2.01 in 0.1 M LiClO_4 acetonitrile solution. Pt Working electrode ($A = 0.4 \text{ cm}^2$), Pt counter electrode, $\text{Ag}/0.1 \text{ M AgNO}_3$ in acetonitrile reference electrode. Scan rate 100 mV/s.

As shown by the lack of any reduction wave upon reversal of the potential sweep, the oxidation is irreversible under the conditions employed. The oxidation observed is diffusion controlled as evidenced by a linear plot of the square root of the sweep rate versus the peak current. Table 2.1 shows the oxidation potential of a number of thioethers that have been investigated electrochemically. In comparison to simple aliphatic sulfides TTCN, 2.01, shows a moderate neighboring group effect. As is evidenced by the trend in the peak potentials, five-membered rings are clearly favored in sulfur-sulfur intramolecular interactions whereas oxidation of 2.01 involves the formation of a less favored four-membered ring (see 2.03). No evidence is seen for participation by the third sulfur.

Controlled potential electrolysis of 2.01 at a carbon electrode with an applied potential of 1.0 V resulted in the



2.02

passage of current corresponding to an "n" value of 1.8 and

Table 2.1
Oxidation of Thioethers





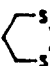
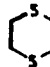
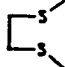

Thioether	Electrochemical Peak Potential (V)	Pulse Radiolysis 2c,3e Bond Absorption (nm) (7)
	1.25 (1)	- (5)
	1.32 (2)	- (5)
	1.13 (2)	- (5)
	1.15 (2)	- (5)
	1.14 (2)	600
	1.25 (2)	650
	0.97 (2)	525
	0.9 (3)	540

Table 2.1 continued
Oxidation of thioethers

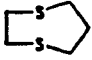
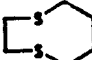
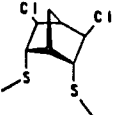
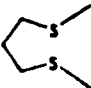
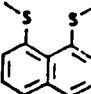
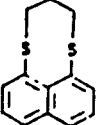

	0.84 (2)	460
	0.81 (2)	-
	0.75 (2)	-
	0.66 (2)	450
	0.7 (4)	-
	0.47 (3)	420 (6)
	0.34 (2)	400

TABLE 2.1 continued

References for table:

- (1) Meites, L; Zuman, P. in "Electrochemical Data, Part 1", Wiley: New York, 1974; Vol. A, p 30.
- (2) Glass, R. S.; Wilson, G. S.; Coleman, B. R.; Setzer W. N.; Prabhu, U. D. G. Adv. Chem. Ser. **1982**, 201, 417.
- (3) This work.
- (4) Zweig, A; Hoffman, A.K. J. Org. Chem., **1965**, 30, 3997.
- (5) Monothioethers form adsorbing dimers- see Bonifacic, M.; Möckel, H.; Bahnemann, D.; Asmus, K.-D. J. Chem. Soc. Perkin Trans. 2, **1975**, 657.
- (6) Observed in isooctane solvent, see Asmus, K.-D; Gillis, H. A.; Teather, G. G. J. Phys. Chem., **1978**, 25, 2677.
- (7) Asmus, K.-D.; Bahnemann, D; Fiscer, Ch.-H.; Veltwisch, D. J. Am. Chem. Soc., **1979**, 101, 5322.

the sulfoxide 2.02 was formed in 75% chemical yield and 80% current yield. The monosulfoxide 2.02 was also prepared chemically by treating 2.01 with sodium metaperiodate and the IR spectrum, ^1H NMR spectrum, and mp of the product formed were identical with those of the electrochemical product and consistent with the formation of 2.02.

Pulse radiolysis of a 0.05 mM aqueous solution of 2.01 (2.01 is only slightly soluble in water) in a nitrous oxide saturated aqueous solution at pH 4 results in the formation of a transient species absorbing in the visible with a peak absorption at 540 nm as shown in Figure 2.2. A weak shoulder with an absorption maximum about 280 nm is assumed to be due to an α -alkylthio radical. The absorption observed at 540 nm shows first-order decay kinetics as shown by the excellent fit of a calculated first-order decay curve overlaid over the actual data from the decay of the species formed shown in Figure 2.3. The half-life of the species formed is 85 μs . The half-life for the decay is independent of the initial concentration of radicals formed, also indicative of first-order decay. The conductivity signal observed upon pulse radiolysis of 2.01 is shown in Figure 2.4. The species formed upon pulse radiolysis is postulated to be the 2c,3e compound 2.03 which is consistent with the absorption maximum observed and the conductivity signal.

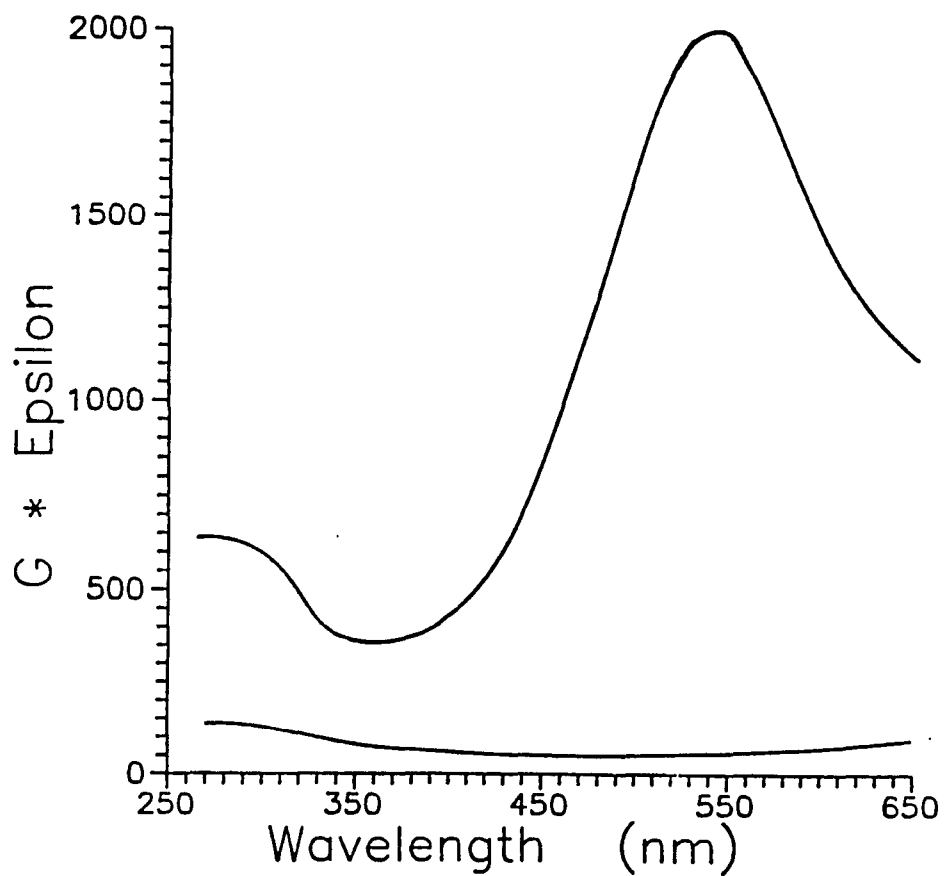


Figure 2.2. Pulse radiolysis of a 0.05 μM solution of 2.02 in N_2O saturated pH 4 water. Upper curve: immediately after application of pulse. Lower curve: 800 μs after pulse. Curves shown are smoothed curves drawn through approximately 25 data points collected between 260 and 650 nm.

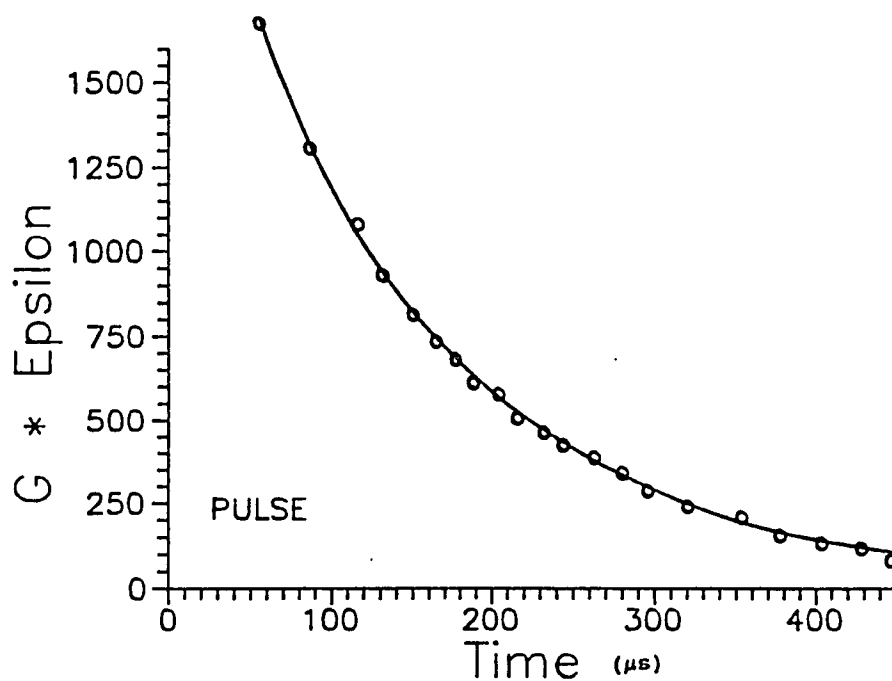


Figure 2.3. Plot of transient absorption decay for 0.05 mM 2.01 in N₂O saturated pH 4 aqueous solution. Measured at 540 nm. Circles: experimental data. Curve: 1st order decay fit, $T_{1/2} = 85 \mu s$.

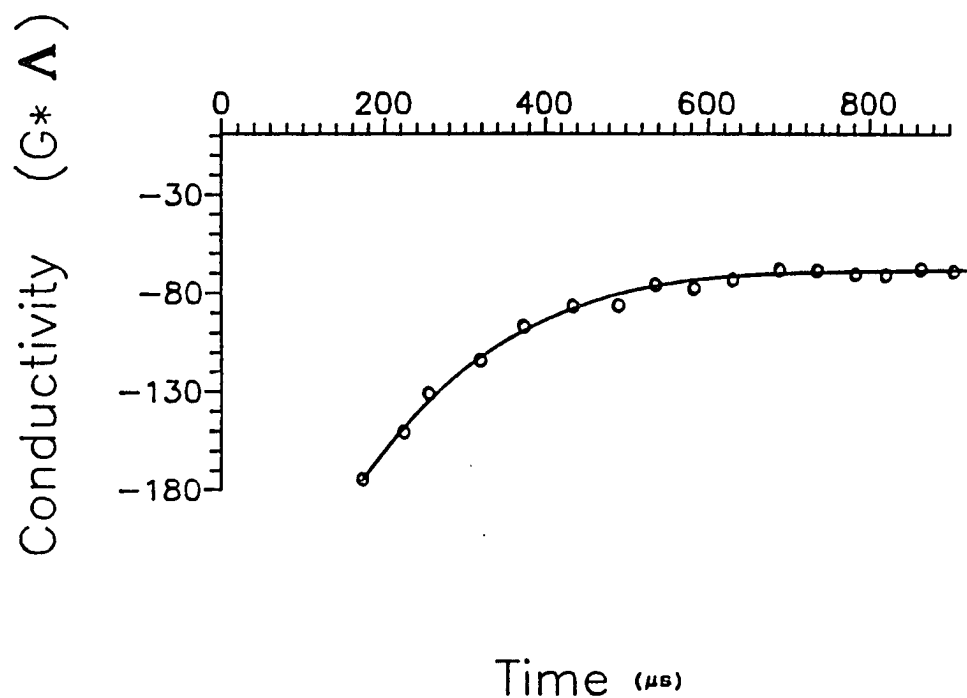
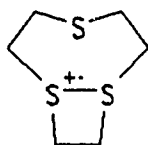


Figure 2.4. Plot of the conductivity signal observed for $\approx 2 \times 10^{-5} \text{ M } 2.01$ in N_2O saturated pH 2.6 water. Circles: experimental data. Curve: 1st order decay fit, $T_{1/2} = 107 \text{ } \mu\text{s}$.

At a pH of 4 the conductivity signal reflects replacement of a proton, which is neutralized by the hydroxide anion



2.03

produced, by the less mobile organic cation radical 2.03. The kinetics of the increase seen in the conductivity signal, $t_{1/2} = 107 \mu s$, parallel those of the absorption observed at 540 nm. A G value of 3.9 can be determined from the conductivity data as follows:

$$\text{Observed } G * \Delta = 1044, \Delta \Lambda \text{ (calc.)} = 315 - 45 = 270$$

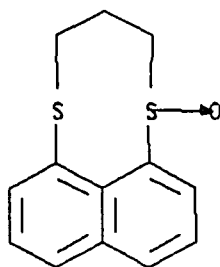
$$G = (1044/270) = 3.9$$

One interesting observation is that unlike most thioethers studied extensively by Asmus *et al.* 2.03 does not appear to decay by direct loss of a proton to form an α -alkylthio radical since the peak at 280 nm does not increase as the absorption at 540 nm decays.

Naphtho Dithiocin 1.02 has the same eight membered dithioether ring as 1.01 but is much more rigid due to the presence and geometry of the naphthalene ring.²³ Compound 1.02 was investigated extensively by Broeker²⁴ using photoelectron spectroscopy and computational analysis.

Cyclic voltammetry of 1.02 in acetonitrile results in

an irreversible oxidation with a peak potential of 0.47 V as shown in Figure 2.5. Several other oxidation waves are present at 1.18, 1.35, and 1.58 V respectively. The peak observed shows no reversible behavior with scan rates up to 500 mV/s. A plot of peak current versus the scan rate between 10 and 200 mV/s is linear, indicating diffusion control of the oxidation (figure 2.6).



2.04

Controlled potential electrolysis of 1.02 at an applied potential of 0.6 V resulted in the passage of 1.8 equivalents of charge before the current had decayed to zero. The product formed in 80% chemical yield (95% current yield) was sulfoxide 2.04. Sulfoxide 2.04 was also prepared by oxidation of 1.02 with sodium metaperiodate and identified by comparison with authentic compound prepared by Broeker²⁴. Cyclic voltammetry on the electrolysis solution before and after electrolysis clearly shows the loss of the oxidation peak at 0.47 V. Cyclic voltammetry on the sulfoxide 2.04 shows peaks corresponding to the

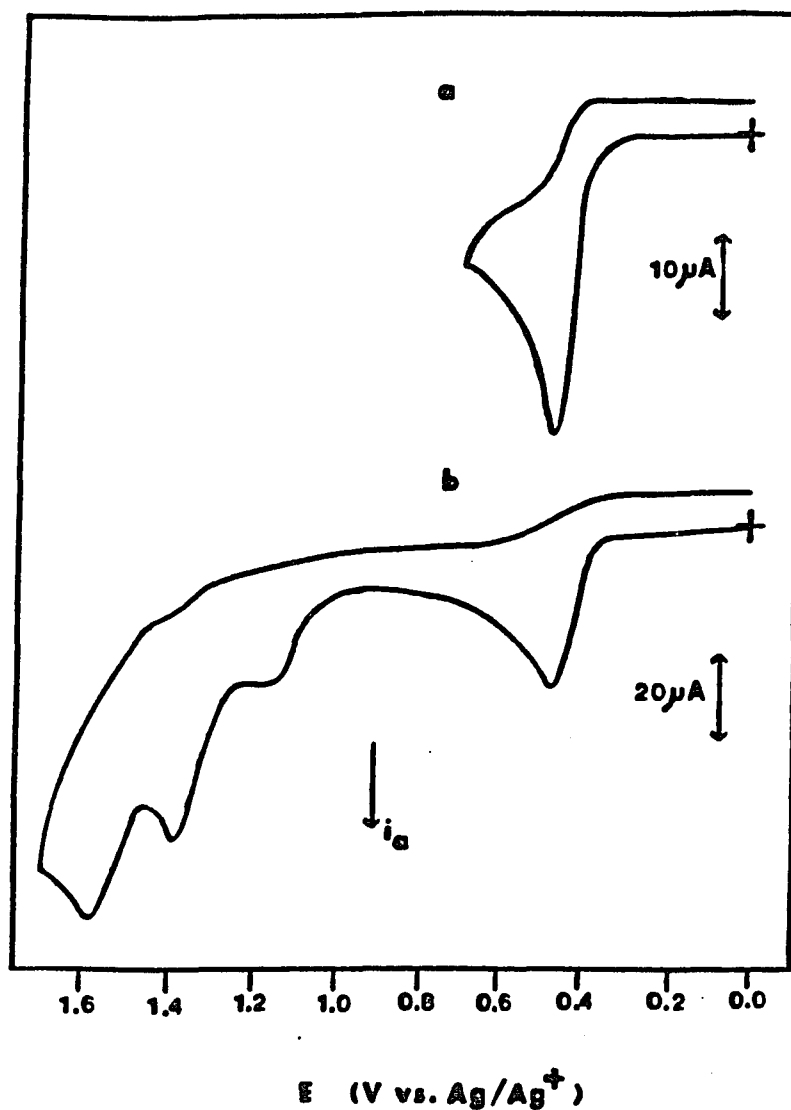


Figure 2.5. Cyclic voltammogram of 1.1 mM 1,02 in 0.1 M LiClO_4 acetonitrile solution. Pt working electrode ($A = 0.3 \text{ cm}^2$), Pt counter electrode, $\text{Ag}/0.1 \text{ M AgNO}_3$ in acetonitrile reference electrode. Scan rate 100 mV/s: (a) cyclic scan in the range 0-0.7 V and (b) cyclic scan in the range 0-1.7 V.

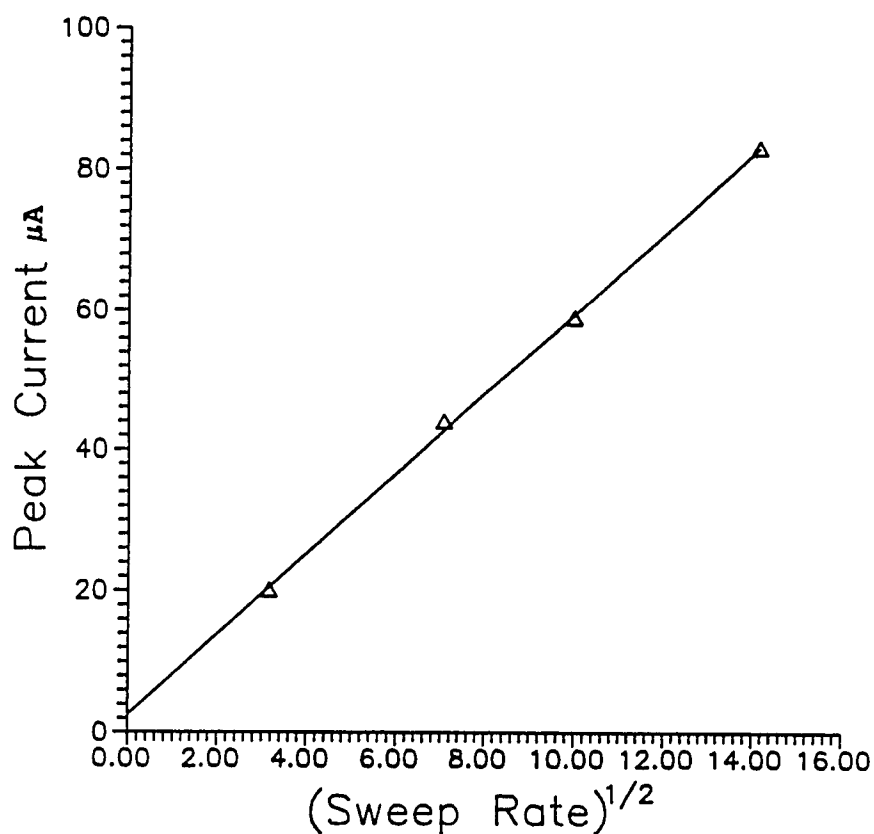
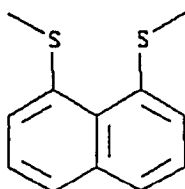


Figure 2.6. Plot of the square root of the sweep rate versus peak current for 1.1 mM 1.02 in 0.1 M LiClO₄ in acetonitrile. Pt working electrode ($A = 0.3 \text{ cm}^2$). Pt counter electrode. Ag/0.1 M AgNO₃ in acetonitrile reference electrode. Scan rates: 10, 50, 100, 200 mV/s.

higher potential peaks seen in the oxidation of 1.02.

Clearly, 1.02 shows strong neighboring group participation in its electrochemical oxidation. The oxidation potential of 1.02 is well below that of the

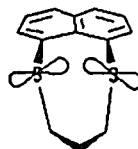


2.05

closely related compound 2.05 which has an E_p of 0.7 V under similar electrochemical conditions. The sulfur atoms in the ground state lowest energy conformers of 1.02 and 2.05 are in significantly different geometries.²⁵ In 2.05 the two methyl carbons are rotated slightly out of the naphthalene plane in conrotatory fashion and the two sulfurs are close to the naphthalene plane resulting in the lone pairs on the sulfur atoms being parallel and tilted slightly with respect to the naphthalene plane. However, in 1.02 the methylene



2.05



1.02

bridge ties the two "methylys" together and forces the

sulfurs to rotate, leading to a conformation where the lone pairs are rotated in towards each other to a much higher degree. The PES and calculations on 1.02 indicate a very large (1.6-2.0 eV) splitting between the two sulfur lone pairs, a clear indication of their interaction. The net result is a much lower oxidation potential for 1.02 than for 2.05. Why is dithiocin 1.02 harder to oxidize than dithiocane 1.01? The electron withdrawing naphthalene ring may destabilize the cation radical by induction. Alternatively, the reason may be that because of the geometric constraints put on the cation radical formed it is destabilized with respect to the cation radical of 1.01. Evidence for this postulate is given in Appendix 1 which reports on preliminary results showing the reversible oxidation of 1.02 to occur with an E^0 of 0.53 V versus 0.3 V for 1.01. It should also be noted that in a hydrocarbon solvent 1.02 shows a pulse radiolysis absorption maximum of between 410 and 430 nm as compared to 400 nm for 1.01 in water.

Experimental

Cyclic Voltammetry

Reagent grade acetonitrile was heated at reflux for at least 12 hours over P_2O_5 and then distilled from P_2O_5 under a nitrogen atmosphere. $LiClO_4$ was dried in a vacuum oven

overnight at 110 °C. Cyclic voltammetry was performed in a three-necked single chambered electrochemical cell. The reference electrode, except where noted, was a silver wire suspended in 0.1 M silver nitrate in acetonitrile encased in a glass case with a sintered glass disk used for contact with the bulk solution. The working and counter electrodes were platinum flag electrodes. The working electrode area was 0.3 cm² and the counter electrode slightly larger. Argon or nitrogen was bubbled through the cell for approximately 10 minutes before recording the cyclic voltammetry curves. Between each cyclic voltammogram the counter and working electrodes were cleaned by rinsing them in nitric acid, then distilled water and then heating to incandescence in a flame. Solutions were prepared by weighing out appropriate amounts of the compounds to be studied and adding them directly to the electrochemical solution after running a background curve. Concentrations, scan rate, and other experimental parameters are as indicated on the individual Figures. A PAR model 362 scanning potentiostat equipped with a Houston model 200 X-Y recorder was used to run the cyclic voltammograms. A Cyprus Systems computer electrochemical data acquisition system (Model CYSY-1) was used for some of the work. The FTIR experiments were performed on a Perkin-Elmer Model 1800

FTIR with a 0.1 mm path length cell using appropriate amounts of the compounds investigated to provide 1 mM solutions.

Controlled Potential Electrolysis of 2.02.

A sample of 2.01 (25 mg, 0.14 mmol) dissolved in acetonitrile (15 ml) 0.1 M in LiClO_4 was electrolyzed at a platinum working electrode at 1.0 V versus a $\text{Ag}/0.1 \text{ M AgNO}_3$ reference electrode with a platinum counter electrode. The working electrode had become passivated (in other words the current flowing dropped to near zero much faster than it should have) after about 20 coulombs of charge had passed and was removed and cleaned. Upon continuing the electrolysis a total of 24 coulombs of charge passed before the current decayed to less than one percent of its original value. The charge passed corresponds to an "n" value of 1.85. Water (100 mL) was added and the solution extracted with dichloromethane (2X50 mL). TLC on silica of the crude extract showed one spot with an R_f of 0.18 eluting with ethyl acetate. Removal of the solvent gave 19.9 mg (74 % yield) of a pale yellow solid: mp 74-77 °C; IR (KBr) 3000, 1414, 1360, 1025 (sulfoxide) cm^{-1} ; ^1H NMR (CDCl_3 , 250 MHz) δ 2.85 (m, 2), 3.00 (ddd, 1, $J = 9.9, 4.9, 2.5 \text{ Hz}$), 3.29 (ddd, 1, $J = 9.8, 7.1, 2.6 \text{ Hz}$), 3.42 (ddd, 1, $J = 9.8, 7.1, 2.7 \text{ Hz}$),

4.01 (ddd, 1, $J = 13, 10.5, 2.6$ Hz); ^{13}C NMR (CDCl_3) δ 52.8, 35.4, 26.1.

Controlled Potential Electrolysis of 2.05.

A sample of 1.02 (19 mg, 0.082 mmol) dissolved in acetonitrile 0.1 M in LiClO_4 (15 mL) was exhaustively electrolyzed at a carbon electrode at a potential of 0.6 V versus a $\text{Ag}/0.1$ M AgNO_3 reference electrode. When the current had decayed to less than one percent of its initial value 14.22 coulombs of charge had passed, corresponding to an "n" value of 1.8. After removal of most of the solvent, the crude mixture was applied to a preparative TLC plate (eluting with ethyl acetate $R_f = 0.2$), and 17.8 mg (80 % yield) of pure sulfoxide 2.04 was obtained: mp 133-134.5; ^1H NMR (CDCl_3 , 250 MHz) δ 1.6 (m, 1), 2.23 (ddd, 1, $J = 15.5, 4.1, 3.7$ Hz), 2.58 (m, 1), 2.68 (dd, 1, $J = 14, 4.2$ Hz), 3.01 (dm, 1, $J = 14$ Hz), 3.73 (ddd, 1, $J = 16, 12.8, 3.3$ Hz); IR (KBr) 2947, 1024 (sulfoxide), 1008, 977, 826, 766 cm^{-1} . The spectral data and melting point are in accord with those reported for sulfoxide 2.04 prepared chemically by Broeker.²⁶

Pulse Radiolysis of 2.02

Millipore filtered water with a resistance of greater than 10 megohm was used for all the pulse radiolysis

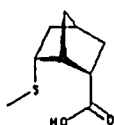
experiments. The solutions were deoxygenated with argon and saturated with N_2O . Thioether 2.01 was only slightly soluble in water but it was possible to dissolve a sufficient amount to generate an approximately 0.05 mM solution. The pH was adjusted by adding standardized $HClO_4$ and was measured just prior to the experiments using an Orion Research pH meter.

The solution was irradiated using a 1.5 MeV van de Graaff accelerator with a pulse duration of 1 μs . Absorbed doses were on the order of 1-5 Gray (1 Gy = 1 J/Kg). The experimental system was calibrated each day by standard pulse radiolysis thiocyanate dosimetry.²⁷ The solution was pumped into the pulse radiolysis cell via a positive pressure flow-through system described elsewhere²⁸. The optical and conductivity apparatus were optimized prior to each experiment. Absorption data were obtained over the range 250-500 nm. Kinetic data were obtained at a wavelength corresponding to the absorption maximum. All the data were acquired and manipulated via a computer-controlled data acquisition system described elsewhere²⁶.

CHAPTER 3
ELECTROCHEMISTRY OF (\pm)-2-EXO-AMINO-6-ENDO-
METHYLTHIOBICYCLO[2.2.1] HEPTANE-2-
ENDO-CARBOXYLIC ACID

Introduction

Neighboring group participation in the electrochemical oxidation of thioethers when the neighboring group is a carboxyl group has been reported²⁹. Endo acid 3.01 oxidizes



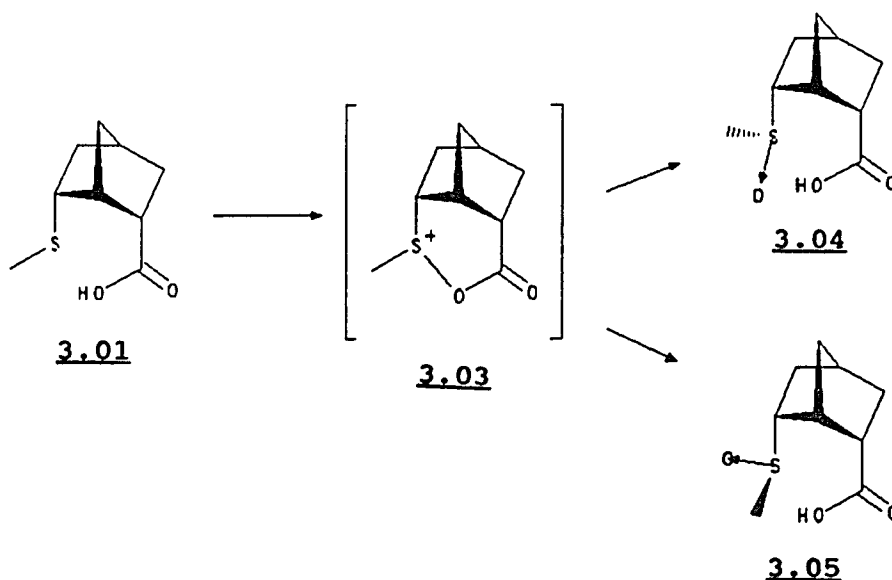
3.01



3.02

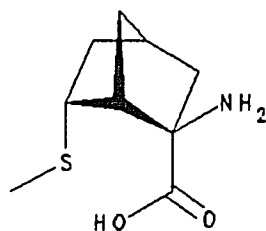
at a much lower potential than its exo derivative 3.02 in the presence of 2,6-di-t-butylpyridine. However, the low peak potential is actually due to the oxidation of bromide. Without bromide present the oxidation potential of 3.01 is only slightly lower than that of exo derivative 3.02 (1.28 V. versus 1.2 V respectively). As discussed thoroughly by Petsom³⁰ the bromide catalysis clearly indicates neighboring group participation but the observed peak potential of 0.6 V is attributed to oxidation of a bromide species, not direct oxidation at sulfur. The need for base to be

present indicates that the species that actually participates in the oxidation is the carboxylate ion. Spectroscopic characterization of acyloxysulfonium salt 3.03 as an intermediate in the chemical oxidation of endo acid 3.01 provided significant evidence for carboxylate neighboring group participation as did analysis of the diastereomer ratios of sulfoxides 3.04 and 3.05 in comparison with the ratios found for chemically prepared 3.04 and 3.05 along with evidence provided by labelling experiments.³¹

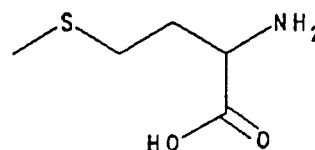


As discussed in the introduction, methionine is present at the active site of a number of redox proteins and may be directly involved in biological electron transfer.

Amino acid 3.06, ((+)-2-exo-amino-6-endo-methylthiobicyclo [2.2.1] heptane-2-endo-carboxylic acid) was developed as a conformationally restricted methionine analog. The synthesis of 3.06 has been described elsewhere.³²



3.06



Methionine

Investigation of compound 3.06 allows one to probe S-Carboxyl interactions which are influenced by the alpha amine but in which direct nitrogen interaction with the sulfur atom is precluded. Amino acid 3.06 crystallizes as the zwitterion and has a short S-C7 (carbon in carboxylate group) distance of 3.158 Å³¹. The amino acid 3.06 has been found to exhibit strong neighboring group participation upon electrochemical oxidation, independent of the presence of bromine, but dependent on the presence of the carboxylate moiety.

Results and Discussion

Cyclic voltammetry of amino acid 3.06 in 0.1 M LiClO₄ in acetonitrile at 100 mV/s shows two oxidation waves. The first wave at about 0.9 V is broad with no distinct peak. There is a second anodic wave with a more normal shape and

a peak potential of 1.35 V versus Ag/0.1 M AgNO₃ in acetonitrile. Figure 3.1 shows the cyclic voltammogram. The two oxidations are irreversible as confirmed by the lack of corresponding cathodic peaks and evaluation of the dependence of the peak potentials on scan rate. Both the oxidations are essentially diffusion controlled. A plot of peak current versus the square root of the sweep rate for the first anodic peak is linear over nearly two orders of magnitude from 20 mV/s up to 10 V/s as shown in Figure 3.2. This suggests that this step is diffusion controlled. The second wave also shows linear behavior between 20 mV/s and 1 V/s. Both peaks shift anodically as the scan rate is increased. Because the peaks are broad it is hard to estimate them accurately but they shift about 70 mV/decade. This corresponds to an irreversible process with one electron in the rate determining step.

The position of the first anodic wave is dependent on concentration. As the concentration is increased from 0.62 mM up to 2.09 mM the peak potential shifts from 0.87 to 0.94 V at 100 mV/s scan rate. The ratio of the currents at the two anodic waves is not affected by the change in concentration. Addition of water to the acetonitrile solution has no effect on the cyclic voltammograms.

The two waves observed were further investigated by

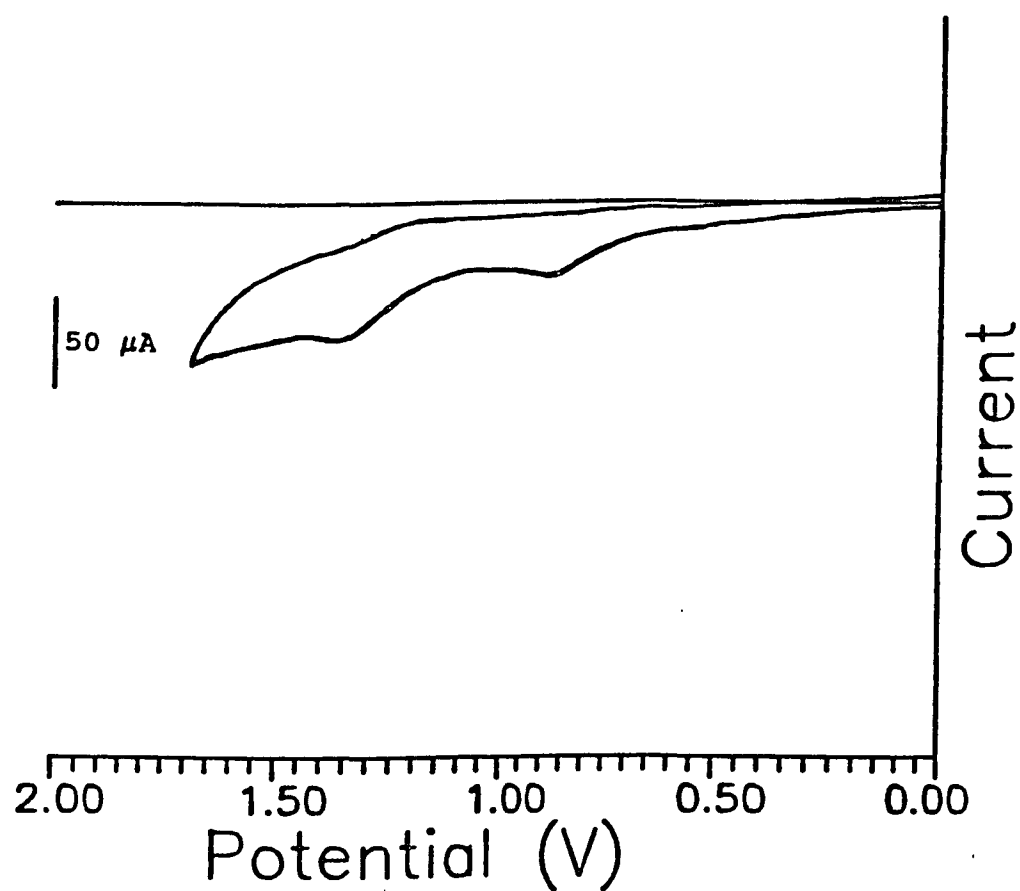


Figure 3.1. Cyclic voltammogram of 0.9 mM 3.06 in 0.1 M LiClO_4 acetonitrile solution. Pt working electrode ($A = 0.4 \text{ cm}^2$), Pt counter electrode, $\text{Ag}/0.1 \text{ M AgNO}_3$ in acetonitrile reference electrode. Scan rate 100 mV/s.

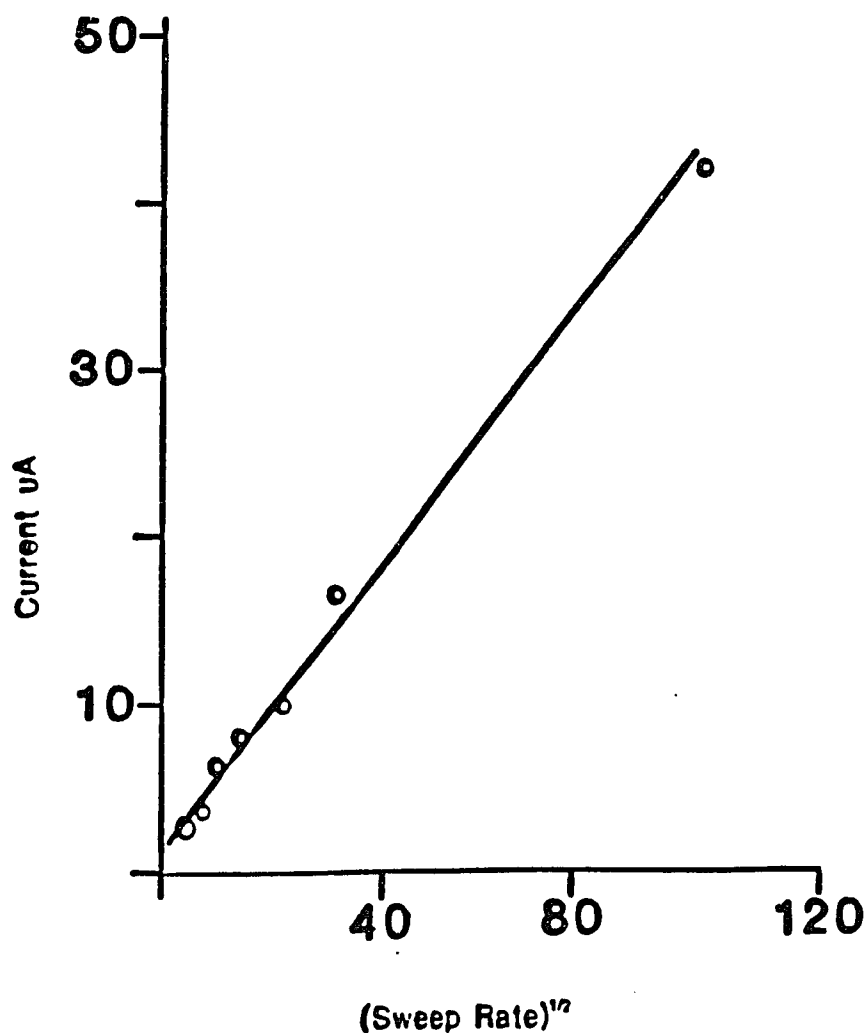


Figure 3.2. Plot of the square root of the sweep rate versus peak current for 0.8 mM 3.06 in 0.1 M LiClO₄ acetonitrile. Pt working electrode ($A = 0.4 \text{ cm}^2$). Pt counter electrode. Ag/0.1 M AgNO₃ in acetonitrile reference electrode. Scan rates: 20, 50, 100, 200, 500, 1000, 2000 mV/s.

rotating disk electrode (RDE) studies. The RDE voltammograms are shown in figure 3.3. A Levich³³ plot for the first oxidation ($E_{\text{appl}} = 1.2$ V versus Ag/0.1 M AgNO₃ reference electrode) is very slightly concave as shown in figure 3.4. A Koutecky-Levich plot (i/i_L vs. $1/\omega^{1/2}$) is linear but does not pass through the origin, indicating some kinetic control for the first wave. An apparent "n" value of 1.1 is obtained from the Levich plot. The second step is found to be diffusion controlled according to the Levich plot ($E_{\text{appl}} = 1.4$ V, see figure 3.4) and an "n" value of 2.2 is obtained for this process.

The addition of a 2:1 mole ratio of base (2,6-di-*t*-butylpyridine) to a solution of amino acid results in a cyclic voltammogram that shows only one broad anodic wave with a peak potential of about 1.07 V. The current measured at the peak is near 90% of the total current for the two separate waves without base present. Addition of an excess of base gives a cyclic voltammogram similar to the 2:1 case except that now the total current is quite close to the simple addition of the currents for the two separate waves without base. Although the base is electroinactive in the region scanned there is a slight increase in the background current at the high end of the potential scale. Figure 3.5 shows the cyclic voltammogram. An RDE voltammogram with

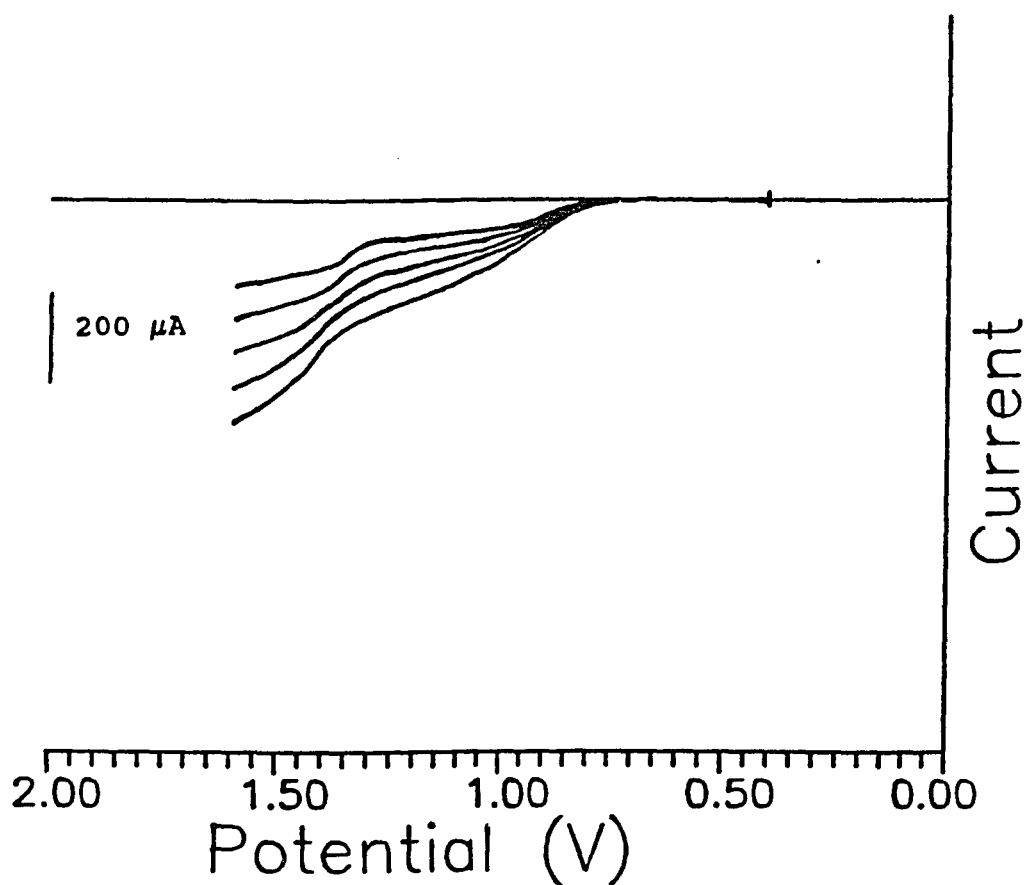


Figure 3.3. Rotating disk voltammogram of 1.15 mM 3.06 in 0.1 M LiClO_4 acetonitrile. Glassy carbon working electrode ($A = 0.3 \text{ cm}^2$). Pt counter electrode. Ag/0.1 M AgNO_3 in acetonitrile reference electrode. Rotation rates: 400, 900, 1600, 2500, 3600 rpm.

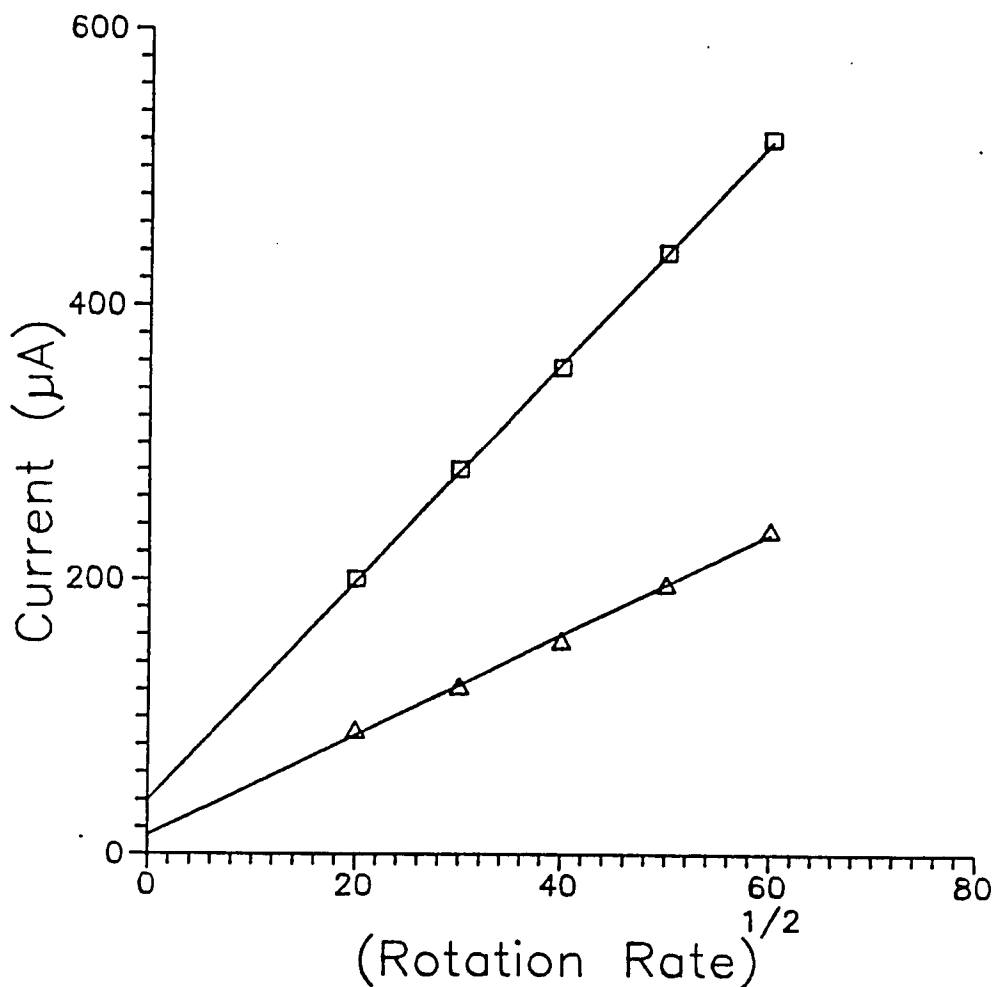


Figure 3.4. Levich plot of 1.15 mM 3.06 in 0.1 M LiClO₄ acetonitrile. The current was measured at 1.2 V for the lower curve and at 1.4 V for the upper curve. Glassy carbon working electrode ($A = 0.3 \text{ cm}^2$). Pt counter electrode. Ag/0.1 M AgNO₃ in acetonitrile reference electrode. Rotation rates: 400, 900, 1600, 2500, 3600 rpm.

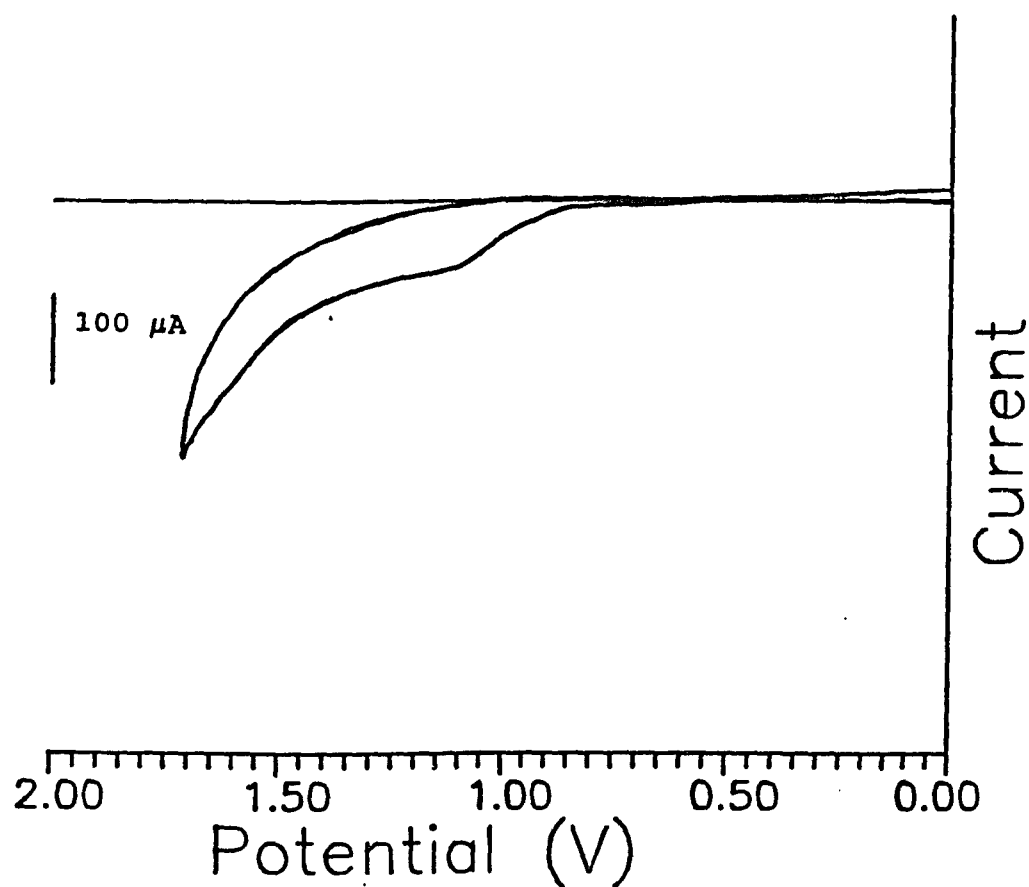


Figure 3.5. Cyclic voltammogram of 1.24 mM 3.06 plus 5.6 mM 2,6-di-*t*-butylpyridine in 0.1 M LiClO_4 acetonitrile solution. Pt working electrode ($A = 0.4 \text{ cm}^2$), Pt counter electrode, Ag/0.1 M AgNO_3 in acetonitrile reference electrode. Scan rate 100 mV/s .

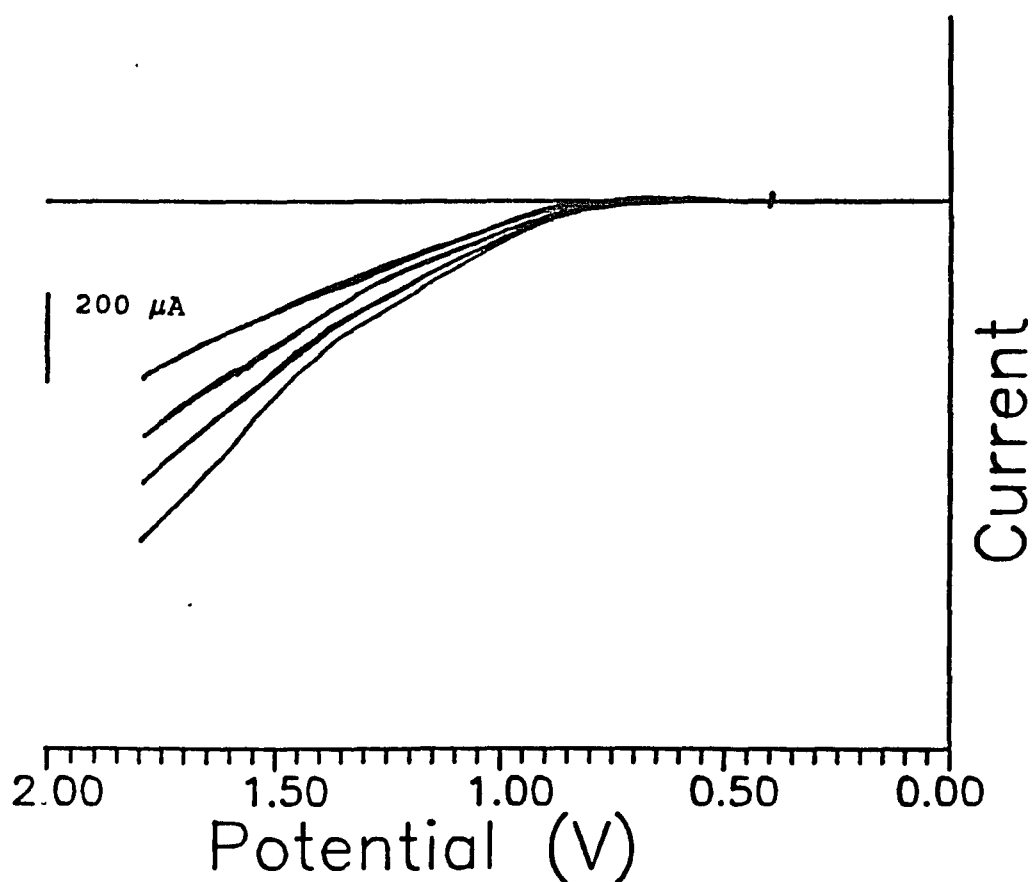


Figure 3.6 Rotating disk voltammogram of 1.13 mM 3.06 and 0.72 mM 2,6-di-*t*-butylpyridine in 0.1 M LiClO_4 acetonitrile. Glassy carbon working electrode ($A = 0.3 \text{ cm}^2$). Pt counter electrode. $\text{Ag}/0.1 \text{ M}$ AgNO_3 in acetonitrile reference electrode. Rotation rates: 400, 900, 1600, 2500, 3600 rpm.

base present shows a drawn-out ill-defined wave as shown in figure 3.6

Cyclic voltammetry of the amino acid in the presence of either trifluoroacetic acid or trifluoromethanesulfonic acid in acetonitrile results in a voltammogram showing one well defined oxidation wave at 1.35 V and as shown in Figure 3.7. The peak current observed is again equal to the sum of the currents from the two waves present in the absence of added acid. A linear plot of the square of the sweep rate versus peak current indicates that the oxidation is diffusion controlled. Rotating disk electrode voltammograms in the presence of trifluoroacetic acid, shown in figure 3.8, exhibit one diffusion controlled oxidation wave with a half wave potential of about 1.3 V.

A differential pulse polarogram of the amino acid, shown in Figure 3.9, exhibits two distinct anodic peaks at 0.870 and 1.24 V corresponding to the two cyclic voltammetric waves observed. The ratio of the first peak current to the second peak current is 0.26, considerably lower than in the cyclic voltammetry. The significance of the peak current ratios will be elaborated upon shortly.

Cyclic voltammetry of the amino acid at a glassy carbon disk electrode results in two waves, one just under 0.9 V and a second wave at 1.3 V. These waves are better defined

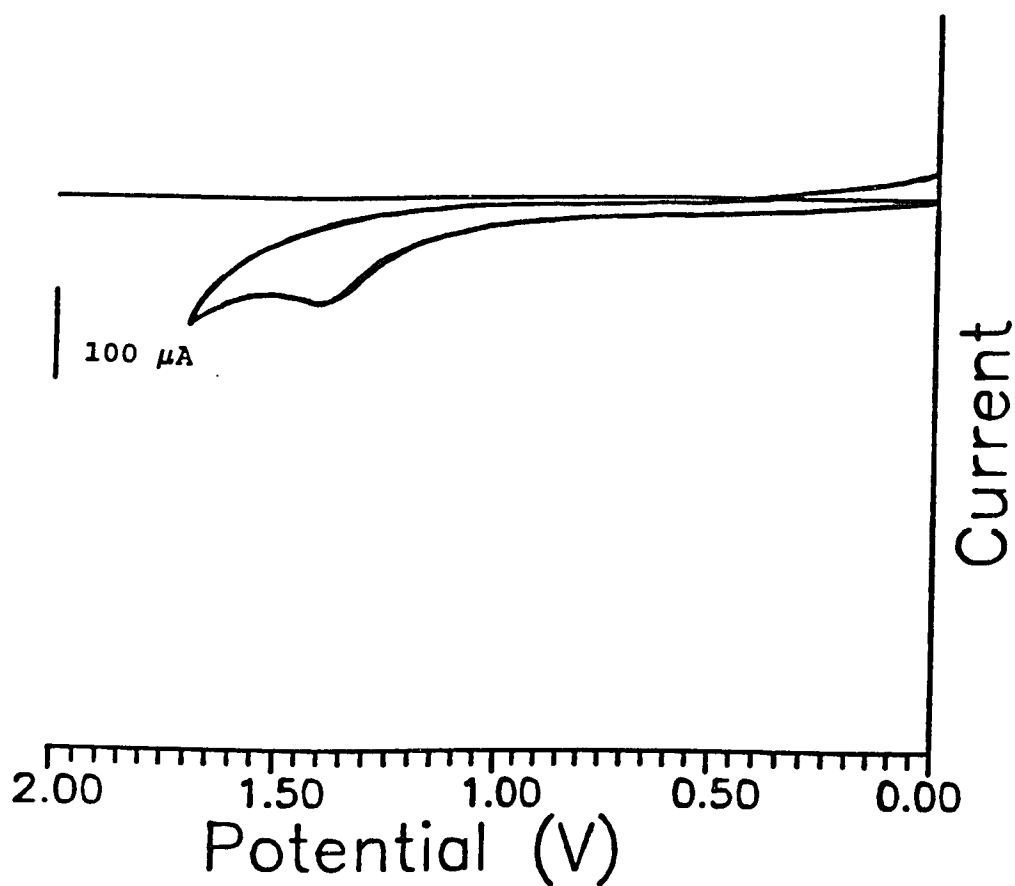


Figure 3.7. Cyclic voltammogram of 1.1 mM 3.06 in the presence of 16 mM trifluoroacetic acid in 0.1 M LiClO_4 acetonitrile solution. Pt working electrode ($A = 0.4 \text{ cm}^2$), Pt counter electrode, $\text{Ag}/0.1 \text{ M}$ AgNO_3 in acetonitrile reference electrode. Scan rate 100 mV/s .

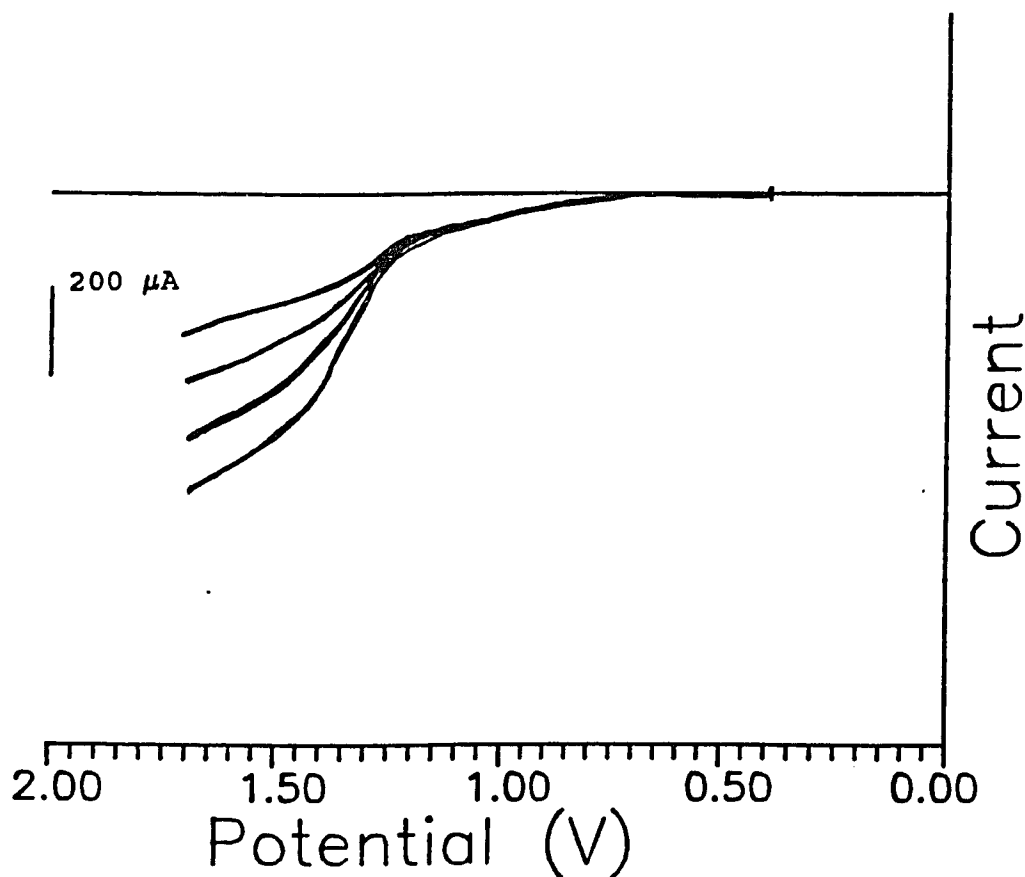


Figure 3.8. Rotating disk voltammogram of 1.15 mM 3.06 and 1.14 mM trifluoroacetic acid in 0.1 M LiClO_4 acetonitrile. Glassy carbon working electrode ($A = 0.3 \text{ cm}^2$). Pt counter electrode. $\text{Ag}/0.1 \text{ M}$ AgNO_3 in acetonitrile reference electrode. Rotation rates: 400, 900, 1600, 2500, 3600 rpm.

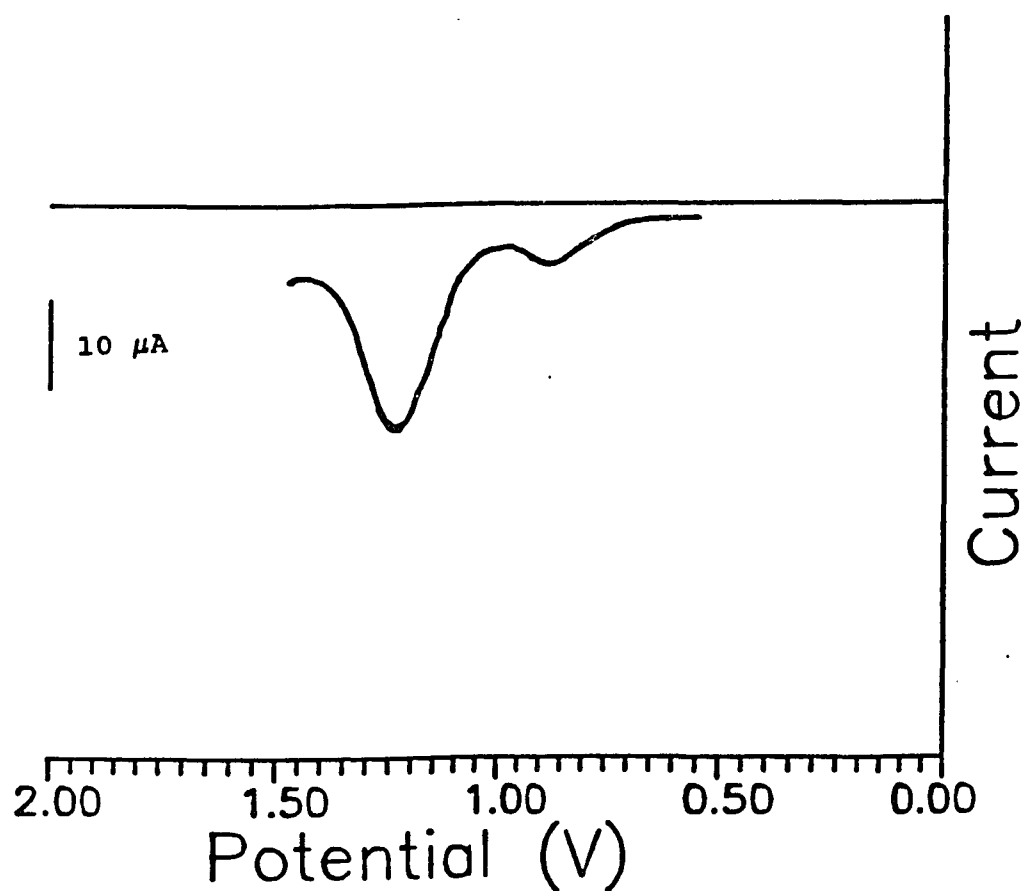


Figure 3.9. Differential pulse voltammogram of 0.8 mM 3.06 in 0.1 M LiClO_4 in acetonitrile. 25 mV pulse amplitude. 2 msec pulse width. 30 mV step height. Pt working electrode ($A = 0.2 \text{ cm}^2$). Pt counter electrode. $\text{Ag}/0.1 \text{ M}$ AgNO_3 in acetonitrile reference electrode.

than the waves at platinum. Addition of trifluoroacetic acid results in a cyclic voltammogram that shows two closely spaced waves at 1.28 and 1.32 V. Since formation of the sulfoxide was a likely reaction, cyclic voltammetry was performed on chemically prepared recrystallized amino acid sulfoxide but the voltammogram showed no discernible peaks up to 1.6 V. Another possibility that needed to be considered was Kolbe oxidation of the acid, however, a 2 mM solution of 1-amino-cyclohexane-1-carboxylic acid showed no oxidation waves below 1.6 V.

The sodium salt of 3.06 was prepared to investigate the effect of deprotonating 3.06 on the voltammograms. A cyclic voltammogram of the sodium salt of the amino acid showed one oxidation wave at 1.02 V as shown in Figure 3.10. Addition of excess amino acid to this solution resulted in two peaks, one drawn out peak with a maximum about 1.0 V and one at 1.35 V. These results indicate that the oxidation is sensitive to whether the nitrogen is protonated or not.

Further experiments to investigate the effect of protonation/deprotonation of 3.06 were as follows. Cyclic voltammetry of the amino acid in the presence of an excess of 2,6-di-*t*-butylpyridinium trifluoromethanesulfonate (this is a salt of the base used earlier, addition of this salt will help establish whether the added base is really

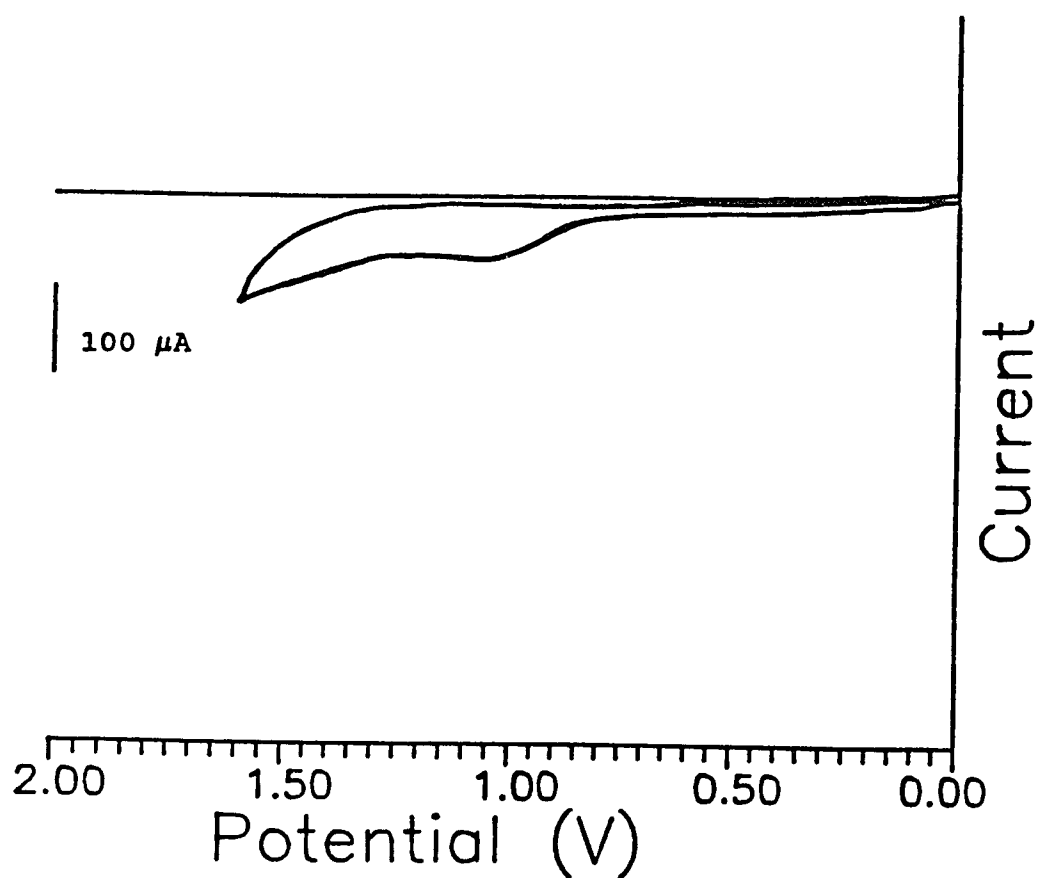


Figure 3.10. Cyclic voltammogram of 1.0 mM sodium salt of 3.06 in 0.1 M LiClO_4 acetonitrile solution. Pt working electrode ($A = 0.4 \text{ cm}^2$), Pt counter electrode, $\text{Ag}/0.1 \text{ M AgNO}_3$ in acetonitrile reference electrode. Scan rate 100 mV/s.

deprotonating 3.06) gave a cyclic voltammogram that showed an oxidation wave beginning at about 0.95 V with a steady, drawn out increase and a broad peak at about 1.33 V. Addition of 2,6-di-*t*-butylpyridine to this solution resulted in a single wave at 1.1 V. Furthermore, addition of trifluoromethanesulfonic acid to the solution such that there was an excess of acid results in a cyclic voltammogram that showed one well-shaped peak at 1.35 V. These results definitely indicate a significant role for the state of protonation of 3.06 in its oxidation.

Cyclic voltammetry in aqueous solutions afforded for better control of the pH. Cyclic voltammetry of 3.06 in pH 2.3 aqueous perchloric acid solution showed one peak with an oxidation potential of 1.10 V versus the SCE. A borate-buffered solution of 3.06, pH 8.4, shows one oxidation peak at 1.13 V versus the SCE. In pH 7.5 sodium acetate solution the cyclic voltammogram shows one peak at 1.14 V versus the SCE. The relevant cyclic voltammograms are shown in Figures 3.11, 3.12 and 3.13 respectively. In all three of the aqueous solutions the anodic solvent limit is close to the peak potential measured, so it was not possible to see further oxidations. Using ferrocene as a reference, the SCE used was 0.295 mV cathodic of the Ag/0.1 M AgNO₃ reference.

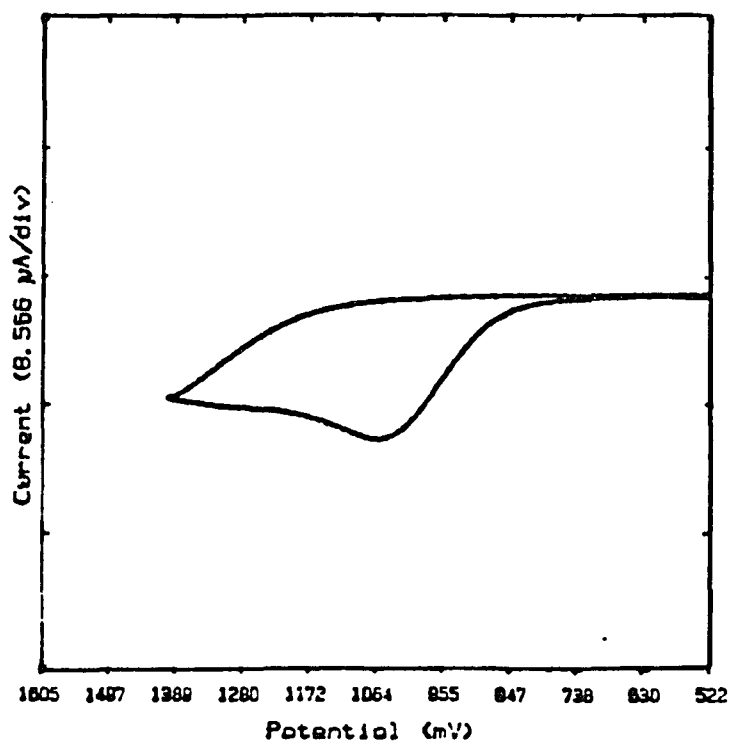


Figure 3.11 Cyclic voltammogram of 0.6 mM 3.06 in pH 2.3 aqueous perchloric acid. Pt working electrode ($A = 0.2 \text{ cm}^2$), Pt counter electrode, SCE reference electrode. Scan rate 100 mV/s.

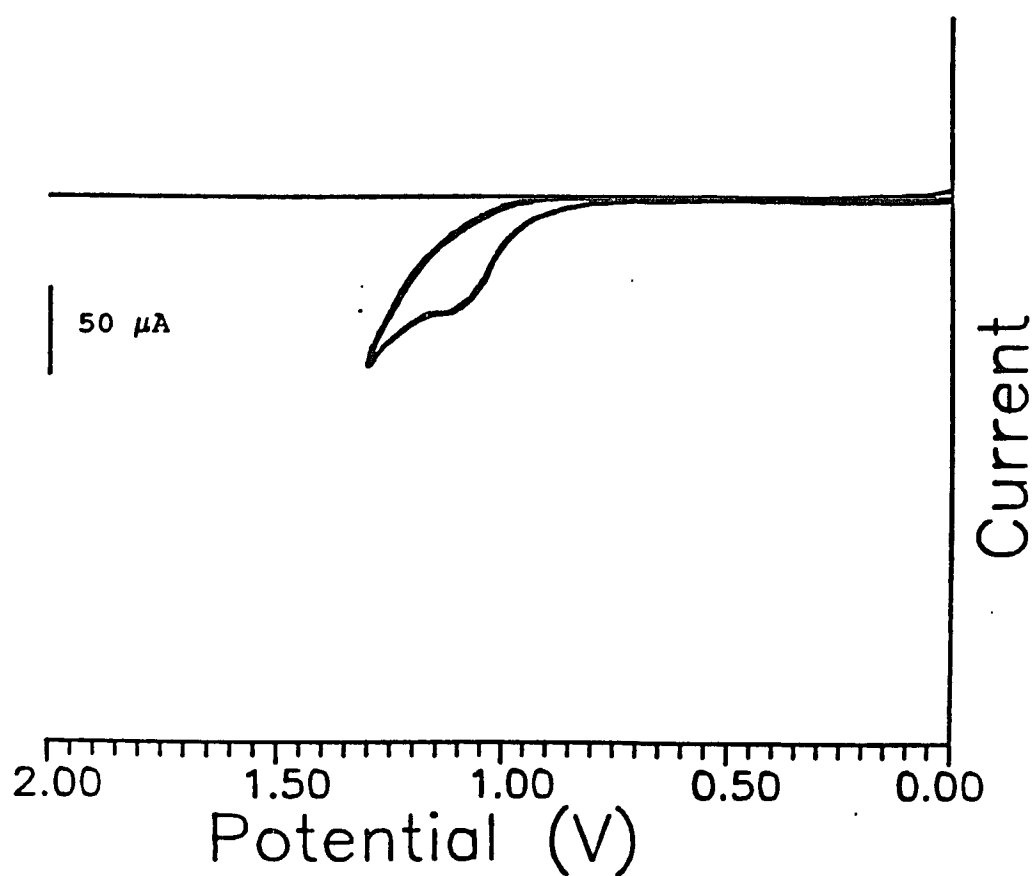


Figure 3.12 Cyclic voltammogram of 1.0 mM 3.06 in pH 8.4 aqueous borate buffer. Pt working electrode ($A = 0.4 \text{ cm}^2$), Pt counter electrode, SCE reference electrode. Scan rate 100 mV/s.

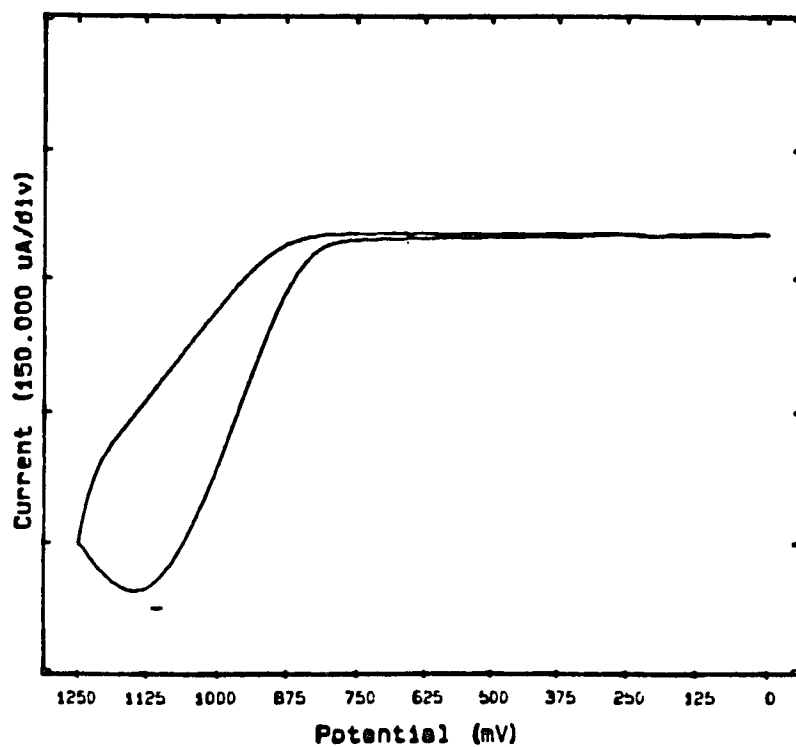


Figure 3.13 Cyclic voltammogram of 1.0 mM 3.06 in pH 7.5 aqueous acetate buffer. Pt working electrode ($A = 0.4 \text{ cm}^2$), Pt counter electrode, SCE reference electrode. Scan rate 100 mV/s.

Table 3.1 summarizes the data obtained from the cyclic voltammetry. The important points are that 3.06 in acetonitrile gives two oxidation waves at 0.9 V and 1.35 V, addition of acid results in a single wave at 1.35 V and the addition of base results in a single wave at 1.1 V.

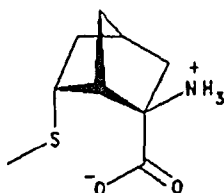
Given that the electrochemical results show a clear dependence on the acid/base properties of 3.06, it was necessary to establish by an independent method the relevant equilibria in acetonitrile. A series of FTIR experiments were carried out to help elucidate which species were actually present in the electrochemical solutions. For most of the FTIR work a solution of 0.1 M LiClO_4 in CH_3CN with an amino acid concentration of about 1 mM was used, conditions which approximate those of the electrochemical studies. There is a clear solvent window from 2000-1570 cm^{-1} allowing one to see the important carbonyl and carboxylate stretching region.

The IR spectrum of the amino acid in acetonitrile solution 0.1 M in LiClO_4 shows one broad band at 1650 cm^{-1} . Methionine shows a similar band at 1657 cm^{-1} . Addition of either trifluoroacetic acid or trifluoromethanesulfonic acid results in the loss of the band at 1650 cm^{-1} and the buildup of two sharper bands at 1760 and 1740 cm^{-1} . Methionine shows one broad band at 1756 cm^{-1} in trifluoroacetic acid.

Table 3.1
Cyclic voltammetry of amino acid 3.06

Cyclic Voltammetry of 3.06					
	Solution	Work. Elect.	Ref. Electrode	Ep 1 Ag/Ag ⁺ (SCE)	Ep 2
1	Ca. 1mM 3.06 in 0.1 M lithium perchlorate in acetonitrile	Pt	Ag/0.1 M AgNO ₃	0.90 (1.20)	1.35
2	As in 1 plus 5 μ L trifluoroacetic acid	Pt	Ag/0.1 M AgNO ₃	1.35 (1.65)	
3	As in 1 plus 10 μ L pyridine base	Pt	Ag/0.1 M AgNO ₃	1.07 (1.37)	
4	As in 1	Glassy Carbon	Ag/0.1 M AgNO ₃	0.89 (1.19)	1.34
5	Na salt of 3.06 in 0.1 M LiClO ₄ CH ₃ CN	Pt	Ag/0.1 M AgNO ₃	1.02 (1.32)	
6	1 mM 3.06 in pH 2.3 perchloric acid	Pt	SCE	0.82 (1.12)	
7	1 mM 3.06 in pH 8.4 borate buffer	Pt	SCE	0.83 (1.13)	
8	1 mM 3.06 in pH 7.5 acetate buffer	Pt	SCE	0.84 (1.14)	

Trifluoroacetate shows bands at 1718 and 1710 cm^{-1} and trifluoroacetic acid has a band at 1792 cm^{-1} . Trifluoromethanesulfonate shows a broad weak band about 1640 cm^{-1} . Addition of 2,6-di-*t*-butylpyridine to a solution of the amino acid gives an IR spectrum very similar to the IR spectrum obtained with just the amino acid. The free pyridine base shows a sharp band at 1577 cm^{-1} and its conjugate acid shows a peak at 1620 cm^{-1} . An IR spectrum of the sodium salt of the amino acid shows one broad peak at 1635 cm^{-1} . These results, which are summarized in Table 3.2, clearly show that in acetonitrile solution 0.1 M in LiClO_4 the amino acid is present primarily as the zwitterion 3.06b as shown.



3.06b

Addition of acid protonates the carboxylate to form the carboxylic acid ammonium species. Addition of the pyridine base does not appear to deprotonate the ammonium significantly although a small band with a wavelength of 1635 cm^{-1} does appear as a shoulder on the large band at 1650 cm^{-1} which by analogy with the sodium salt may be some of the carboxylate amine. These results indicate that the

Table 3.2

FTIR DATA		
Solution	Absorptions observed in the carbonyl region cm ⁻¹	Assignment
acetonitrile 3.0 mM 3.06	1630	Carboxylate of 3.06b
0.1 M lithium perchlorate in acetonitrile. 3.9 mM 3.06	1650	Carboxylate of 3.06b
0.1 M lithium perchlorate in acetonitrile. 5.6 mM triflic acid 1.4 mM 3.06	1760, 1740	Carboxylic acid of 3.06d
0.1 M lithium perchlorate in acetonitrile. 6.1 mM base (1) 2.1 mM 3.06	1650 1635 shoulder	Carboxylate of 3.06b Carboxylate of 3.06c
0.1 M lithium perchlorate in acetonitrile. 1.8 mM Na salt 3.06	1635	Carboxylate of 3.06c
acetonitrile 1 mM methionine	1632	Carboxylate of zwitterion
0.1 M lithium perchlorate in acetonitrile 1 mM methionine (2)	1657	Carboxylate of zwitterion

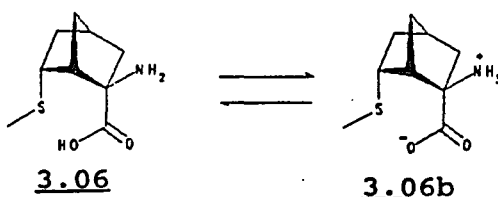
Table 3.2 continued

0.1 M lithium perchlorate in acetonitrile. 3.9 mM trifluoroacetic acid 3.1 mM methionine	1756	Carboxylic acid
0.1 M lithium perchlorate in acetonitrile. 6.1 mM base (1) 1 mM methionine (2)	1657	Carboxylate of zwitterion
0.1 M lithium perchlorate in acetonitrile. 3.9 mM trifluoroacetic acid	1792	Carboxylic acid of TFA
0.1 M lithium perchlorate in acetonitrile. 3.9 mM trifluoroacetic acid 6.1 mM Base (1)	1718	Carboxylate of TFA
(1) Base = 2,6-di-t-butylpyridine		
(2) methionine is only slightly soluble in acetonitrile		

zwitterion is the major species present in neutral solution. With the base 2,6-di-*t*-butylpyridine present the zwitterion is still the major species but there may be a small amount of carboxylate-amine. With acid present the carboxylic acid-ammonium form predominates. The fourth species, the amine carboxylic acid, is never seen. The results with methionine support the results for the amino acid. Addition of 2,6-di-*t*-butylpyridinium trifluoromethanesulfonate to a solution of the amino acid results in the decrease of the carboxylate peak at 1650 cm^{-1} and a build-up of the two carboxyl peaks at 1760 and 1740 cm^{-1} and a peak at 1577 cm^{-1} which appears to be associated with the free base. If an excess of the pyridinium salt is added one begins to see a peak at 1620 cm^{-1} , due to the pyridinium salt, build up. It is uncertain whether all of the carboxylate is converted to carboxylic acid because of the broad band which occurs for the trifluoromethanesulfonate at 1640 cm^{-1} . These results indicate that the carboxylate is actually a better base than the pyridine and will deprotonate the pyridinium ion under these conditions, a surprising result considering the measured pK_a of 2.6 for 3.06. Excess acid present in the sample of the pyridinium trifluoromethanesulfonate could be responsible for these results but titration of the pyridinium salt against standardized sodium hydroxide

actually showed a slight excess of base. This may help explain the electrochemical result in that one sees the pyridinium salt acting as a weak acid.

To understand the FTIR results it is necessary to consider the various ionic forms which might be present in solution. The amino acid in 0.1 M LiClO_4 in acetonitrile can exist as both a neutral and a zwitterionic species as shown. If one adds a base such as 2,6-di-*t*-butyl pyridine

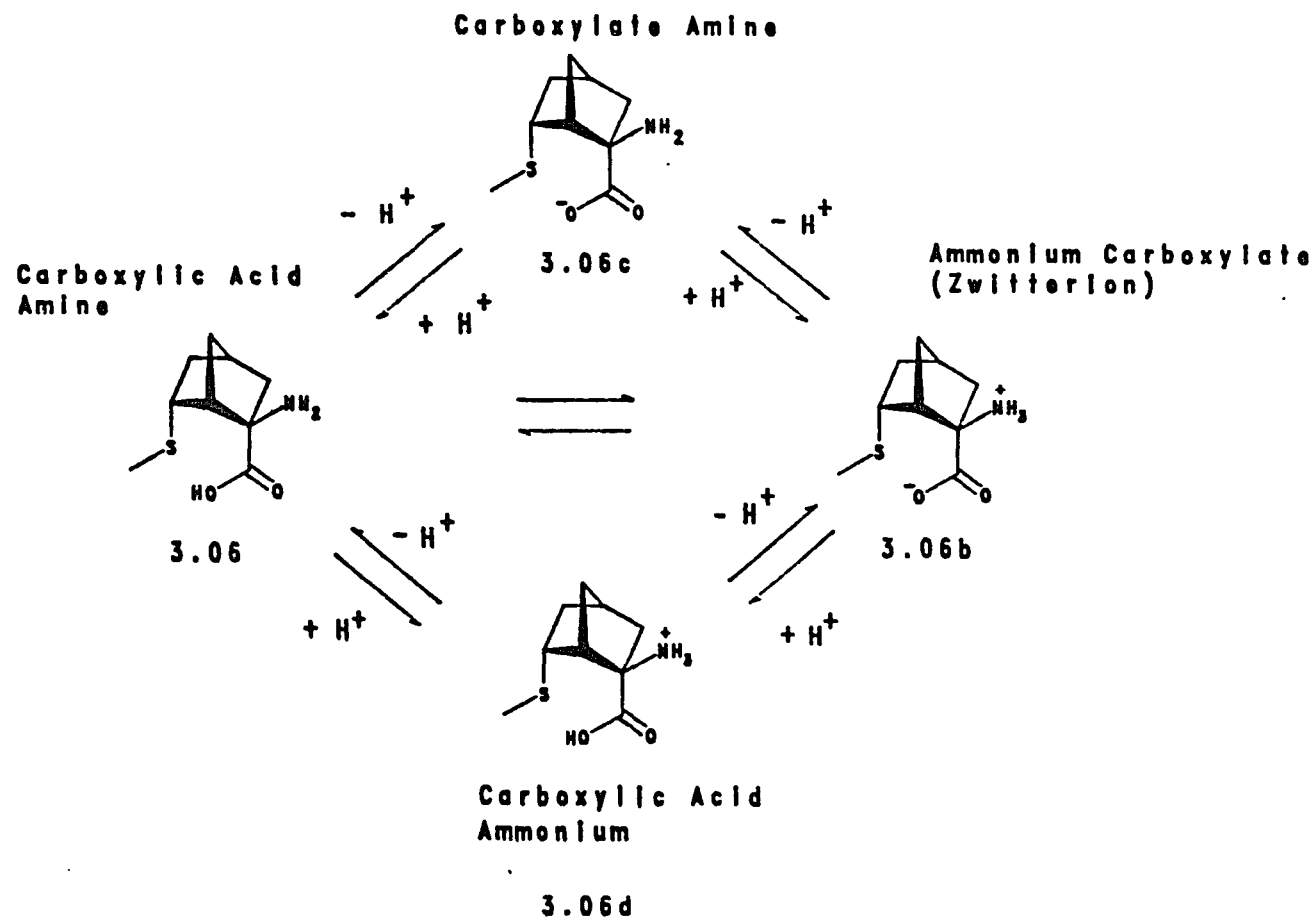


it could in principle deprotonate either of the species shown. The pK_b of the 2,6-di-*t*-butylpyridine is very solvent dependent ranging from 9 in pure water to as high as 11.8 in 90% methanol-water. In acetonitrile it is likely to be closer to the methanol-water value than the value for pure water. The pK_b of 3.06b, *i.e.* formation of the carboxylate amine as shown in figure 3.14 this corresponds to going from 3.06b to 3.06c, was determined to be 9.3. It is expected that the pyridine will deprotonate the carboxylic acid in acetonitrile but the IR spectra indicated it does not deprotonate the ammonium. Addition of acid would result in protonation of the amine and possibly

protonation of the carboxylate (3.06b --> 3.06d) depending on the concentration of acid and the pKa of the 3.06 which was determined to be 2.4. The overall equilibria are illustrated in one diagram, Figure 3.14.

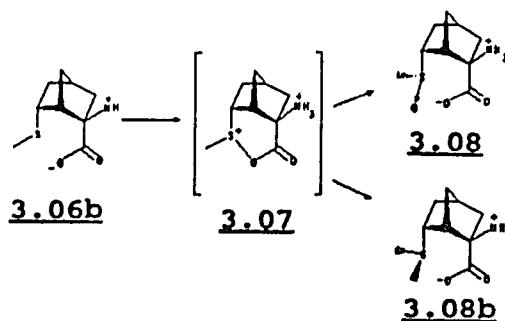
With the knowledge obtained from the FTIR experiments it is now possible to understand the electrochemical results. The first wave is the oxidation of the carboxylate-ammonium form, or zwitterion 3.06b, and the second is the carboxylic acid-ammonium species (3.06d). The IR studies indicate that only the zwitterion 3.06b is present in the electrochemical solution at the beginning. Where does the carboxylic acid ammonium 3.06d, which is oxidized at the second peak, come from? The key is that initial oxidation releases protons (i.e. formation of the sulfoxide by reaction of the acyloxysulfonium salt with water; see the following section) resulting in the protonation of the incoming amino acid which is then oxidized at 1.35 V. This is compatible with the results where base is added since the base would neutralize any protons formed. Only one peak is observed for the oxidation of the carboxylate-ammonium species which may be slightly harder to oxidize possibly due to hydrogen bonding between the base and the ammonium. In other words, even though the base is not strong enough to deprotonate the ammonium but

Figure 3.14
Acid-base equilibria of 3.06



it certainly could form a hydrogen bond which would decrease the electron-withdrawing character of the ammonium and subsequently destabilize the sulfur-oxygen bond. At the same time this interaction would increase the nucleophilicity of the carboxylate. The cyclic voltammetry of the sodium salt supports the analysis since it is indeed harder to oxidize the amine carboxylate. However, the presence of a large excess of lithium cation in solution may affect the results obtained.

The rotating disk electrode experiments help confirm the protonation idea. Initial oxidation is immediately followed by a second oxidation to form acyloxysulfonium salt



3.07 which is then attacked by residual water to form diastereomeric sulfoxides 3.08 and 3.08b and two protons (further evidence for this reaction sequence will be presented in the controlled potential electrolysis section

to follow). The two protons produced for each 3.06b oxidized will protonate 3.06b diffusing toward the electrode to form the harder to oxidize 3.06d. Thus an "n" value for the first wave of only 0.67 is expected (*i.e.* 1/3 of the total 2 electron current needed to oxidize all of 3.06b to the sulfoxide. The other two thirds of the diffusing substrate will be protonated and will not oxidize at the applied potential). The actual value of 1.1 indicates that some of the protons escape from the reaction layer allowing for more oxidation at the lower potential. The broad flat nature of the first oxidation in the cyclic voltammogram may be caused by the establishment of an equilibrium between protonation and escape from the reaction layer. The ratio of the peak currents in the differential pulse polarography is 0.26, a low value but much closer to the theoretical 0.33.

The cyclic voltammetry in aqueous pH 2.3 perchloric acid solution shows one observable wave at approximately 0.8 V versus Ag/AgNO₃, which is attributable to the oxidation of the ammonium-carboxylate 3.06b. At pH 2.3, which is near the pK_a of 3.06, both protonated and unprotonated carboxyl and completely protonated ammonium will be present. There is probably an oxidation wave at higher potential but the anodic solvent limit is reached before a second wave is

observed. The oxidation waves seen in the mildly basic borate and acetate solutions can also be attributed to oxidation of the ammonium-carboxylate 3.06b.

Because of the possibility that the lower oxidation peak was due to bromine redox catalysis^{28,34}, a number of experiments were carried out. A sample of the amino acid was submitted for neutron activation analysis. The sample and a blank were irradiated for 3 hours in a TRIGA reactor³⁵ at 100kW with a neutron flux of 3.6×10^{11} n/cm² s and the samples were counted the next day for 4800 s. The results showed that 3.3 ppm bromine was present in the sample. It was not clear whether or not this was a sufficient amount of bromine to facilitate the electrocatalysis seen for other similar endo norbornane derivatives. If silver nitrate is added to a solution of the amino acid to precipitate the bromide as silver bromide there is no effect on the resulting cyclic voltammogram. By calculating the amount of silver nitrate added and taking into consideration the K_{sp} of silver bromide (using the value for water, and assuming it will be nearly the same or greater in acetonitrile) the bromide ion concentration in solution should have decreased by a factor of 350 or more. More convincingly, if lithium bromide is added directly to a solution of the amino acid so that there is a 0.07:1

bromide/substrate ratio on a molar basis one does not see any significant effect on the cyclic voltammogram. Increasing the concentration to a ratio of about 0.33:1 results in a distorted cyclic voltammogram which still has the two oxidation peaks and a small peak perhaps due to bromide oxidation at about 0.7. If a slight molar excess of bromide ion is present only the oxidation of bromide at about 0.6 V is observed which indicates that bromide catalysis does occur after one mole equivalent of bromine is added. If base is present with no bromide, then one again sees only one peak for just the amino acid at about 1.1 V. Addition of lithium bromide to make the concentration of bromide as high as 0.9:1 bromide/substrate results in a cyclic voltammogram which shows simply a bromide oxidation at about 0.6 V and the sulfur species oxidation at about 1.1 V although both waves are very broad. If an excess of bromide is present a bromide oxidation wave is observed at 0.6 V but no clear wave at 1.1 V. These data indicate that the amino acid can be oxidized by bromine species formed electrochemically but there is some complexation with the bromide added so that one needs to add a slightly more than 1:1 ratio of bromide to see the catalysis. Figures 3.15 and 3.16 illustrate the effect of bromide on the cyclic voltammetry of 3.06.

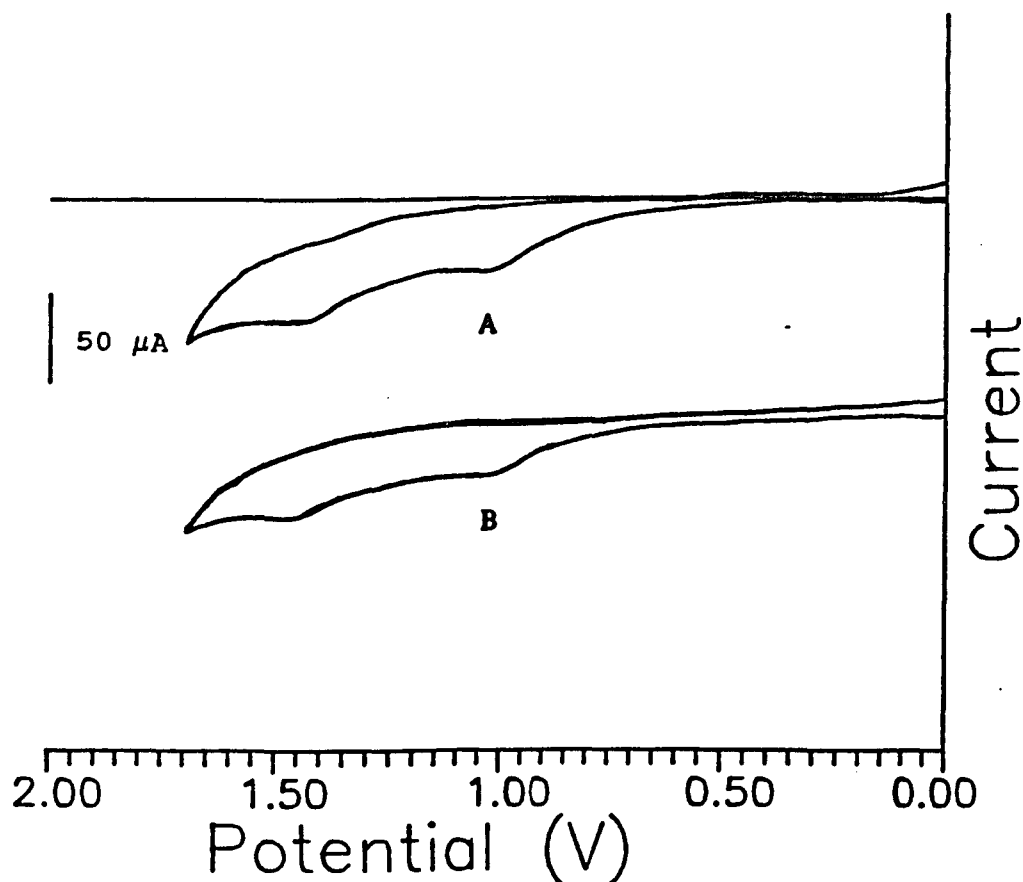


Figure 3.15. Effect of Addition of Bromide.

A. Cyclic voltammogram of 1.1 mM 3.06 in 0.1 M LiClO_4 acetonitrile solution. 5.6 mM 2,6-di-*t*-butylpyridine. Pt working electrode ($A = 0.4 \text{ cm}^2$), Pt counter electrode, Ag/0.1 M AgNO_3 in acetonitrile reference electrode. Scan rate 100 mV/s .

B. Cyclic voltammogram of 1.1 mM 3.06 plus 0.07:1 LiBr in 0.1 M LiClO_4 acetonitrile solution. 5.6 mM in 2,6-di-*t*-butylpyridine. Pt working electrode ($A = 0.4 \text{ cm}^2$), Pt

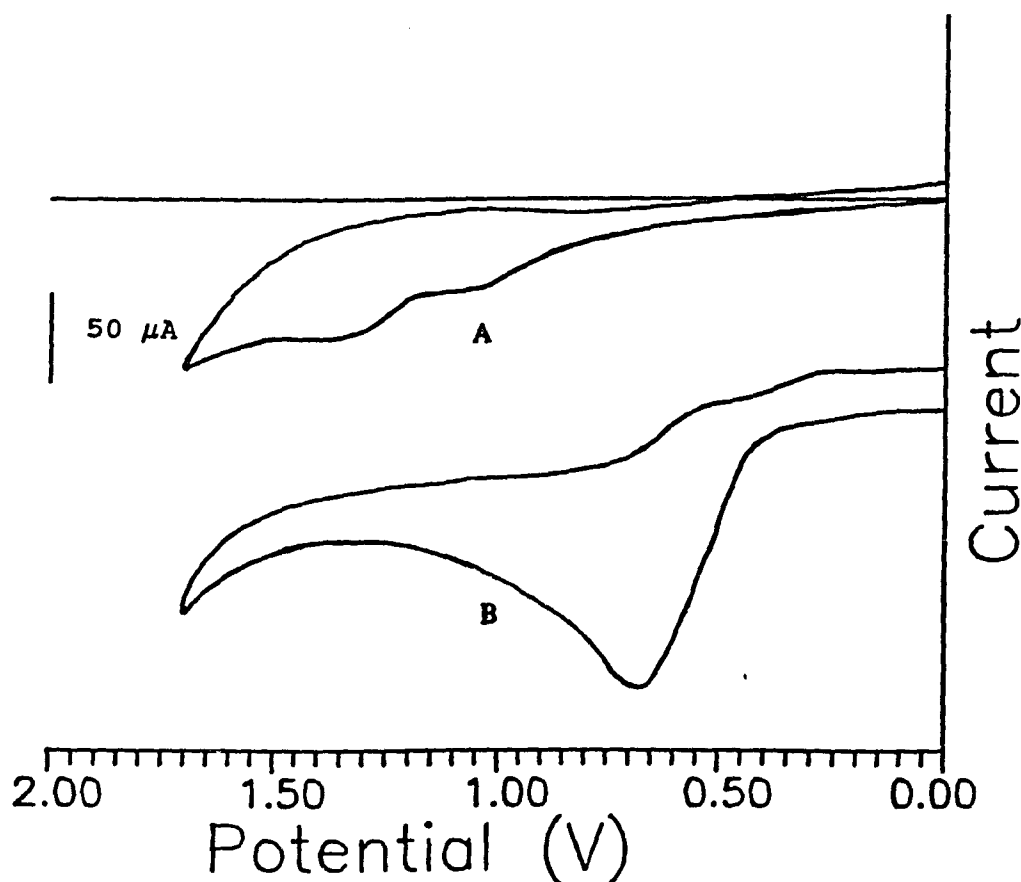


Figure 3.16. Effect of Addition of Bromide Continued.

A. Cyclic voltammogram of 1.1 mM 3.06 plus 0.33:1 LiBr in 0.1 M LiClO_4 acetonitrile solution. 5.6 mM 2,6-di-*t*-butylpyridine. Pt working electrode ($A = 0.4 \text{ cm}^2$), Pt counter electrode, Ag/0.1 M AgNO_3 in acetonitrile reference electrode. Scan rate 100 mV/s.

B. Cyclic voltammogram of 1.1 mM 3.06 plus 1.1:1 LiBr in 0.1 M LiClO_4 acetonitrile solution. 5.6 mM 2,6-di-*t*-butylpyridine. Pt working electrode ($A = 0.4 \text{ cm}^2$), Pt

What factors account for the difference in the ease of oxidation of the various species shown in Figure 3.14? Assuming oxidation occurs first at the sulfur one is asking what the likely effect is of the four possible forms (carboxylic acid-amine, carboxylate-amine, carboxylate-ammonium, carboxylic acid-ammonium) on the interaction between the sulfur cation radical which begins to form upon initial oxidation and the neighboring carboxylic acid or carboxylate group. There are two important effects to consider. As the nucleophilicity of the carboxyl group increases a stronger interaction with the developing positive charge on sulfur is expected. Considering that electron withdrawal by induction decreases the nucleophilicity the least nucleophilic moiety would be the carboxylic acid-ammonium, followed by the carboxylic acid-amine. The carboxylate-ammonium or zwitterion species is the next best nucleophile and the carboxylate-amine should be the best nucleophile since the free amine does not have as strong of an electron-withdrawing inductive effect as the ammonium ion. Since the initial stabilized species is likely to contain a 2c,3e bond one also needs to consider the effect that the various groups will have on the stability of this bond. The 2c,3e bond contains an electron in an antibonding orbital, therefore electron-withdrawing

groups will help stabilize the bond. Considering this the carboxylate-amine should be the least stable followed by the carboxylic acid amine and the ammonium carboxylate. The carboxylic acid-ammonium is expected to form the most stable species. However, results obtained on the endo tertiary alcohol 5.02 and on the endo acid 3.01 indicate that the protonated S-O species will be a very strong acid and will rapidly deprotonate to give the unprotonated species.³⁶ These results, coupled with the observation that the endo acid salt of 3.01 shows only a weak neighboring group interaction, indicate that when looking at the carboxylate species both nucleophilicity and stabilization of the S-O bond are important. The zwitterion provides the best balance of these two factors and indeed the experimental evidence support this. There is one important caveat to the argument presented which is illustrated by the broad drawn-out waves seen when the pyridine base is present. The 2,6-di-t-butylpyridine may adsorb on the electrode surface itself or may promote adsorption of the thioether leading in either case to distorted voltammograms.

As evidenced by an over 400 mV cathodic shift in the peak potential for oxidation, amino acid 3.06, which exists primarily as the zwitterion 3.06b in solution, clearly undergoes neighboring group participation in its oxidation.

In comparison with the endo acid 3.01 the stabilizing effect of the ammonium group is apparent, since 3.06b oxidizes at a potential 300 mV lower than 3.01. The only other known systems with sulfur adjacent to another non-sulfur heteroatom with such low oxidation potentials are the endo secondary alcohol discussed in Chapter 5 and the amide of 3.01 which has a reported oxidation potential of 0.85 V³⁷.

Experimental

Reagent grade acetonitrile was heated at reflux for at least 12 hours over P₂O₅ and then distilled from P₂O₅ under a nitrogen atmosphere. LiClO₄ was dried in a vacuum oven overnight at 110 °C. Reagent grade 2,6-di-*t*-butylpyridine, trifluoroacetic acid, and LiBr were used as received from Aldrich Chemical Co. Cyclic voltammetry was performed in a three-necked single-chambered electrochemical cell. The reference electrode, except where noted, was a silver wire suspended in 0.1 M silver nitrate in acetonitrile encased in a glass case with a sintered glass disk used for contact with the bulk solution. The working and counter electrodes were platinum flag electrodes. The working electrode area was 0.3 cm² and the counter electrode was slightly larger. Argon or nitrogen was bubbled through the cell for approximately 10 minutes before recording the cyclic

voltammetry curves. Between each cyclic voltammogram the counter and working electrodes were cleaned by rinsing them in nitric acid, distilled water and then heating to incandescence in a flame. Solutions were prepared by weighing out appropriate amounts of the compounds to be studied and adding them directly to the electrochemical solution after running a background curve. Concentrations, scan rate, and other experimental parameters are as indicated on the individual Figures. A PAR model 362 scanning potentiostat equipped with a Houston model 200 X-Y recorder was used to run the cyclic voltammograms. A Cyprus Systems computer electrochemical data acquisition system (Model CYSY-1) was used for some of the work. The FTIR experiments were performed on a Perkin-Elmer model number 1800 FTIR with a 0.1 mm path length cell using appropriate amounts of the compounds investigated to provide 1 mM solutions.

Rotating Disk Electrode (RDE) Voltammetry.

A platinum disk electrode, surface area 0.79 cm^2 , was used as the working electrode and was placed in the center of a three-chambered electrochemical cell with fritted glass disk separators. A platinum counter electrode, surface area $\approx 1 \text{ cm}^2$, was placed in one side compartment and a $\text{Ag}/0.1 \text{ M AgNO}_3$ reference electrode was placed in the other side

compartment. A Pine Instrument Model PIR analytical rotator was used to rotate the working electrode at rotation rates between 400 and 3600 rpm. A PARC model 362 potentiostat was used to sweep the potential at 20 mV/s and the current/voltage response measured on a Houston Model 200 x-y recorder. Solutions of approximately 10^{-3} M in amino acid 3.06 were used.

Differential Pulse Polarography.

Differential Pulse Polarography was performed using the same electrodes, cell and concentration of substrate as for the cyclic voltammetry and the Cypress electrochemical system. The step height was 30 mV, the pulse amplitude was 25 mV and the pulse width 2 ms.

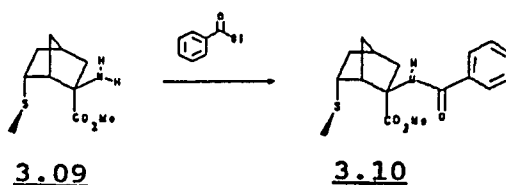
Controlled Potential Electrolysis of 3.06b

Cyclic voltammetry of 3.06b in acetonitrile at a carbon cloth anode in the presence of base and water shows a broad oxidation wave with an oxidation potential of near 1.0 V versus the Ag/0.1M AgNO₃ reference electrode. Controlled potential electrolysis of a millimolar solution of 1 at 1.1 V under similar conditions results in the passage of 1.9 equivalents of charge. This corresponds to an "n" value of 2. The major product formed is sulfoxide 3.08b. The

product was identified by comparison of NMR and IR spectra with those of authentic sulfoxide prepared by chemical oxidation of 3.06b. Since the ^1H NMR spectrum of 3.08b was pH dependent and also changed by the presence of the supporting electrolyte, lithium perchlorate, the NMR studies on 3.08b prepared chemically were performed under identical conditions as the NMR spectrum of 3.08b prepared electrochemically. This was accomplished by adding a known amount of 3.08b prepared chemically to an NMR tube containing 3.08b prepared electrochemically and observing the spectra obtained to determine if new peaks were present or if the peaks already present grew proportionately to the amount of 3.08b added. Indeed, the latter was the case and it was possible to determine that the yield of 3.08b obtained was about 62% in the initial reaction. There is another set of smaller peaks seen in the NMR spectrum which correspond to the other diastereomer of 2 that is formed in the electrochemical reaction with a yield of 25-30%. The ratio of diastereomers is approximately 70/30 and is similar to that found³⁸ in the oxidation of endo acid 3.01.

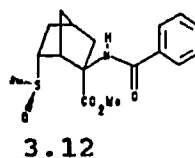
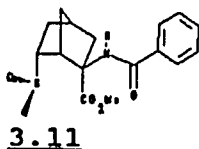
To confirm the analysis based on the ^1H NMR spectrum of the crude reaction mixture and to provide authentic samples of the separated diastereomeric sulfoxides it was decided to synthesize easily characterized derivatives of the amino

acid sulfoxide. These derivatives could then be compared to derivatives obtained from the initial electrochemical mixture. Amino ester 3.09 was converted into amide 3.10 by benzoylation as shown.



Amide 3.10 was then converted into sulfoxides 3.11 and 3.12 by oxidation with NaIO₄ in methanol with 3.11 predominating by about 10:1. Pure, crystalline 3.11 was isolated by recrystallization of this mixture and a small amount of 3.12 has been isolated and is pure by ¹H NMR spectroscopic analysis. The relative stereochemistry was determined by analogy with the oxidation done on endo acid 3.01³⁶ and its ester. Oxidation of 3.10 with DABCO•2Br₂ gives an approximately 60/40 ratio of 3.12/3.11 from which after repeated HPLC a small amount of pure 3.12 as determined by ¹H NMR spectroscopic analysis was isolated.

Cyclic voltammetry of 3.06 in pH 8.4 aqueous borate buffer solution showed an oxidation wave at 1.13 V versus the SCE at a glassy carbon electrode (this corresponds to



about 0.83 V versus Ag/0.1 M AgNO₃ in acetonitrile). Controlled potential electrolysis in the borate solution resulted in the formation of a sulfoxide as indicated by the presence of an S-Methyl peak at 2.5 ppm in the ¹H NMR spectrum. The prominent sulfoxide peak in the IR spectrum was obscured by large absorptions due to borate. However, the sulfoxide formed was not 3.08b as determined by ¹H NMR spectroscopy but instead possibly a borate ester (carbonyl peak at 1736 cm⁻¹ in the IR). Addition of authentic 3.08b to the borate buffer followed by lyophilization as was done in the electrolysis left 3.08b unreacted, suggesting that the new compound formed is formed during the electrochemical reaction, possibly by interception of the acyloxysulfonium salt by borate.

Cyclic voltammetry of 3.06b in acetate buffer solution resulted in a voltammogram with an E_p of 1.14 V versus the SCE reference electrode. Controlled potential electrolysis of 3.06 in 0.1 M sodium acetate with acetic acid added to adjust the pH to 7.5 resulted in the formation of sulfoxide

3.08 in 73% yield as determined by ^1H NMR spectroscopic analysis. The species observed was actually the sodium salt of 3.08b as determined by adding sodium acetate to a D_2O solution of 3.08b and observing the ^1H NMR spectrum which was identical with that of the observed product. Also, as was done in the acetonitrile electrolysis, addition of authentic sulfoxide 3.08b to the electrochemical product confirmed the formation of sulfoxide which gave a similar 71% yield. The integration in the ^1H NMR spectrum indicated that only 10% of the minor diastereomer formed.

Clearly controlled potential electrolysis under a variety of conditions at peak potentials indicative of neighboring group effects leads to the formation of sulfoxide as the major product, a formal two-electron oxidation overall at sulfur. This is in contrast to the preferred single-electron decarboxylation process seen in the pulse radiolysis (vide supra).

Experimental

All melting points are uncorrected and were taken in open-ended glass capillary tubes using a Thomas-Hoover melting point apparatus. IR spectra were obtained on a Perkin-Elmer Model 983 spectrometer. ^1H NMR spectra were measured at 250 MHz using a Bruker WM-250 spectrometer on samples containing an internal standard: tetramethylsilane

in deuteriochloroform. HPLC was performed with an Altex/Beckman 110b pump equipped with a preparative pump head. An Altex Ultrasil-ODS 10mm X 250mm reverse phase and Phenomenex Maxisil 10mm X 250 mm normal phase 10 μ m particle size columns were used. An ISCO V⁴ absorbance detector along with a Linear model 0555 strip chart recorder were used to monitor the HPLC.

Chemical oxidation of 3.06b.

To a suspension of 3.06b (50 mg, 0.25 mmol) in chilled (10 °C) acetic acid in a 25 mL round bottom flask was added dropwise 30% hydrogen peroxide (300 μ L, 0.265 mmol) with a syringe. The suspended 3.06b dissolved forming a peach colored solution. The solution was stirred for three hours and allowed to warm to room temperature. The acetic acid was stripped off by rotary evaporation and the solid obtained was dissolved in water (2 mL). Acetone was then added resulting in the formation of a white precipitate. The product was filtered and by ¹H NMR spectroscopic analysis in D₂O shown to be the sulfoxide along with acetic acid. The product was recrystallized from hot ethanol to yield pure 3.08b (39mg, 75% yield): mp 258-260 °C d; ¹H NMR(D₂O, 250 MHz) δ 3.01(ddd, 1, $J=15, 10, 5$ Hz), 2.71(br s, 1, bridgehead H), 2.52(s, 3, S-Me), 2.43(br s, 1,

bridgehead H), 2.20(dd, 1, $J=20, 10$ Hz), 1.92(ddd, 1, $J=20, 5, 5$ Hz), 1.75(dd, 1, $J=15, 4$ Hz), 1.54(m, 2), 1.41(ddd, 1, $J=15, 10, 4$ Hz). IR (KBr): 3100-2300 (ammonium), 1597(carboxylate), 1537(ammonium), 981 cm^{-1} (sulfoxide); MS m/z 217 (M^+ , 0.2%), 172($M-\text{CO}_2\text{H}$, 1.8%), 154($M-\text{CO}_2\text{H}, \text{H}_2\text{O}$, 33%).

Controlled Potential Electrolysis of 3.06b in Acetonitrile.

A three-chambered electrochemical cell was fitted with a platinum counter electrode (surface area approximately 1 cm^2) in one side compartment, a carbon cloth working electrode (nominal surface area of 0.5 cm^2) in the center compartment, and a Ag/0.1M AgNO_3 in acetonitrile reference electrode in the other side compartment. The center chamber was filled with 15 mL acetonitrile 0.1 M LiClO_4 solution and the side chambers filled to the same height as the center chamber. Argon was bubbled through the solution for 1/2 hour and then 2,6-di-*t*-butylpyridine (44 μL , 0.2 mmol) and water (10 μL , 0.5 mmol) were added. A sample of 3.06b (21 mg, 0.1 mmol) was added and the potential set to 1.1 V with the cell electrically disconnected. The coulometer was zeroed and the cell connected. Current immediately began to flow and after 19.2 coulombs of charge had passed the current had decayed to zero. This corresponds to an "n" value of 1.91. Distilled water (2 mL) was added to the

solution and the acetonitrile removed by rotary evaporation. The aqueous solution was then purified by applying 200 μ L samples to a reverse phase semipreparative C-18 column HPLC system using isocratic elution with 30% aqueous acetonitrile at a flow rate of 4.4 mL/min. Four fractions were collected. No discernible products were obtained from the first and fourth fractions in order of elution. The second fraction contained 22 mg of an off-white solid which by ^1H NMR spectroscopic analysis had significant amounts of 3.08 present. The third fraction was mostly supporting electrolyte. Addition of a known amount of authentic 3.08b prepared chemically (see above) to fraction two resulted in an NMR spectrum qualitatively similar to that obtained before addition of 3.08b but with the height of a number of peaks enhanced. By measuring the increase in area due to the S-methyl peak it was determined that 3.08b formed with a yield of 62%. If the singlet at 2.38 is due to the other diastereomer (3.08) then its yield is about 25-30%. An IR spectrum of fraction two showed the broad ammonium peak, the carboxylate peaks and a peak at 991 cm^{-1} for the sulfoxide but there was also a large peak at 1100 cm^{-1} attributable to some residual perchlorate left over from the supporting electrolyte. There was no indication of starting material in this run although on earlier attempts at this reaction

when the n value was lower a singlet possibly corresponding to starting material was seen at δ 1.82.

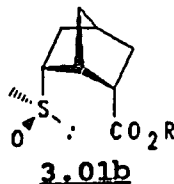
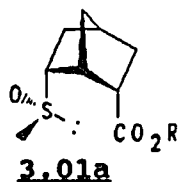
The electrochemical oxidation was repeated on 3.06b (30 mg, 0.15 mmol) under conditions identical to those above. Analysis of the crude ^1H NMR again showed formation of the sulfoxides with a yield of 61% for the major diastereomer and 22-28% of the minor (in the crude spectrum there is some overlap of a peak from the norbornyl ring of the major diastereomer with the S-methyl peak of the minor, leading to some error in measuring the amount of minor diastereomer formed). This product mixture was applied to a semipreparative C-18 HPLC column as indicated above and the appropriate fraction collected. The supporting electrolyte was removed by this HPLC but the diastereomer ratio was similar to that observed for the crude reaction mixture.

The mixture of diastereomers (approximately 32 mg, 0.12 mmol) was dissolved in a minimal amount of 3 M sodium hydroxide solution. The solution was cooled to $-5\text{ }^\circ\text{C}$ in an ice/salt water bath and the pH periodically checked to keep it between pH 9 and 11. Benzoyl chloride (32 μL , 0.27 mmol) was added slowly in 10 μL portions with vigorous shaking after each addition over about 40 min. The solution was kept immersed in the ice bath as much as possible. After stirring for an hour the solution was allowed to stir at RT

overnight. The solution was filtered to remove a white precipitate that had formed and then made acidic using 4 M hydrochloric acid and extracted with ethyl acetate. A white solid was obtained after removal of the ethyl acetate by rotary evaporation. A weight was not obtained on this solid.

The solid obtained was dissolved in chloroform and cooled to -76°C in a dry ice/acetone bath. A solution of light yellow diazomethane in ether was added dropwise while cooling. Addition of diazomethane was halted when the yellow color persisted for more than one minute. Evaporation of the solvent gave a white solid (13 mg, yield based on starting amino acid 3.06b = 24%) whose ^1H NMR spectrum showed the presence of protected amino acid sulfoxides 3.11 and 3.12 in a ratio of 68:32 based on the S-methyl peaks or 71:29 based on the aromatic peaks at δ 7.71 and 7.82.

The diastereomer assignments were based on comparison with the endo acid sulfoxides and endo methyl ester sulfoxides formed from oxidation of 3.01 and its methyl



ester. Electrochemical oxidation of 3.01 leads to formation of a 3:2 ratio of sulfoxides 3.01a and 3.01b. The S-methyl protons show singlets at δ 2.8 and 2.6 respectively for these diastereomers in deuteriochloroform. Considering the relative positions of the S-methyl groups seen in the endo sulfoxides 3.01a and 3.01b the major product sulfoxide formed in the electrochemical oxidation of 3.06b which shows singlets at δ 2.55 and 2.4 in deuterated water was assigned the structure shown in 3.08b. The shift to lower ppm is ascribable to the presence of the shielding carboxylate ion. The diastereomeric assignments are further confirmed by comparing the methyl esters formed upon esterification of 3.01a and 3.01b which show S-methyl peaks at δ 2.62 and 2.45 respectively which compares with the S-methyl peaks shown for the endo methyl ester exo benzoyl derivatives 3.11 and 3.12 of δ 2.62 and 2.44. Also, for the endo esters of 3.01a and 3.01b the C-1 bridgehead proton is at δ 2.85 and 3.24 respectively. A large shift due to the anisotropic effect of the sulfoxide is evident. The protected amino acid esters 3.11 and 3.12 have C-1 bridgehead resonances at δ 2.75 and 3.29 respectively which again confirms the diastereomer assignment.

Controlled Potential Electrolysis of 3.06b in pH 7.8 Acetate

Buffer.

A sample of 3.06b (22 mg, 0.11 mmol) was dissolved in pH 8.3 sodium acetate solution in the center compartment of a three-chambered electrochemical cell. A carbon cloth working electrode was placed in the center compartment. A Pt counter and an SCE reference electrode were placed in the two side compartments. A cyclic voltammogram run on the solution before starting the electrolysis showed one peak with a peak potential of 1.14. After zeroing the coulometer the potential was set at 1.18 V and the cell connected. Since the cyclic voltammogram showed considerable background current at this potential the current was allowed to flow until 2.5 equivalents of charge had passed to facilitate complete oxidation. When the electrolysis was complete the pH was 7.8. A cyclic voltammogram run after the electrolysis showed only background current. The reaction mixture was put into a 25 mL round bottom flask and the carbon cloth electrode ground up and triturated with distilled water which was added to the reaction mixture. The water was lyophilized off to yield a white solid. A ^1H NMR spectrum of the crude mixture revealed a 72% yield of major diastereomer sulfoxide. Addition of authentic sulfoxide 3.08b prepared chemically indicated a yield of 74%. The ^1H NMR spectrum of pure chemically prepared 3.08b

in D₂O was not identical to that obtained but upon adding a small amount of sodium acetate an identical ¹H NMR spectrum was obtained. The other diastereomer was present in only 10-12% yield.

Synthesis of Protected Amino Acid 3.10.

Amino ester 3.09 (75 mg, 0.34 mmol) was dissolved in 0.5 mL acetonitrile and cooled to -5 °C in an ice bath. Saturated aqueous sodium bicarbonate solution (1 mL) was added to keep the pH basic. Benzoyl chloride (80 µL, 0.66 mmol) was added slowly with rapid stirring over 30 min. The solution was allowed to stir overnight at room temperature. Water (5 mL) was then added and the acetonitrile removed by rotary evaporation. The aqueous solution was then extracted with ethyl acetate (3X20 mL) with the final extraction done on a sodium chloride saturated solution. Evaporation of the solvent gave a white solid which upon purification by preparative TLC on silica gel (50% EtOAc in hexanes, R_f 0.6) gave pure 3.10 with a yield of 60%: mp 120-122 °C; ¹H NMR(250MHz)δ 7.7 (dd, 2, o-ArH, J=5.8, 1.2 Hz), 7.4 (m, 3, m, p ArH) 3.73 (s, 3, methoxy), 3.06 (ddd, 1, R₂CHS, J = 15.1, 11.1, 17.4 Hz) 2.80 (dd, 1, J = 13.6, 2.9 Hz), 2.66 (br s, 1, bridgehead) 2.44(br s, 1, bridgehead), 2.15 (m, 2), 2.04 (s, 3, S-Me),

2.02 (m, 1), 1.93(ddd, 1, $J = 11.3, 9.4, 1.2$ Hz), 1.12 (ddd, 1, $J=10.6, 5.4, 3.1$ Hz); IR (KBr) 3378 (NH), 1725 (CO₂Me), 1649, 1520 cm⁻¹; MS m/z 319 (M⁺, 10.4%).

Oxidation of 3.10 by Sodium Metaperiodate.

A sample of 3.10 (30 mg, 0.09 mmol) was dissolved in methanol (0.5 mL) and cooled in an ice bath to -5° C. Sodium metaperiodate (72mg, 0.34 mmol) was dissolved in a minimum amount of water and methanol (0.5 mL) was added. The sodium metaperiodate solution was then added to the first solution over about 10 min. The solution was allowed to warm to room temperature and left stirring overnight. A white precipitate was filtered off and after saturating with sodium chloride the solution was extracted with ethyl acetate (3X20 mL). ¹H NMR spectroscopic analysis of the crude showed the presence of a sulfoxide methyl at δ 2.62 and a small sulfoxide methyl at δ 2.44 in an ~ 10:1 ratio. Preparative HPLC (20% methanol in ethyl acetate, C18 column, 4.4 mL/min flow rate) gave three fractions. Fraction one contained a small amount of starting material. Fraction two contained mostly one diastereomer of the sulfoxide and fraction three contained a mixture of sulfoxides, still dominated by the sulfoxide in fraction 2. Vapor diffusion recrystallization of the residue from fraction two with

ethyl ether into methanol gave thin clear needles of major sulfoxide diastereomer 3.11: mp 218-219 °C; ^1H NMR (CDCl_3 , 250MHz) δ 7.69 (d, 2, o-ArH, $J=7.9$, 2.6 Hz), 7.4 (m, 3, m,p ArH), 6.4 (s, 1, amine proton), 3.75 (s, 3, OMe), 3.06 (ddd, 1, $\text{R}_2\text{CHS(O)}$, $J=15.0$, 6.8, 3.4 Hz), 2.89 (dd, 1, $J=13.9$, 2.9 Hz), 2.75 (br s, 1, bridgehead), 2.62 (br s, 4, bridgehead and S(O)Me), 2.23 (m, 1), 2.14 (dd, 1, $J=10.4$, 1.3 Hz), 1.98 (ddd, 1, $J=14.0$, 4.2, 4.2 Hz), 1.81 (ddd, 1, $J=13.4$, 6.9, 2.0 Hz), 1.70 (dd, 1, $J=11.9$ Hz); IR (KBr) cm^{-1} 3378 (NH stretch), 3000 (CH stretch), 1721 (ester carbonyl), 1649 (amide I band) 1523, 1488, 1037 (sulfoxide), 692; MS m/z 335 (M^+ , 0.05%). Anal. Calcd. for $\text{C}_{17}\text{H}_{21}\text{O}_4\text{SN}$: C, 60.88; H, 6.31; N, 4.18. Found: C, 60.81; H, 6.32; N, 4.14.

Oxidation of 3.10 by DABCO \cdot 2Br $_2$

A sample of 3.10 (20 mg, 0.06 mmol) was dissolved in 1.5 mL 80% acetic acid. To the stirred solution was added DABCO \cdot 2Br $_2$ (35 mg, 0.08 mmol) all at once. The complex slowly dissolved and a clear solution was obtained. After stirring for 30 min the bulk of the acetic acid was removed by rotary evaporation to yield a white solid. The solid was triturated with methylene chloride and then the solution obtained was filtered through a fine glass frit. Rotary evaporation of the methylene chloride left a white semisolid

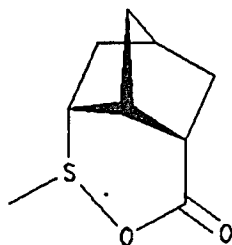
whose ^1H NMR spectrum indicated the presence of the two sulfoxides 3.11 and 3.12 in a ratio of about 40/60 with a yield of 80%. The sample was applied to a silica gel HPLC column eluting with 20% methanol in ethyl acetate at a flow rate of 4.4 mL/min and the fractions enriched in 3.12 were recycled twice to obtain pure 3.12: ^1H NMR (CDCl_3 , 250MHz) δ 7.75 (d, 2, o-ArH), 7.45 (m, 3, m-,p- ArH), 6.75 (s, 1, amine proton), 3.79 (s, 3, OMe), 3.01 (ddd, 1, R_2CHS , \underline{J} =14.0, 6.5, 3.6 Hz), 2.91 (dd, 1, \underline{J} =15.1, 6.1Hz), 2.59(br s, 1, bridgehead), 2.44 (s, 3, SMe), 2.12 (d, 1, ring proton); 1.91(m,2, ring protons); 1.65(br d, 1, \underline{J} =14.3 Hz), 1.25 (m, 2); IR (KBr) cm^{-1} , 3380(NH stretch), 3000(CH stretch), 1725(ester carbonyl), 1640(amide I band), 1045(sulfoxide), 685; MS $\underline{m/z}$ 335(M^+ , 0.04%)

CHAPTER 4
PULSE RADIOLYSIS OF (\pm)-2-EXO-AMINO-6-
ENDO-METHYLTHIOBICYCLO [2.2.1] HEPTANE-2-ENDO-
CARBOXYLIC ACID

Introduction

Pulse radiolysis of simple thioethers leads to the formation of cation radicals of the type $R_2S^{\cdot+}$.³⁹ and the cation radicals formed can be stabilized inter- or intramolecularly by other sulfur atoms as discussed in Chapters 1 and 2. Other heteroatoms, including oxygen⁴⁰, nitrogen⁴¹, and halogens⁴², may also stabilize the radicals formed. Unlike the case where the other heteroatom is a sulfur the bonding interaction is not expected to be symmetrical but instead the excess electron density will be shifted towards the more electronegative atom. Experimental data and theoretical calculations⁴³ indicate that the closer the two heteroatoms are in electronegativity the stronger the 2c3e electron bond should be. Accordingly one would expect S-N interaction to be strong, S-O interaction to be somewhat weaker and S-halogen interaction to increase as one goes from fluorine down to iodine. An entropic advantage, as mentioned in the introduction, can lead to stabilization of even relatively

weak intramolecular interactions. In the case of species such as alcohols and carboxylates one needs to consider the effect of the ionic state and possible conjugation upon the incipient bond.



3.01c

Sulfur carboxylate adducts have been investigated by thermolysis of t-butylperoxy benzoates which have thioether substituents⁴⁴. EPR spectroscopy of the radicals observed indicated formation of a so called 9-S-3 radical involving formation of a three-center three-electron bond as discussed in Chapter 1.⁴²

Carboxylate groups have been shown to be capable of stabilizing sulfur cation radicals formed via pulse radiolysis.⁴⁵ Pulse radiolysis of 3.01 results in the formation of a transient which absorbs in the UV at 390 nm, has a half-life of between 30 and 60 μ sec depending on the pH⁴³ and which has been postulated to be the 2c,3e bonded 3.01c.

By comparing the concentration at which competition to

form an intermolecularly bound 2c,3e species becomes significant it was shown that 3.01a has a much stronger S-O interaction, the bond strength is on the order of 50 kJ/mol which is considerably higher than that found for simple open chain carboxylate-thioethers. The following section will discuss the results obtained upon pulse radiolysis of amino acid 3.06b (at most of the pHs investigated the zwitterion will be the major species present) and compare the results obtained with similar carboxylate-containing species including methionine.

Results and Discussion

The absorption spectrum of a pH 2.6 solution of 3.06b immediately after a pulse shows two absorption maxima, one at 280 nm and a broad one centered about 355 ± 5 nm as seen in Figure 4.1. The short wavelength absorption at 280 nm is presumed to be an α -thioalkyl radical by analogy with numerous other thioether compounds which show similar absorption⁴⁶. The peak at 355 ± 5 nm has a half-life of 29 μ sec and exhibits strict first-order decay as indicated by an excellent fit for a calculated first-order decay curve overlaid on the actual data (Figure 4.2). Also, changing the concentration of radicals by a factor of five by adjusting the initial pulse width had no significant effect on the

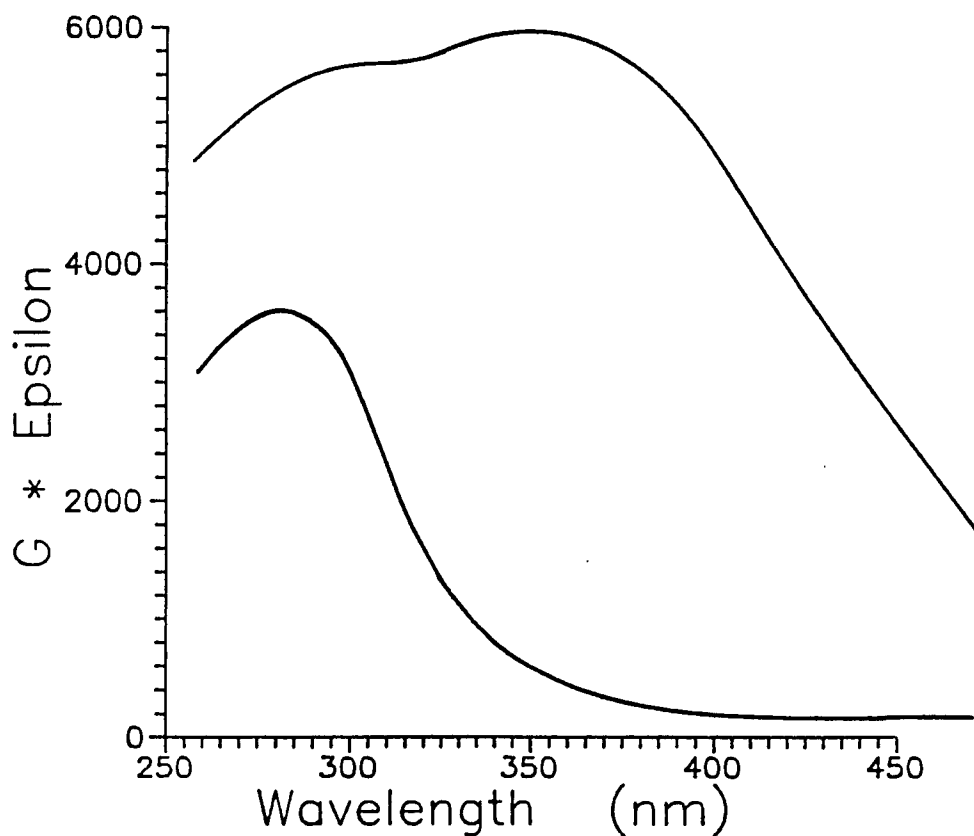


Figure 4.1. Pulse radiolysis of a 0.2 mM solution of 3.06b in N₂O saturated pH 2.6 water. Upper curve: immediately after application of pulse. Lower curve: 300 μ s after application of the pulse. Curves shown are smoothed curves drawn through approximately 20 data points collected between 260 and 500 nm.

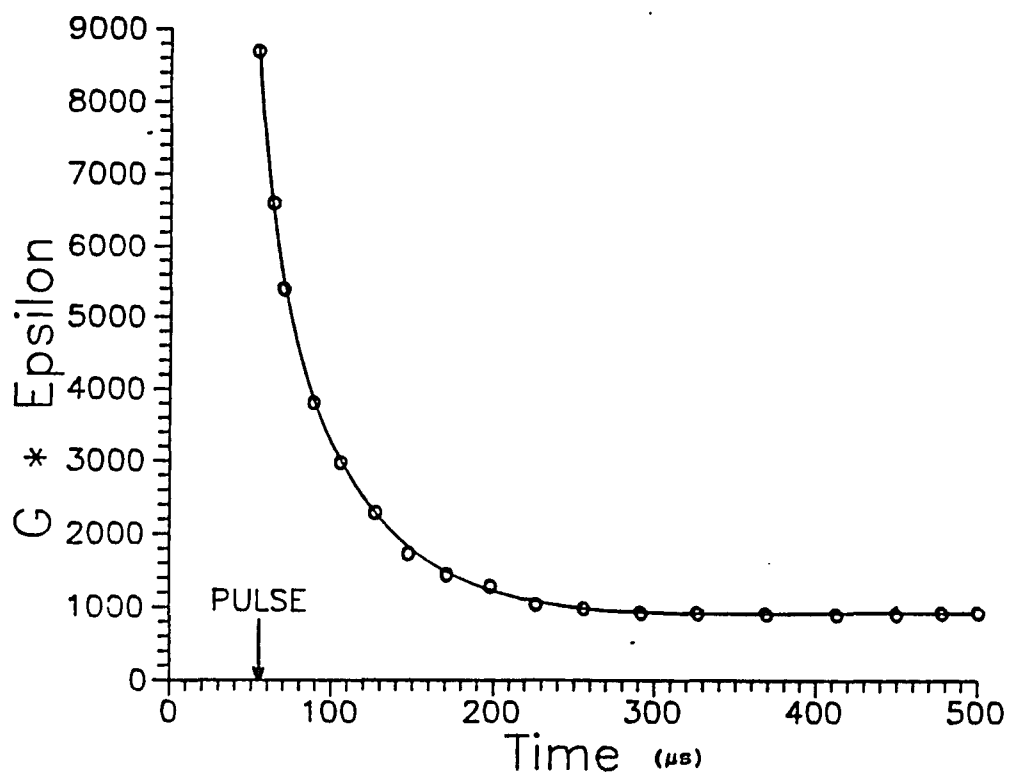
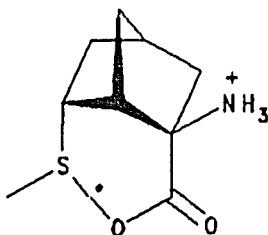


Figure 4.2. Plot of the transient absorption decay for ≈ 0.02 mM 3.06b in N_2O saturated pH 2.6 aqueous solution. Measured at 360 nm. Circles: Experimental data. Curve: 1st order decay fit, $T_{1/2} = 29 \mu s$.

half-life, again indicating a first-order decay. A long wavelength peak usually associated with intermolecular 2c,3e bonded species was not seen at this concentration. The time dependent conductivity (Figure 4.3) shows a net decrease followed by a build up, the half-life of which is close to the half-life decay seen in the absorption spectrum at pH 2.6 where the 355 nm species is the strongest. Given this evidence and evidence from related molecules it is postulated that the species formed is the intramolecularly stabilized radical species 4.01. The exact bonding structure in 4.01 and related molecules⁴⁷ is not known and is shown arbitrarily as a direct sulfur to oxygen bond with the radical in an antibonding orbital formed between the oxygen and sulfur. Experimental and theoretical studies are in progress to help clarify the bonding in such species.



4.01

In the pH 2.6 solution one would expect the amino acid to be present as both the zwitterion and as the cationic species. An initial loss of conductivity would be expected

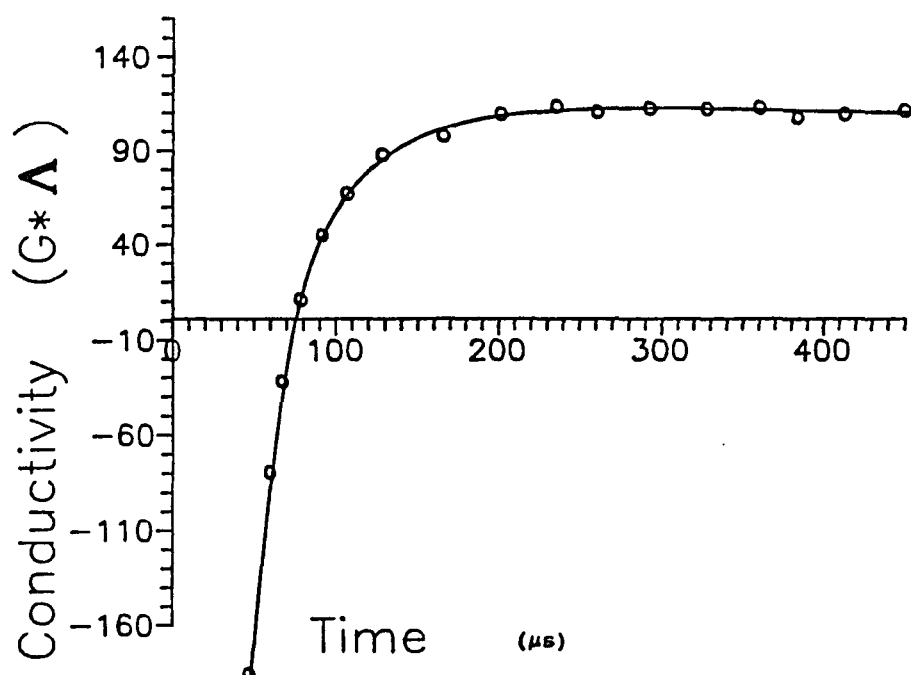


Figure 4.3. Plot of the conductivity signal observed for $\approx 0.02 \text{ mM } 3.06\text{b}$ in N_2O saturated pH 2.6 aqueous solution. Circles: experimental data. Curve: 1st order decay fit, $T_{1/2} = 22 \text{ } \mu\text{s}$.

since the net ionic reaction is the loss of a highly mobile proton and the gain of the less mobile organic ammonium ion. A G value of ≈ 1.6 can be calculated from the conductivity data by assuming a specific conductance of 315 for the proton and ≈ 45 for the organic ion and looking at the largest decrease in conductivity of $G \times \text{Specific Conductance}$ of about -450 ($G = 1.6 = -450 / (315 - 45)$)

The yield of the species which absorbs at 355 nm is dependent on pH. Figures 4.4-4.6 illustrate the effect of pH on the observed absorptions. Table 4.1 summarizes the data. A plot of the yield of adsorbing species expressed as $G \times \epsilon$ versus pH is shown in Figure 4.7. A number of interesting observations can be made by comparing the amino acid with the endo acid 3.01⁴⁸. The one-electron oxidation product of endo acid 3.01 also shows two peaks in its absorption spectrum, one at 280 nm and one at 390 nm. As in the electrochemical oxidation the ammonium group alpha to the carboxylate appears to help stabilize the S-O species thermodynamically by inductively removing electron density. As discussed in Chapter 1 a blue shift in the UV/vis absorption maximum of a 2c,3e species indicates a strengthening of the bond.⁴⁹ Indeed one sees a 30-40 nm blue shift down to 355 ± 5 nm compared to the adduct formed from one-electron oxidation of endo acid 3.01. However the S-O

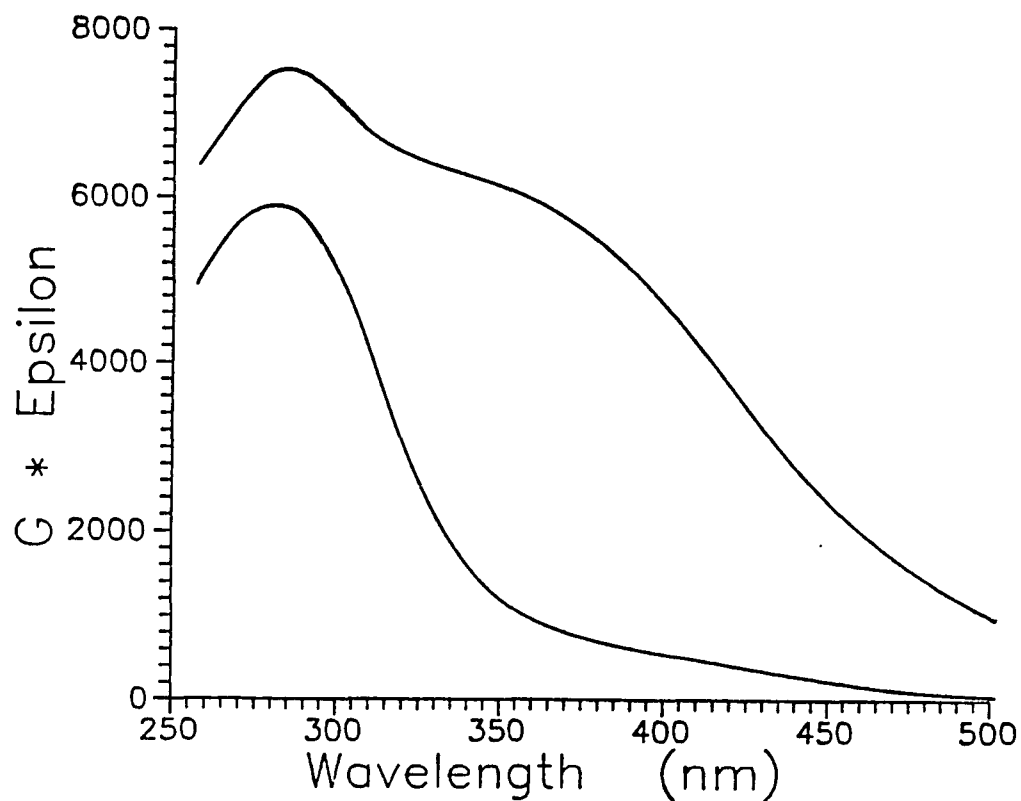


Figure 4.4. Pulse radiolysis of ≈ 0.2 mM 3,06b in N_2O saturated pH 3.1 aqueous solution. Upper curve: immediately after application of pulse. Lower curve: 200 μs after application of the pulse. Curve shown are smoothed curves drawn through approximately 20 data points collected between 260 and 500 nm.

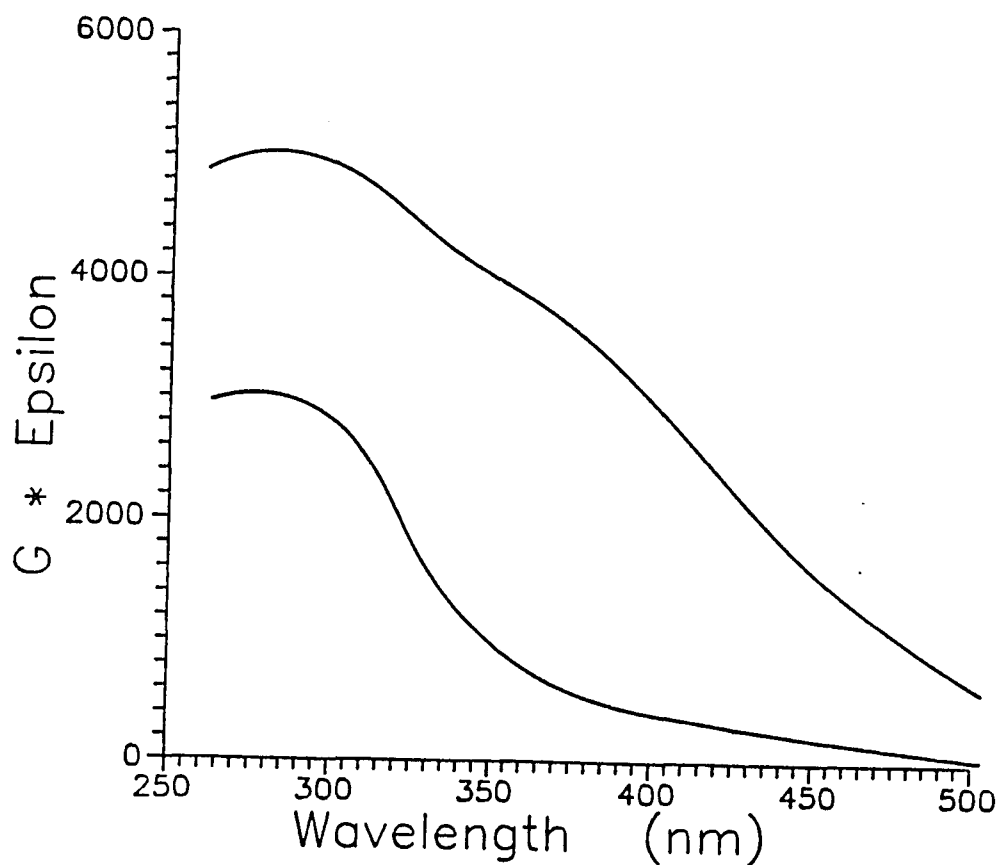


Figure 4.5. Pulse radiolysis of ≈ 0.2 mM 3.06b in N_2O saturated pH 5.5 aqueous solution. Upper curve: immediately after application of pulse. Lower curve: 200 μs after application of the pulse. Curve shown are smoothed curves drawn through approximately 20 data points collected between 260 and 500 nm.

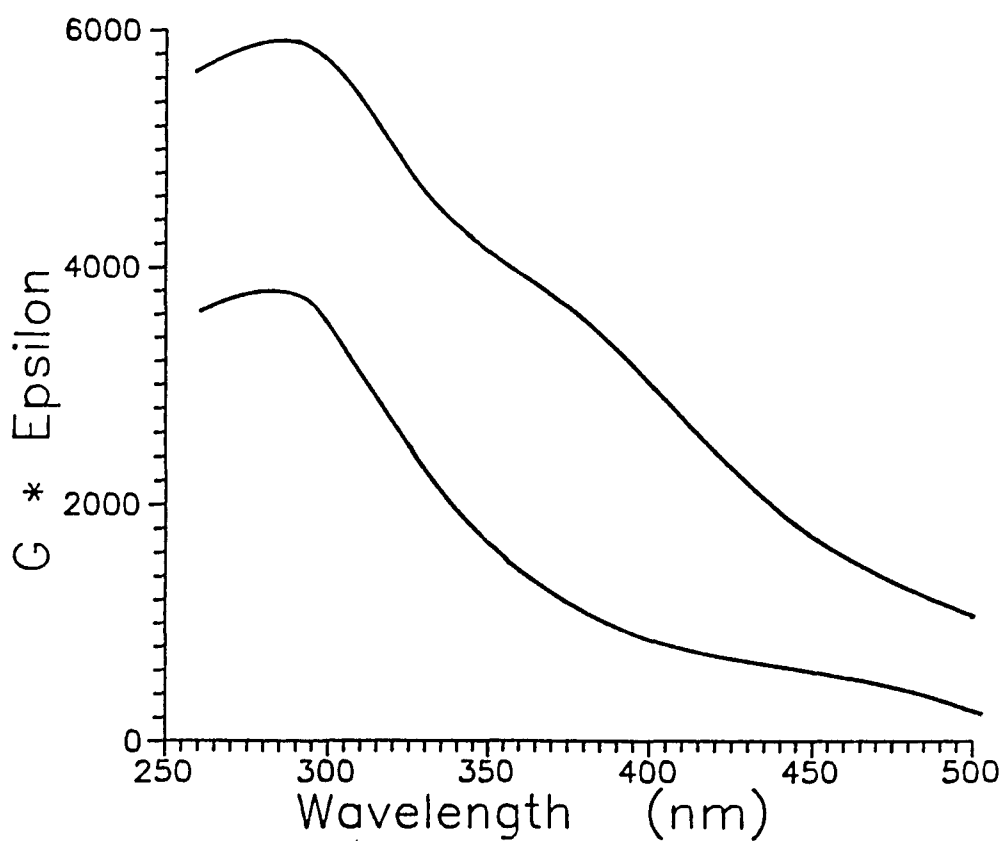


Figure 4.6. Pulse radiolysis of ≈ 0.2 mM 3.06b in N_2O saturated pH 6.9 aqueous solution. Upper curve: immediately after application of pulse. Lower curve: 200 μs after application of the pulse. Curve shown are smoothed curves drawn through approximately 20 data points collected between 260 and 500 nm.

Table 4.1
Pulse radiolysis data for 3.06b

Pulse Radiolysis of 3.06b Absorption data			
pH	Transient Max.	First Order T 1/2 usec	G*epsilon at 360 nm
1	355 +/- 5 nm	8	4100
2.1	"	24	5690
2.6	"	29	6830
3.1	"	27	4980
3.6	"	26	4180
4.2	"	32	3800
5.5	"	40	2850
6.9	"	16	2100
8.4	"	5	1100
9.6	"	-	1000

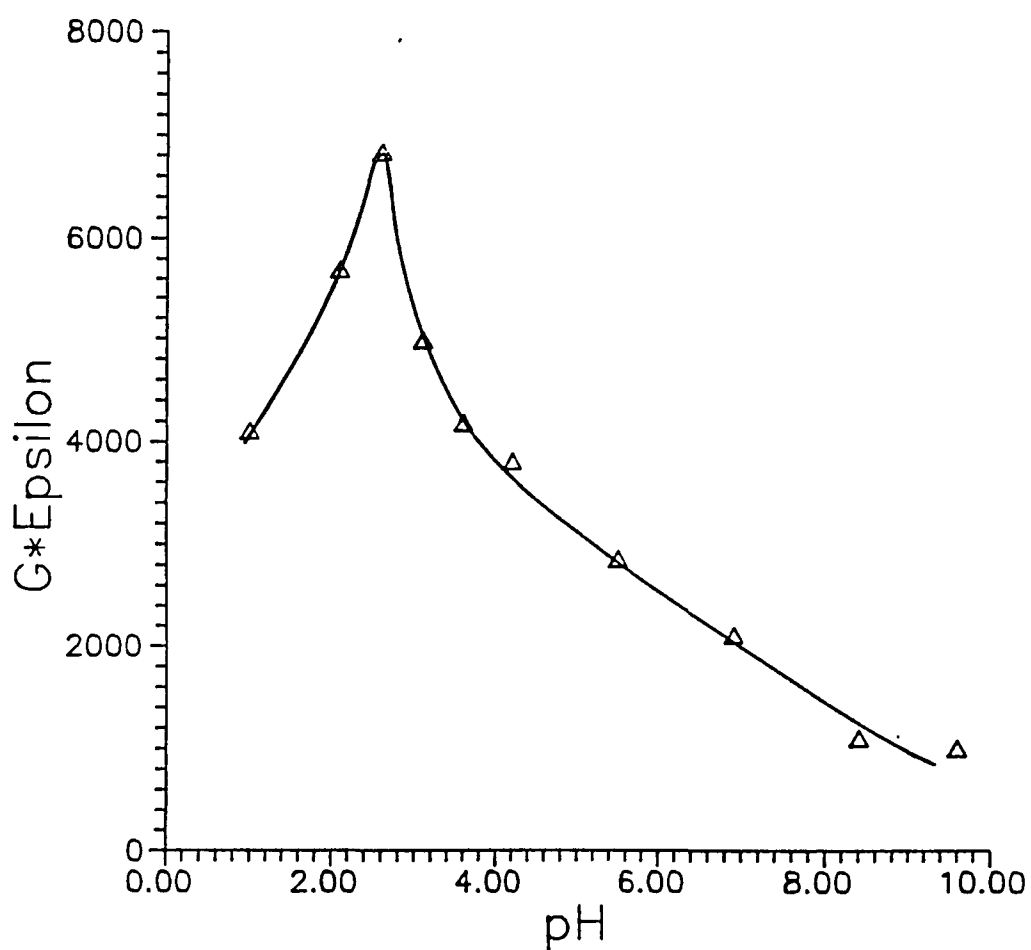


Figure 4.7. Plot of the yield of the transient species observed at 355 ± 5 nm upon pulse radiolysis of ≈ 0.2 mM 3.06b in N_2O saturated aqueous solutions at various pH's. See Table 3.3 for data. Measured at 360 nm.

adduct obtained upon one-electron oxidation of 3.06b is kinetically less stable than the adduct obtained from one electron oxidation of 3.01 over most of the pH range studied as evidenced by the shorter half-life of 3.06b. Another interesting observation is that the endo acid S-O species is obtained in higher yield than the corresponding amino acid species ($G=3.7$ for the endo acid 3.01 and $G= 1.53$ for the amino acid 3.06b).

Gamma radiolysis of the amino acid⁵⁰ 3.06b indicated decarboxylation as a major decomposition pathway. The yield of decarboxylation as measured by monitoring the amount of CO_2 produced (measured as bicarbonate by ion chromatography) was pH dependent as shown in Figure 4.8.

The 2c,3e S-O species in the endo acid 3.01 is favored at higher pH where the carboxylate is present as evidenced by a greater yield and longer half-life for the species absorbing at 390 nm. The half-life of the endo acid S-O increases with increasing pH in acidic solution ($\text{pH} < 4$) reaches a maximum between pH 4 and 7 and then begins to slowly fall off. The effect of protonation on the S-O species is seen below pH 4. On the basic side the S-O species can be attacked by hydroxyl anions. The amino acid would be expected to give similar behavior except that the pK_a would be lower. The pK_a of 3.06b has been determined to

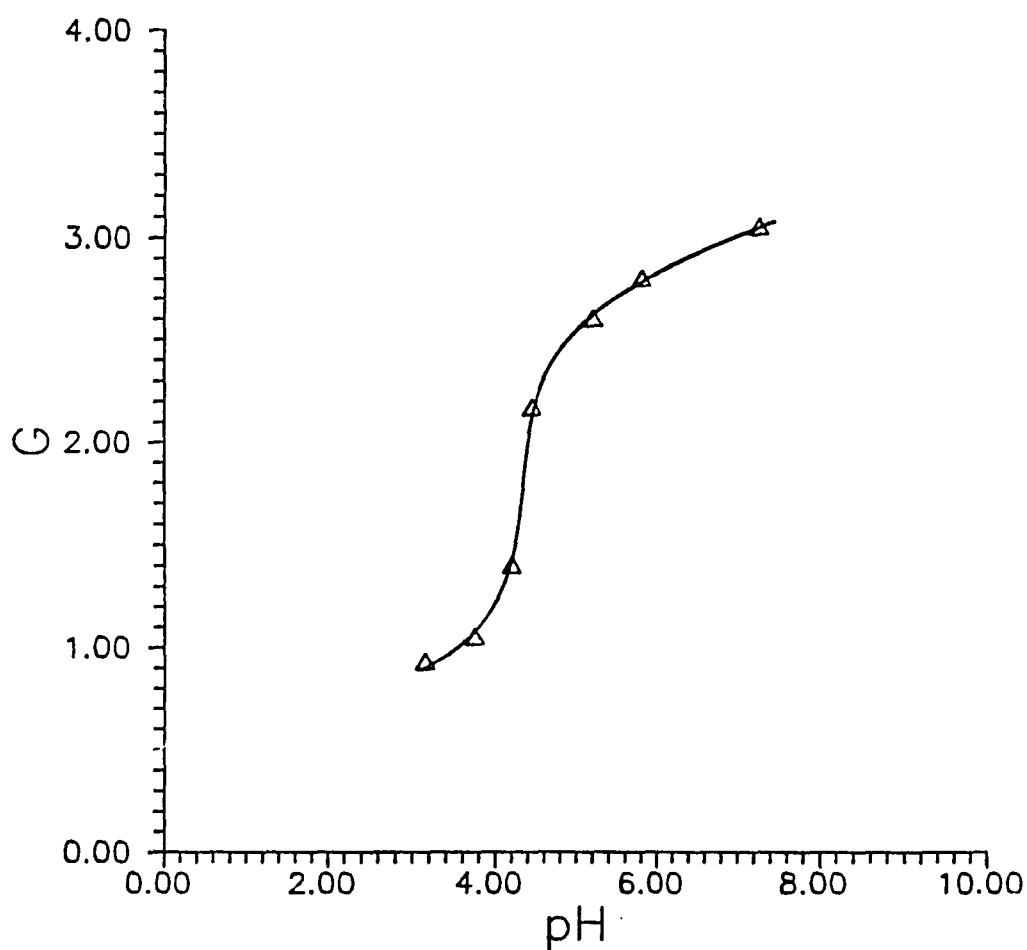


Figure 4.8. Plot of the radiation chemical yield of decarboxylation upon ^{60}Co -gamma- irradiation of 0.5 mM 3.06b in N_2O saturated aqueous solutions at various pH's.

be 2.4. These considerations can be used to explain the initial portion of the pH versus $G \cdot \epsilon$ curve for amino acid in that there is a rapid increase in yield passing through the pK_a of the amino acid. However, instead of rising smoothly to a plateau as one might expect the yield drops off rapidly at pH's above about 2.8. The dropoff correlates well with the marked increase in the yield of CO_2 in the gamma radiolysis as shown in Figure 4.9.

The conductivity data as a function of pH are quite complex. Table 4.2 summarizes the data. Some important points to note are that at low pH the signal immediately after the pulse, 1-2 μs , is negative and the decay kinetics are similar to those of the species absorbing at 355 nm. Between pH 4 and 5 the initial signal switches sign to an increase in conductivity and one sees very rapid decay kinetics unrelated to the decay observed for the 355 nm species. At high pH one sees a net increase in conductivity with little subsequent kinetics.

What then is the fate of 3.06b upon pulse radiolysis? Although not directly observed there is precedent for postulating formation of a hydroxyl radical-sulfur 2c,3e bond adduct⁵¹ 4.02 as the initial species as shown in Figure 4.10. A significant amount, approximately 30%, of α -thioalkyl radicals such as 4.03 (the radical resulting from abstraction

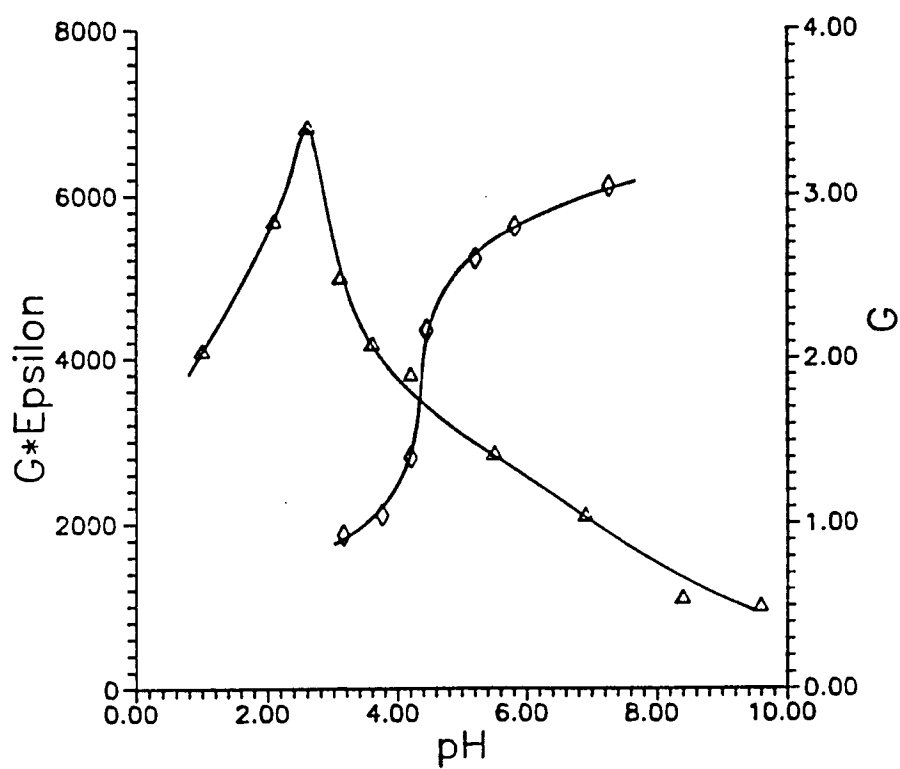


Figure 4.9. Comparison of pulse radiolysis versus ^{60}Co -gamma- radiolysis yields upon irradiation of 3.06b at various pH's.

Table 4.2
Conductivity data for 3.06b

Pulse Radiolysis Conductivity Data for 3.06b			
pH	Initial Signal	Final Signal	Kinetics observed T 1/2 in microseconds
2.6	-200	120	22
3.1	-450	0	20
3.6	-500	-100	24
4.2	-350	-110	32
5.5	200	-100	4
6.9	190	20	5
8.4	60	35	Slow decay
9.6	130	160	Slow linear increase

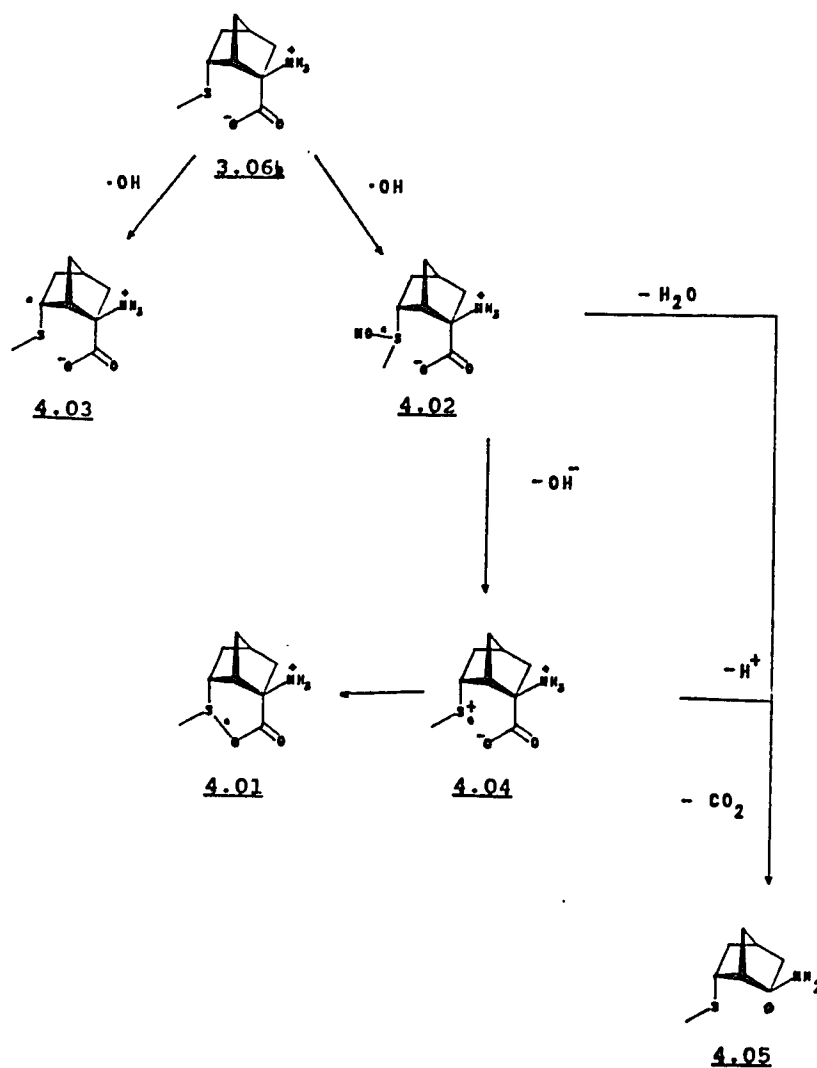


Figure 4.10. Outline of the possible pulse radiolysis products formed upon radiolysis of 3.06 under various conditions.

of one of the methyl hydrogens could form but it is not possible to distinguish between the two sites of attack under the conditions used) is also formed which accounts for the absorption at 280 nm. Adduct 4.02 can react via a number of pathways depending on pH. At low pH protonation of the adduct 4.02 followed by loss of water by an S_N1 process would lead to formation of the sulfur cation radical 4.04. Alternatively, loss of water by an S_N2 displacement by the carboxylate could lead to formation of S-O adduct 4.01 directly. The absorption observed at 355 nm is assigned to 4.01. At more moderate pH 4.02 could simply lose hydroxyl anions, which of course would still be protonated at pH below 7, to form 4.01 and 4.04. Sulfur cation radicals such as 4.04 are known⁵² but they are usually quite unstable and therefore short lived. The radical cation 4.04 could collapse to the S-O stabilized 4.01 or it could undergo a pseudo Kolbe⁵³ decarboxylation reaction along with subsequent loss of an amino proton to form 4.05. The S-O species 4.01 undergoes clean first-order decay with apparent release of a proton as evidenced by the concomitant increase seen in the conductivity. Based on previous work on thioethers⁵⁴ it is reasonable that this decomposition leads to formation of 4.03, however, unlike with endo acid 3.01, which shows the peak at 280 nm increasing as the peak at 390 nm decreases,

the 280 nm peak for the amino acid 4.01 does not increase as the peak at 355 nm decreases. The absorption versus decay over time curves reveal that the peak at 280 nm decays very little while significant amounts of 4.01 are present, an indication that 4.01 may be deprotonating to form some 4.03 at a slower rate comparable to the rate of decay of 4.03. Unfortunately, the decay at 280 nm is a complex second order process and insufficient kinetic data were collected at this wavelength to quantify this possibility. Opening of 4.01 to 4.04 is possible but would be expected to lead to a decrease in the half-life of 4.01 as decarboxylation becomes more significant which is not seen.

Decarboxylation becomes a dominant pathway at pH's above about 3.5. Since the half-life of 4.01 remains relatively constant above pH 3.5 4.01 is not the species which decarboxylates and is not in equilibrium with the species which decarboxylates. Also, the decrease in the yield of 4.01 above pH 2.6 appears related to the increase in decarboxylation which leads to the conclusion that formation of 4.01 and decarboxylation to form 4.05 are competing reactions arising from a common precursor. The most likely precursors are the initial hydroxyl adduct 4.02 and the thioether cation radical 4.04. If adduct 4.02 is the species which decarboxylates one would expect to see no net increase

in the conductivity signal immediately after the pulse. However, adduct 4.04 would be expected to give rise to a large decrease in the conductivity since a proton is consumed in its production. Table 4.2 shows a net initial increase in conductivity in the region where decarboxylation becomes significant. However, the half-life of 4.04 is likely to be on the order of a few μ s at best, leading to the same overall conductivity change expected in the decarboxylation of 4.02. Therefore, differentiation between 4.02 and 4.04 as the precursor to decarboxylation using the conductivity data is not conclusive. Why is decarboxylation such a facile reaction? The alpha amino radical 4.05 formed is expected to be relatively stable⁵⁵ and similar radicals are known to have pKa's in the region of pH 3-4 where decarboxylation becomes significant. The availability of a low energy pathway to form the alpha amino radical, followed by either a concerted loss of hydroxyl anion, decarboxylation and loss of a proton from the ammonium (this corresponds to going directly from 4.02 to 4.05) or initial charge transfer from the sulfur cation radical 4.04 to the carboxylate to form a carboxylate radical followed by decarboxylation and deprotonation of the ammonium, would lead to 4.05. On the basis of precedent the second pathway, which terminates in the aforementioned pseudo Kolbe reaction, would seem to be

the most likely.

Comparison of the results obtained for 3.06b and methionine upon pulse radiolysis further substantiates Asmus,⁵⁶ assertion that methionine decays via an S-N intermediate and not a S-O intermediate. In methionine the adduct formed has a much shorter half-life (220 ns) and the absorption maximum is at 400 nm. Also the pH dependence of the methionine adduct indicates an S-N interaction. The behavior of S-methylcysteine upon pulse radiolysis⁵⁷, which is believed to involve a protonated sulfur carboxylate intermediate, compares very well with 3.06b. S-Methylcysteine at very low pH shows a absorption in the UV at 385 nm which has a half-life of 27 μ s. At pH's where the carboxylate would be present S-methylcysteine rapidly decarboxylates in a fashion analogous to that seen for 3.06b.

Amino acid 3.06b exhibits strong neighboring group participation upon pulse radiolysis. The 40 nm shift in lambda max in comparison with 3.01a indicates that the 2c,3e bond formed is actually stronger than the bond formed in 3.01a due most reasonably to the presence of the electron withdrawing ammonium group alpha to the carboxylate. In comparison with the adduct formed from S-methylcysteine 4.01 is seen to be more stable as evidenced by a 30 nm shift to lower wavelength and greater resistance to decarboxylation,

an indication of the extra stability provided by the fixed conformation of the norbornyl ring. Decarboxylation also clearly indicates a strong neighboring group effect in the presence of the ammonium moiety since the initial oxidation takes place primarily at sulfur and in the case of 3.01 no decarboxylation occurs.

Experimental

Millipore filtered water with a nominal resistance of 10 megohm was used for all the pulse radiolysis experiments. The solutions were deoxygenated with argon and saturated with N_2O . Sufficient quantities of amino acid were added to make 0.1 mM solutions. The pH was adjusted by adding standardized NaOH or $HClO_4$ and was measured just prior to the experiments using a Orion research pH meter.

The solutions were irradiated using a 1.5 or 3.8 MeV van de Graaff accelerator with pulse durations of 1 μs and 50 ns respectively. Absorbed doses were on the order of 1-5 Gray (1 Gy = 1 J/Kg). The irradiation results in the formation of hydroxyl radicals, solvated electrons and a low concentration of hydrogen radicals. The solvated electrons react rapidly with the dissolved nitrous oxide to form N_2 and more hydroxyl radicals. The net result is the formation of a solution containing greater than 90% hydroxyl radicals in terms of total radical species produced. The G value (G is

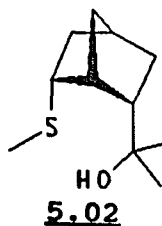
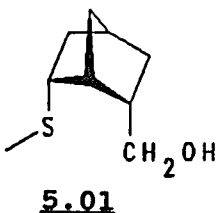
a measure of the pulse radiolysis yield expressed as the number of radicals formed for every 100 eV of energy imparted to the solution) is 5.6 which corresponds to an actual concentration of hydroxyl radicals of about $2-6 \times 10^{-6}$ M depending on the pulse duration. The experimental system was calibrated each day by standard pulse radiolysis thiocyanate dosimetry⁵⁸. The solution was pumped into the pulse radiolysis cell via a positive pressure flow through system described elsewhere⁵⁹. The optical and conductivity apparatus were optimized prior to each experiment. Absorption data were obtained over the range 250-500 nm. Kinetic data were obtained at individual wavelengths as desired. Conductivity data could be obtained at pH > 2.5 and < 11.0. All the data were acquired and manipulated via a computer-controlled data acquisition system described elsewhere⁵⁶.

Gamma radiolysis was initiated by irradiation in a field of about 6000-Ci ^{60}Co - γ -source. The total absorbed doses were on the order of 50-200 Gy at a dose rate of 700 Gy/h. The initially sealed sample vials were made basic to drive the CO_2 bicarbonate equilibrium toward bicarbonate and then a Dionex 2010i ion chromatograph equipped with an ion exchange column using a conductivity detector was used to monitor the bicarbonate concentration in the test solutions⁶⁰.

CHAPTER 5
ELECTROCHEMICAL AND CHEMICAL OXIDATION OF
(±)-endo-2-HYDROXY-6-endo-METHYLTHIO-BICYCLO-
[2.2.1] HEPTANE

Introduction

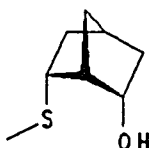
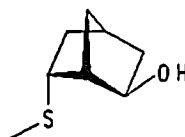
Facilitation of oxidation of thioethers by neighboring hydroxyl group participation has been reported.⁶¹ The primary and tertiary endo alcohol groups in 5.01 and 5.02 respectively both show evidence for neighboring group participation upon electrochemical oxidation, as indicated by very low oxidation potentials of about 0.6 V and formation of S-O species upon pulse radiolytic oxidation in the case of 5.02.⁴⁶ However, in the electrochemical oxidation the strong neighboring group participation is dependent upon the presence of a catalytic amount of bromide.⁶² In the absence of bromide the difference between the peak potentials observed for 5.01 and 5.02 and their analogous exo derivatives is less than 150 mV and the peak



potentials for the endo derivatives are in the low range

expected for normal thioethers. Pulse radiolysis of 5.02 indicates the formation of an S-O species of moderate kinetic stability as evidenced by a first-order half-life of 30 μ s. Primary alcohol 5.03 does not exhibit such behavior.

This chapter presents results obtained in the oxidation by electrochemical and chemical means of the endo alcohol 5.03 using exo alcohol 5.04 as a control compound.

5.035.04

Results and Discussion

Cyclic Voltammetry and FTIR of 5.03

Cyclic voltammetry of 5.03 in 0.1 M LiClO₄ in acetonitrile at a glassy carbon electrode with a sweep rate of 100 mV/sec results in a single irreversible oxidation with a peak potential of 0.88 V versus Ag/0.1 M AgNO₃ in acetonitrile. The cyclic voltammogram is shown in Figure 5.1. The oxidation is diffusion controlled as evidenced by a linear plot of the square root of the sweep rate versus the peak current over a two order of magnitude change in sweep rate between 20 and 2000 mV/sec as shown in Figure 5.2. At higher scan rates a small shoulder is seen

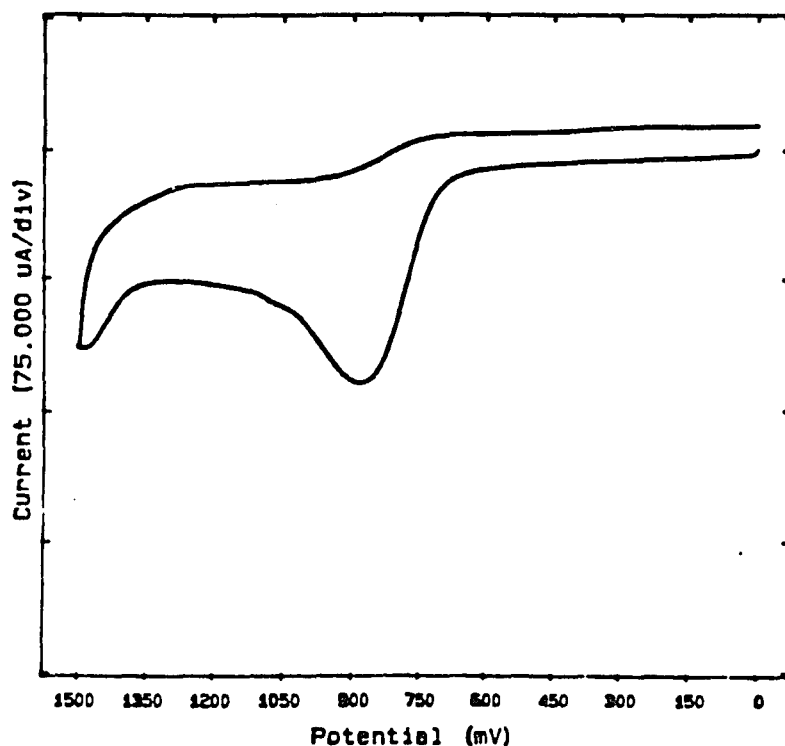


Figure 5.1. Cyclic voltammogram of 1.6 mM 5.03 in 0.1 M LiClO₄ acetonitrile solution. Glassy carbon working electrode ($A = 0.09 \text{ cm}^2$), Pt counter electrode, Ag/ 0.1 M Ag/NO₃ in acetonitrile reference electrode. Scan rate 100 mV/s.

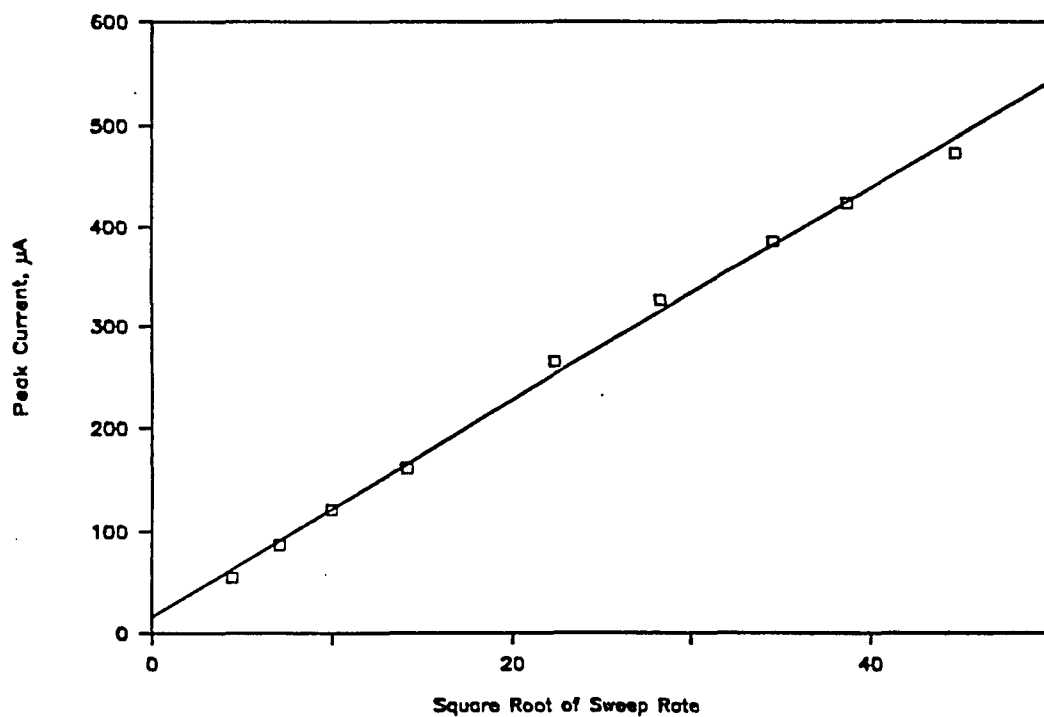


Figure 5.2. Plot of the square root of the sweep rate versus peak current for 1.5 mM 5.03 in 0.1 M LiClO_4 acetonitrile solution. Glassy carbon working electrode ($A = 0.09 \text{ cm}^2$), Pt counter electrode, Ag/ 0.1 M Ag/ NO_3 in acetonitrile reference electrode. Scan rates 20, 50, 100, 200, 500, 800, 1200, 1500, 2000, 3000 mV/s.

superimposed on the current decay of the main oxidation at about 1.1 V. The peak potential shifts in an anodic direction as the sweep rate is increased but at a rate considerably faster than the expected $30/\alpha n$. Addition of 2,6-di-*t*-butylpyridine to the solution results in a very small cathodic shift in the peak potential of about 10 mV. Upon addition of sufficient lithium bromide to result in a 0.3 molar ratio of bromide the large oxidation wave at 0.54 V in the cyclic voltammogram shown in Figure 5.3 shows bromide catalysis of the oxidation of 5.03. The catalysis observed is similar to that seen upon oxidation of 5.01 in the presence of bromide with a catalytic current enhancement of approximately 8 times. Table 5.1 summarizes the cyclic voltammetry data. Differential pulse voltammetry of 5.03 shows one peak at 0.85 V as shown in Figure 5.4. Rotating disk electrode voltammograms of 5.03 are shown in Figure 5.5. A Levich plot of the square root of the rotation rate versus the diffusion current, shown in Figure 5.6, shows definite curvature at 1.2 V, indicating some kinetic control of the current. At 1.3 V the curve is more linear, indicative of pure diffusion control. An "n" value of 1.9 was determined from the RDE curves.

Cyclic voltammetry of exo alcohol 5.04 under the same conditions as used for the cyclic voltammetry of 5.03 shows

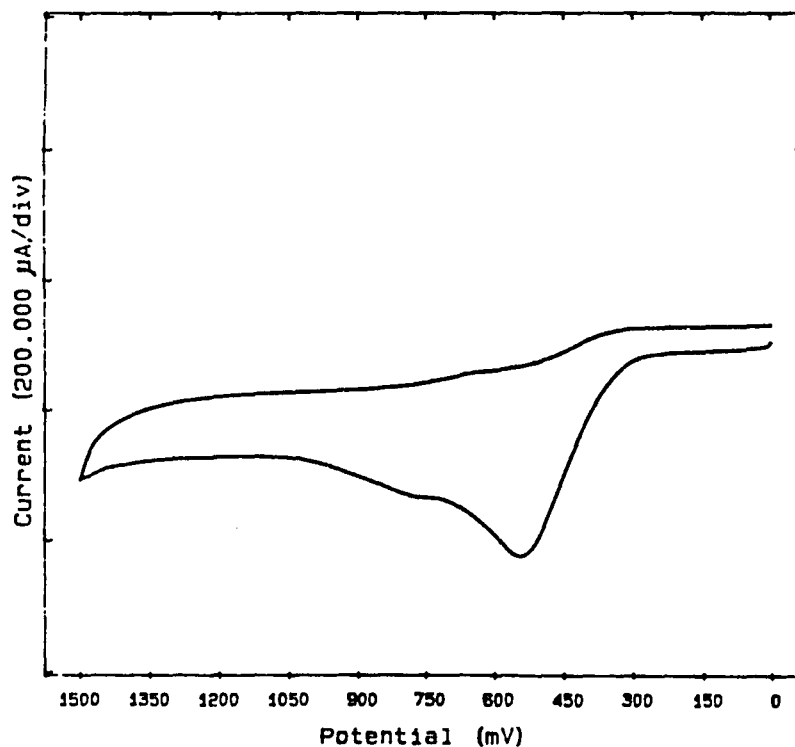


Figure 5.3. Cyclic voltammogram of 1.6 μM 5.03 plus 30 mole % LiBr and 0.3 μM 2,6-di-*t*-butylpyridine in 0.1 M LiClO₄ acetonitrile solution. Glassy carbon working electrode ($A = 0.09 \text{ cm}^2$), Pt counter electrode, Ag/ 0.1 M Ag/NO₃ in acetonitrile reference electrode. Scan rate 100 mV/s.

Table 5.1
Cyclic and rotating disk voltammetry data
for endo alcohol 5.02

Cyclic Voltammetry Data for 5.03		
Sweep Rate (mV/sec)	Peak Current (A)	Peak Potential (V)
20	55.5	0.85
50	87.3	0.87
100	121.7	0.88
200	162.2	0.91
500	264.5	0.95
800	326	0.96
1200	385.3	0.99
1500	423.6	1.01
2000	473.6	1.03
3000	492.5	1.06

Rotating Disk Electrode Voltammetry Data for 5.03		
Rotation Rate (rpm)	Diffusion Current (uA) E = 1.2 V	Diffusion Current (uA) E = 1.3 V
400	725	766
900	1120	1148
1200	1449	1490
1600	1740	1790
3600	2015	2090

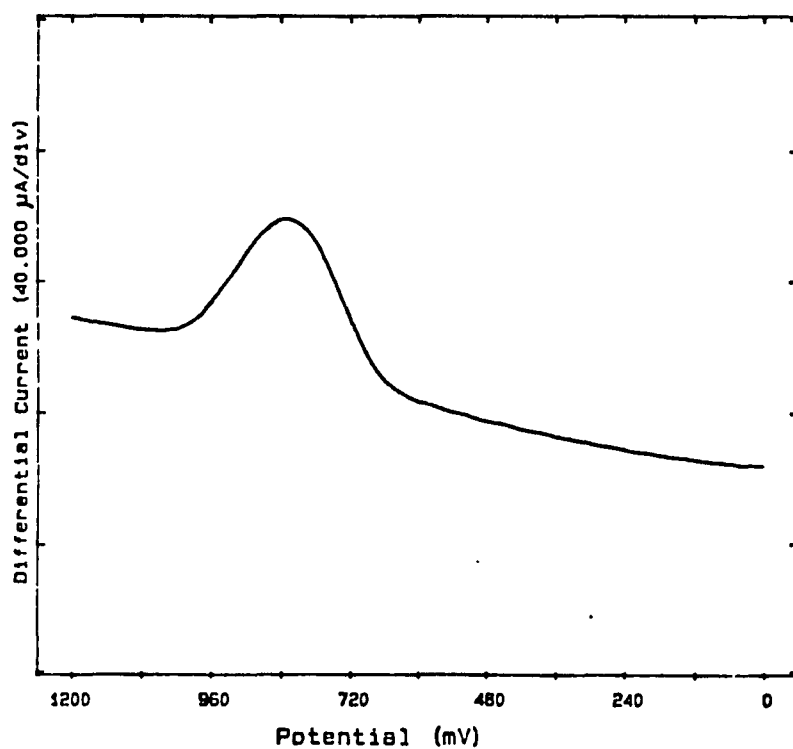


Figure 5.4. Differential pulse voltammogram of 1.5 mM 5.03 in 0.1 M LiClO_4 acetonitrile solution. Glassy carbon working electrode ($A = 0.09 \text{ cm}^2$), Pt counter electrode, Ag/ 0.1 M Ag/NO_3 in acetonitrile reference electrode. 50 mV pulse amplitude, 50 ms pulse width. 2 mV step height.

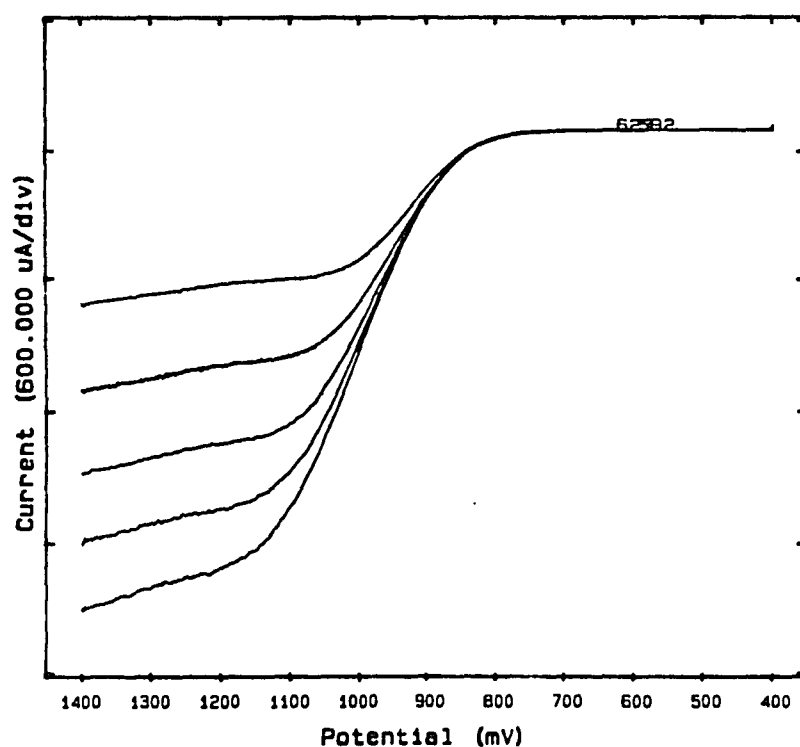


Figure 5.5. Rotating disk voltammograms of 1.9 mM 5.03 in 0.1 M LiClO₄ acetonitrile solution. Glassy carbon working electrode ($A = 0.3 \text{ cm}^2$), Pt counter electrode, Ag/ 0.1 M Ag/NO₃ in acetonitrile reference electrode. Rotation rates : 400, 900, 1600, 2500, 3600 rpm.

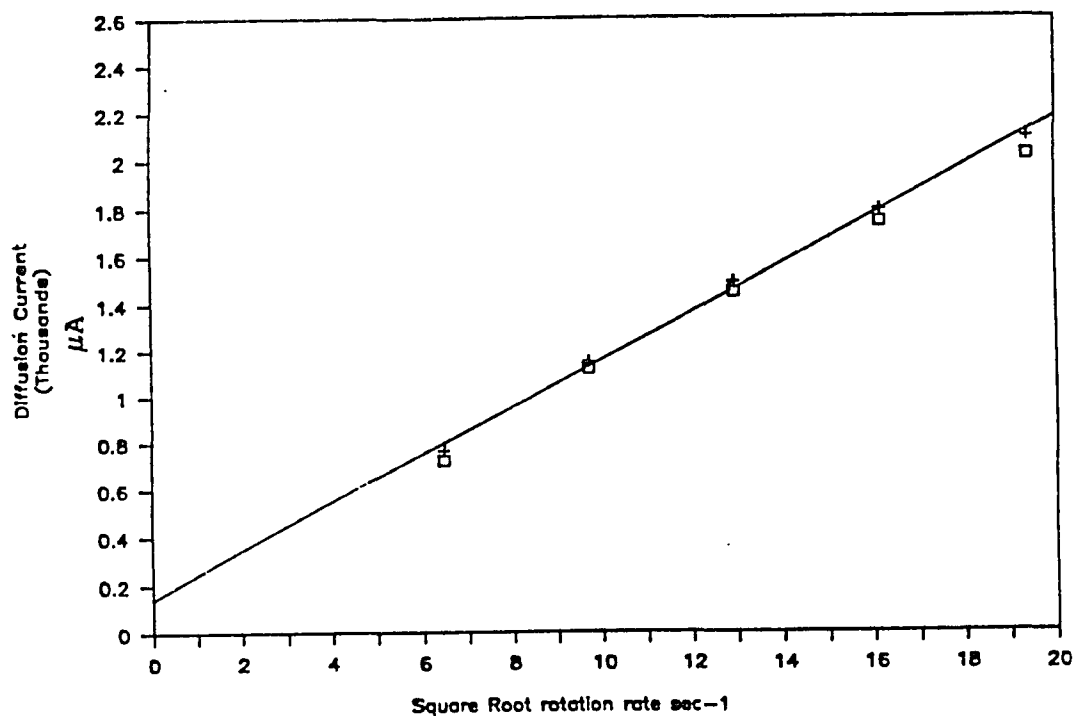


Figure 5.6. Levich plot of 1.9 mM 5.03 in 0.1 M LiClO₄ in acetonitrile. The current was measured at 1.2 V for the squares and at 1.3 V for the crosses. Glassy carbon working electrodes ($A = 0.3 \text{ cm}^2$). Pt counter electrode. Ag/0.1 M AgNO₃ in acetonitrile reference electrode. Rotation rates: 400, 900, 1600, 2500, 3600 rpm.

one irreversible oxidation wave with a peak potential of 1.23 V versus Ag/0.1 M AgNO₃, as shown in Figure 5.7. The oxidation of 5.04 also is diffusion controlled as determined by a linear plot of the square root of the sweep rate versus the peak current. Addition of 2,6-di-*t*-butylpyridine to the electrochemical solution of 5.04 also has only a slight effect, shifting the peak potential in a cathodic direction about 10 mV at a sweep rate of 100 mV/s. As expected, 5.04 does not show bromine catalysis upon addition of bromide to the electrochemical solution.

A cyclic voltammogram of a solution containing both 5.03 and 5.04 shows a greater than 300 mV shift in peak potential between the two derivatives as illustrated in Figure 5.8. This large shift in peak potential is convincing evidence of neighboring hydroxyl group participation in the oxidation of thioethers with neighboring hydroxyl groups. In comparison with endo alcohols 5.01 and 5.02 one can see the advantage of the formation of a five-membered ring over formation of a six-membered ring in neighboring group participation. Neighboring group participation resulting in sulfur-sulfur interactions have also been reported to be more favorable if a five-membered ring is formed rather than a six membered ring.⁶³

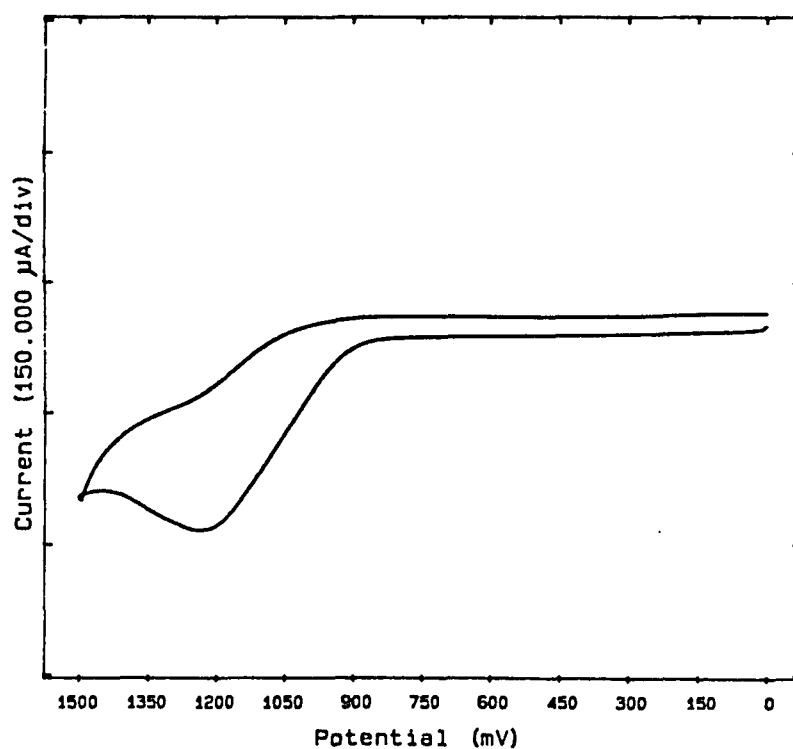


Figure 5.7. Cyclic voltammogram of 2.2 mM 5.04 in 0.1 M LiClO_4 acetonitrile solution. Glassy carbon working electrode ($A = 0.09 \text{ cm}^2$), Pt counter electrode, $\text{Ag}/0.1 \text{ M Ag/NO}_3$ in acetonitrile reference electrode. Scan rate 100 mV/s.

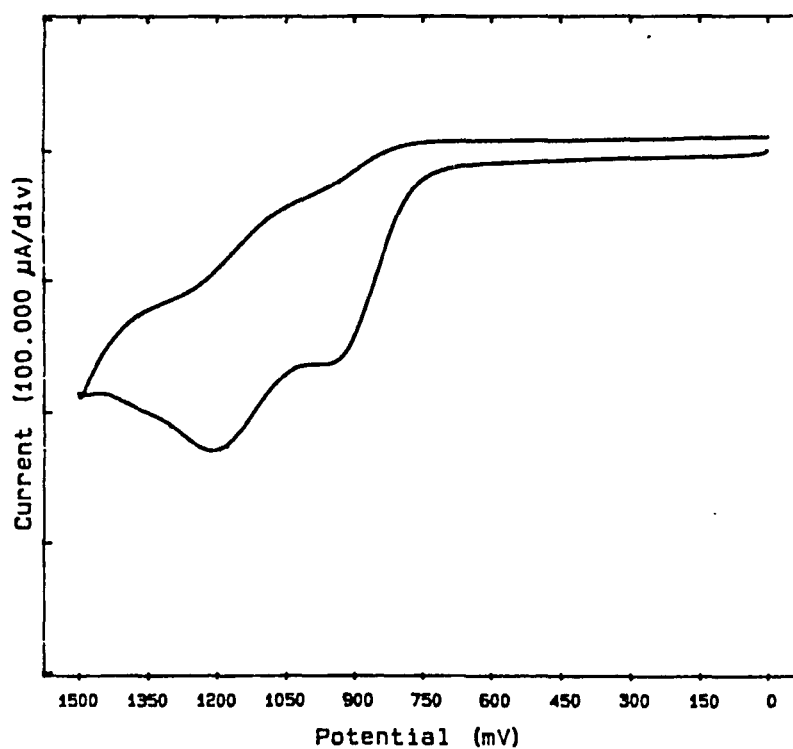


Figure 5.8. Cyclic voltammogram of 2.2 mM 5.04 and 1.5 mM 5.02 in 0.1 M LiClO_4 acetonitrile solution. Glassy carbon working electrode ($A = 0.09 \text{ cm}^2$), Pt counter electrode, $\text{Ag}/0.1 \text{ M Ag/NO}_3$ in acetonitrile reference electrode. Scan rate 100 mV/s .

The lowest ionization potentials of 5.03 and 5.04 determined by PES are 8.56 and 8.38 respectively.⁶⁴ The PES indicate that in the gas phase 5.04 is easier to oxidize than 5.03, results exactly the opposite of those obtained in the electrochemical investigations just outlined. The difference in gas phase ionization potentials may be due to the formation of a relatively strong intramolecular hydrogen bond in 5.03 which is geometrically precluded in 5.04. A series of FTIR experiments were carried out to investigate this possibility and the results are summarized in Table 5.1. Compound 5.04 in carbon tetrachloride at high concentration (0.3 M) shows a broad intermolecular hydrogen peak at 3394 cm^{-1} and a small sharp free hydroxyl band at 3623 cm^{-1} . Dilution to low concentration (0.016 M) results in an IR spectrum with just the free hydroxyl band at 3624 cm^{-1} . The IR spectrum of 5.03 in carbon tetrachloride shows only one peak in the OH region at 3440 cm^{-1} over the concentration range 0.46 M down to 2.5 mM. This independence on concentration is indicative of an intramolecular hydrogen bond. Intramolecular hydrogen bonds between thioethers and hydroxyl groups have been reported⁶⁵ and the ones which involve the formation of a six membered ring show absorptions near 3440 cm^{-1} .⁶⁶ Clearly, 5.03 is intramolecularly hydrogen-bonded in carbon tetrachloride.

Table 5.2
FTIR data for endo and exo alcohols
5.02 and 5.03

FTIR of 5.03 and 5.04		
Solution	Peaks Observed cm ⁻¹ (intensity)	Hydrogen Bond Assignment
Neat 5.04	3357	Intermolecular
0.31 M 5.04 carbon tetrachloride	3623 (85.8) 3394 (87.5)	Free OH, Intermolecular
0.016 M 5.04 CCl ₄	3624 (97.7)	Free OH
0.32 M 5.04 Acetonitrile	3630 (5) 3528 (60.4)	3528: Intermolecular to Solvent (see note below)
0.07 M 5.04 Acetonitrile	3630 (90) 3532 (78.8)	Inter to solvent
0.029 M 5.04 Acetonitrile	3621 (97.4) 3536 (95.6)	Inter to solvent
Neat 5.03	3426	Intra?
0.46 M 5.03 CCl ₄	3440 (36.7)	Intramolecular
0.09 M 5.03 CCl ₄	3444 (82.0)	Intra
0.0025 M 5.03 CCl ₄	3439 (99.2)	Intra

Table 5.2 continued

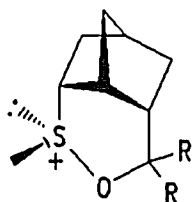
0.30 M 5.03 Acetonitrile	3621 (96.6) 3528 (87.8) 3418 (77.0)	Inter to solvent (3528) and intra (3418)
0.068 M 5.03 Acetonitrile	3627 (96.7) 3536 (94.2) 3416 (92.6)	Inter to solvent and intra
0.027 M 5.03 Acetonitrile	3625 (96.6) 3531 (96.4) 3415 (97.9)	Inter to solvent and Intra
Note: peak at approximately 3625 in acetonitrile is due to a subtraction error in the FTIR.		

What about in acetonitrile? The hydroxyl region of the FTIR spectrum of 5.03 in acetonitrile at high concentration (0.3 M) shows three peaks, one at 3621, one at 3528 and one at 3418 cm^{-1} . The peak at 3621 has been determined to be due to a subtraction error in removing the absorptions due to acetonitrile. The peak at 3418 cm^{-1} is assumed to be the intramolecular hydrogen bonded species shifted due to the acetonitrile. The peak at 3528 cm^{-1} is too broad to be for a free hydroxyl but too high to be for an intermolecular hydrogen bond. Compound 5.04 in acetonitrile gives a band at 3528 cm^{-1} which therefore must correspond to the hydrogen bond between 5.04 and the solvent, acetonitrile. Indeed, methanol in acetonitrile shows a hydrogen bonding peak at 3565 cm^{-1} . In acetonitrile there is an equilibrium between 5.03 intermolecularly hydrogen-bonded to the solvent and intramolecular hydrogen-bonded 5.03. The intermolecularly hydrogen-bonded species should be easier to oxidize than the intramolecularly hydrogen-bonded species in which the sulfur is hydrogen bonded. The oxidation wave at 0.88 V is for the oxidation of the intermolecularly bonded 5.03. As the intermolecular species is oxidized at 0.88 V the equilibrium between the inter- and intramolecularly hydrogen-bonded species is shifted towards the intermolecular species. The results obtained present a clear example of hydroxyl

neighboring group participation in thioether oxidation. The change in the relative ease of oxidation of 5.03 and 5.04 between PES and electrochemical data illustrates the importance of using multiple approaches to investigating thioether oxidations.

Controlled Potential Electrolysis and Chemical
Oxidation of 5.03

Controlled potential electrolysis of 5.01 and 5.02 leads to the formation of alkoxysulfonium salts 5.05 and



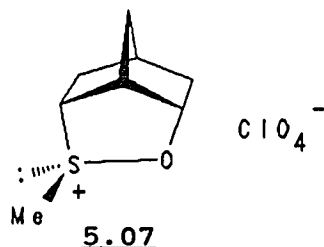
5.05 $R = H$

5.06 $R = CH_3$

5.06 in an overall two-electron process⁶⁷ analogous to that already reported for the formation of the endo alkoxysulfonium salt 3.01a. The major diastereomers formed are shown. Electrolysis is carried out at an applied potential of 0.65 V and requires the presence of bromide to facilitate the oxidation. Stereochemical and electrochemical evidence indicates that these oxidations are accompanied by neighboring group participation of the

hydroxyl group via displacement of a bromine adduct initially formed, this is again analogous to the results obtained upon oxidation of endo acid 3.01. This section reports on the controlled potential electrolysis of 5.03. The product formed is shown to be identical to the major product formed upon chemical oxidation of 5.03 by bromine in acetonitrile.

Controlled potential electrolysis of 5.03, at a carbon



cloth electrode in 0.1 M LiClO_4 in acetonitrile solution with 2,6-di-*t*-butylpyridine present, results in the passage of nearly two equivalents of charge before the current decays to zero. The major product formed in 80% crude yield has been determined by ^1H NMR spectroscopy to be alkoxy sulfonium salt 5.07. The IR spectrum obtained from the product also indicates the formation of 5.07. The crude ^1H NMR of the electrochemical mixture also indicated the formation of about 15% of another compound similar to 5.07, possibly its diastereomer, but this minor component

was not isolated. The crude mixture was applied to an HPLC column and after collection of the appropriate fraction pure 5.07 was obtained.

Oxidation of 5.03 by bromine in acetonitrile followed by workup of the reaction gave alkoxysulfonium salt 5.07 as the only product seen in the ^1H NMR spectrum of the crude mixture. Purification by HPLC and recrystallization gave crystalline 5.07 identical by ^1H NMR and IR spectroscopy with the product obtained via electrochemical oxidation.

Controlled potential electrolysis of 5.03 at a potential indicative of neighboring group participation and the isolation of alkoxysulfonium salt 5.07 provides, along with the analytical electrochemistry, convincing evidence for the neighboring alcohol group participation of alcohols in the oxidation of thioethers.

Experimental

Cyclic voltammetry, RDE, and DPP

The cyclic voltammetry, rotating disk electrode voltammetry, and differential pulse polarography were all done using the same conditions as those reported for the investigation of 3.06b except that all the data were collected on the Cypress Systems model CYSY-1 Electroanalysis System. Also, a glassy carbon electrode, surface area 0.09 cm^2 , was used as the working electrode and

was cleaned between each run using fine polishing powder.

Controlled potential electrolysis of 5.03.

A sample of 5.03 (22 mg, 0.14 mmol) was dissolved in acetonitrile 0.1 M in LiClO_4 (20mL) in the central compartment of a three chambered electrochemical cell. 2,6-Di-*t*-butylpyridine (75 μL , 0.3 mmol) was added to the solution. Using a carbon cloth working electrode (surface area 1 cm^2) in the center compartment, a platinum counter electrode in one side compartment and a $\text{Ag}/0.1 \text{ M AgNO}_3$ in acetonitrile reference electrode in the other side compartment, the electrolysis was started. The current decayed to zero after 25 coulombs had passed corresponding to an "n" value of 1.9. After removing the solvent a ^1H NMR spectrum of the crude showed downfield peaks at δ 5.62 and 4.68 ppm which indicated formation of the alkoxysulfonium salt. A set of smaller peaks at δ 5.32 and 4.81 which may correspond to the other diastereomer are also present in a ratio of 85:15 major to minor diastereomer. Analysis of the ^1H NMR peak positions for the bridgehead and SMe peaks indicates that the diastereomer shown, 5.07, is the major diastereomer as follows. The proton resonance for the SMe methyl in the major diastereomer of 5.02 shown above is at δ 3.42 and the minor diastereomer SMe proton resonance is

at δ 3.25. In 5.07 the SMe proton resonance is at δ 3.16 for the major diastereomer and the minor diastereomer is at upfield at δ 2.85. The bridgehead proton at C1 is shifted to lower field, δ 3.63 versus δ 3.51, in the major diastereomer of 5.07 which is consistent with the structure shown due to the anisotropic effect of the proximate alkoxysulfonium group. The crude yield was 80% as determined by addition to the NMR solution a known amount of piperonal as an internal standard. The crude product was subjected to HPLC purification using a reverse phase C-18 column (Altex ODS, 25 X 250 mm) eluting with acetonitrile at a flow rate of 4.4 mL/min with the detector set at 230 nm. The two major peaks were collected in several fractions. Upon removal of the solvent the first peak was determined to be alkoxysulfonium salt 5.05 (\approx 10 mg, 30% yield): ^1H NMR (CDCl_3 , 250 MHz) δ 1.51 (dd, 1, J = 8, 3.6 Hz), 1.77 (dd, 1, J = 15, 2.5 Hz), 1.95 (m, 2), 2.50 (bs, 1, C4 bridgehead), 2.67 (m, 1), 3.16 (s, 3, SMe), 3.63 (bs, 1, C1 bridgehead); IR (KBr) 3000, 1445w, 1327w, 1085s (ClO_4), 900w, 820m, 623m, cm^{-1} .

Oxidation of 5.03 with bromine.

A sample of 5.03 (60 mg, 0.38 mmol) was dissolved in acetonitrile (5 mL) and degassed with argon. 2,6-Di-t-

butylpyridine (100 μ L, 0.44 mmol) was added by syringe and the solution cooled to -35°C . Bromine (20 μ L, 0.38 mmol) dissolved in acetonitrile (1 mL) was added dropwise over 10 min to the solution of 5.03. Silver perchlorate (156 mg, 0.75 mmol) was added and the solution stirred for 30 min at -35°C and then allowed to warm to room temperature. After filtration and rotary evaporation an NMR spectrum of the crude product indicated formation of 5.07 in 90% yield. Vapor diffusion recrystallization of diethyl ether into a dichloromethane solution of the crude product resulted in the formation of clear crystalline plates of 5.07. The ^1H NMR spectrum and IR spectrum were identical with those reported for the electrochemical product.

APPENDIX I
REVERSIBLE ELECTROCHEMISTRY OF
NAPHTHO[1,8-b,c]-1,5-DITHIOCIN

It has been shown that hydrolytically unstable cation radicals can be generated electrochemically in dichloromethane with a tetraalkylammonium supporting electrolyte and a mixture of trifluoroacetic acid and trifluoroacetic anhydride present to scavenge trace amounts of water.⁶⁸ Since interception of cationic sulfur species by water was indeed seen in the electrochemical oxidation of 1.02 a question arose as to whether reversible behavior could be seen in the non-nucleophilic, anhydrous solvents mentioned.

Addition of a sufficient amount of 1.02 to make a 2 mM solution in 10 mL dichloromethane/0.2 mL TFA/0.5 mL TFAA gave a brilliant green solution. Cyclic voltammetry of the solution at a platinum working electrode results in two quasi reversible electrochemical waves with $E^{\circ'}$ of 0.51 and 0.95 V respectively as shown in Figure I.1. The $E^{\circ'}$ for 1,5-dithiocane, 1.01, is 0.32. The first wave was shown to be reversible at least between 10 and 500 mV/s. The peak separation for the first wave is 160 mV at a scan rate of 100 mV/s. The brilliant colored solution obtained was reminiscent of that reported for thianthrene cation radical and indeed an RDE, shown in Figure I.2, of the solution showed that the species in solution was positively charged as indicated by an initial cathodic current. Also, an EPR

spectrum of the colored solution gave a large triplet spectrum with a g of 2.012 and a splitting of 16.5 gauss as shown in Figure I.3. It is not known at this time why the cation radical was formed in the solution before anodic oxidation; apparently there was a trace oxidant impurity present. Addition of thianthrene to the electrochemical solvent also resulted in the formation of the thianthrene cation radical as evidenced by RDE, cyclic voltammetry and UV/vis.

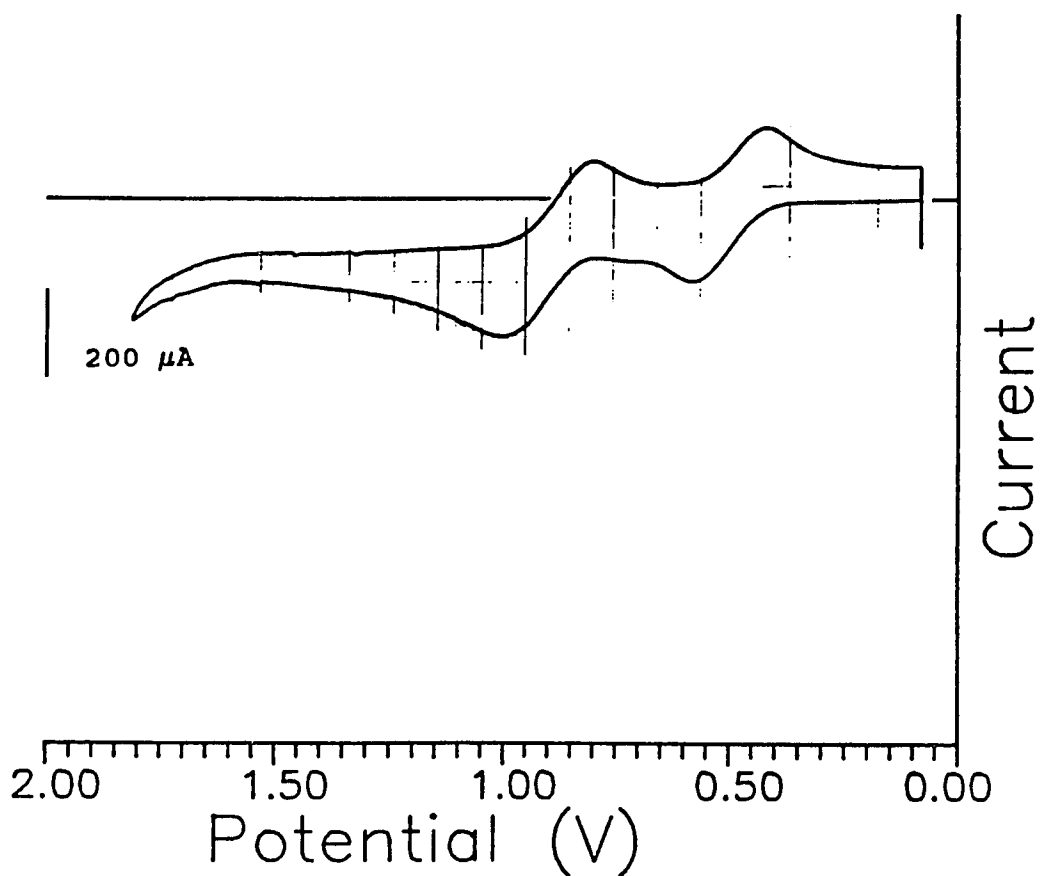


Figure I.1. Cyclic voltammogram of 2.2 mM 1.02 in a solution of 10 mL dichloromethane/0.2 mL trifluoroacetic acid/0.5 mL trifluoroacetic acid anhydride. Pt working electrode ($A = 0.4 \text{ cm}^2$), Pt counter electrode, Ag/0.1 M AgNO_3 in acetonitrile reference electrode. Scan rate 100 mV/s.

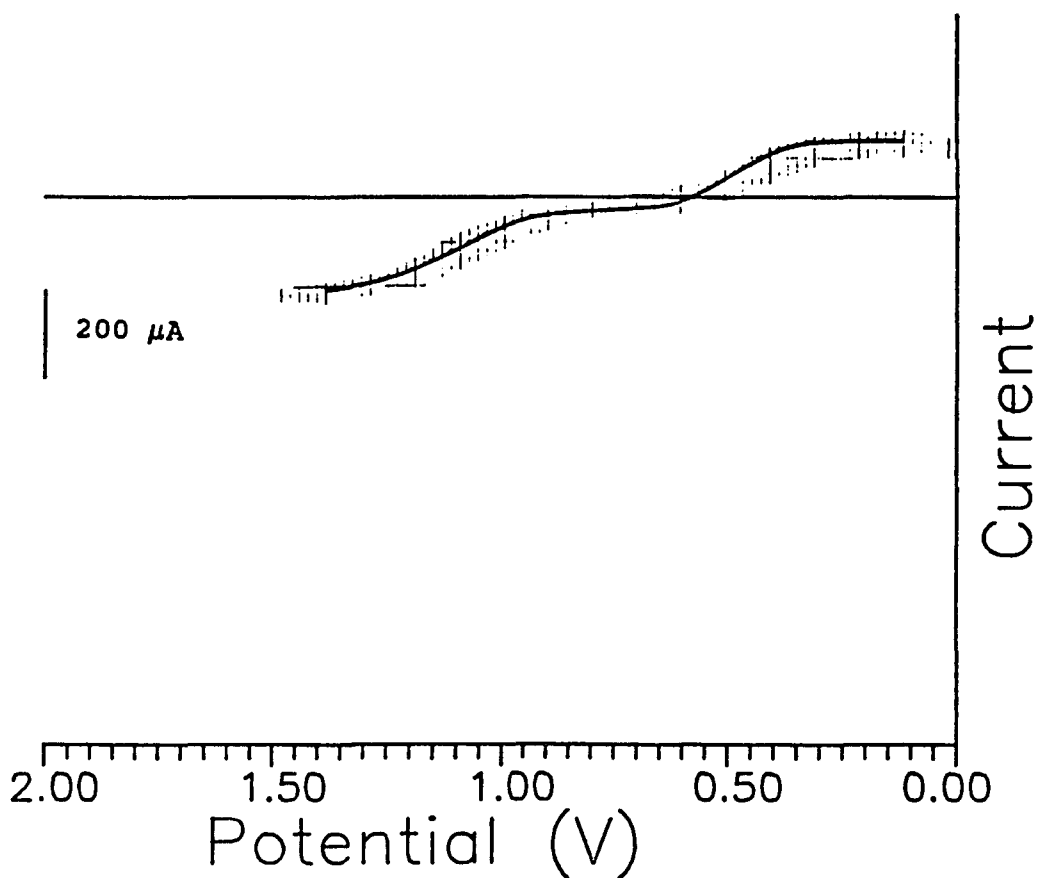


Figure I.2. Rotating disk electrode voltammogram of 2.2 mM 1.02 in the cyclic voltammetry solution. Pt working electrode ($A = 0.4 \text{ cm}^2$), Pt counter electrode, Ag/0.1 M AgNO₃ in acetonitrile reference electrode. Rotation rate: 1200 rpm.

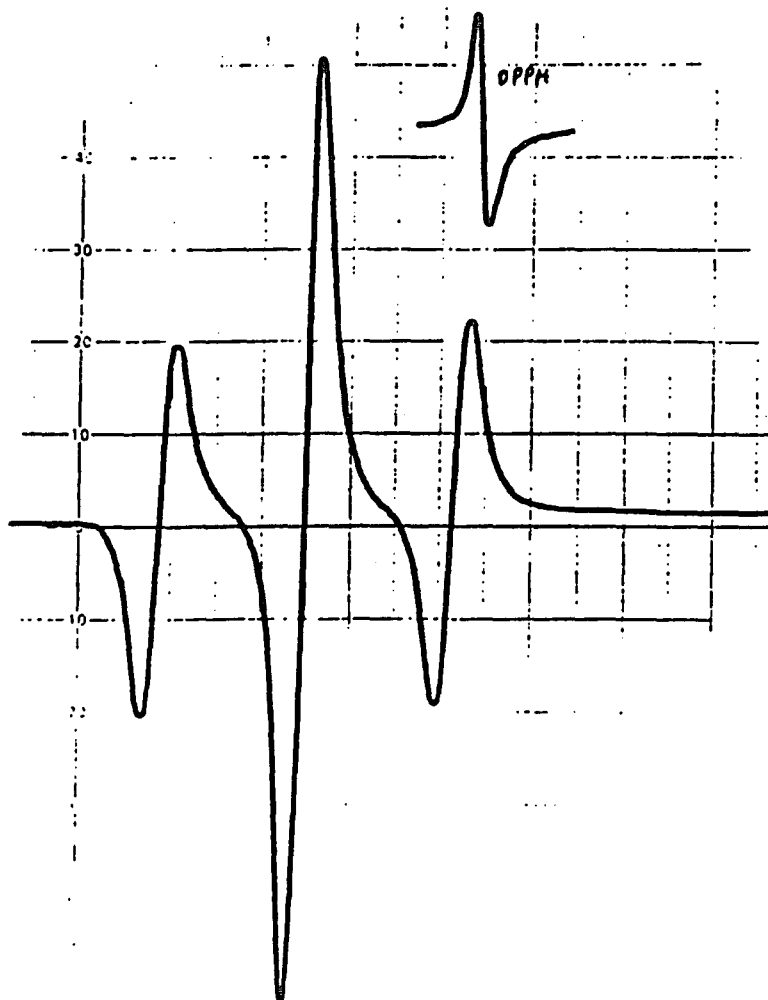


Figure I.3. EPR spectrum of 2 mM 1.02 in the electrochemical solvent system. Microwave Power: 2.50 mW. Microwave Frequency: 9.510 GHz. Modulation frequency: 100 Hz. Modulation amplitude: 0.1 G. Small curve = DPPH.

APPENDIX II

$\text{Cd}(\text{TTCN})_2^{2+}$ AND $\text{Cd}(\text{Cu})(\text{TTCN})_2^{2+}$ METAL COMPLEXES

The mesocyclic thioether 1,4,7-trithianonane, 2.01 (TTCN), has proven to be an excellent tridentate ligand for transition metals. Bis-TTCN complexes have been made with Ni(II), Cu(II), Co(II),⁶⁹ Pd(II), Pd(III),⁷⁰ Fe(II), Fe(III)⁷¹ and many other transition metal ions. The endodentate structure adopted by TTCN⁷² allows it to form very robust octahedral metal complexes. High and low oxidation states of transition metals can be stabilized by TTCN. There is considerable interest in the redox, electronic, and magnetic properties of these complexes. This appendix reports on the synthesis and crystal structure of Cd(II)(TTCN)₂(BF₄)₂·2CH₃NO₂, Cu(II)(TTCN)₂(BF₄)₂·2CH₃NO₂ and also the synthesis of mixed crystals of the cadmium complex and the copper complex. Cu(II)(TTCN)₂(BF₄)₂ with acetonitrile as the solvent of recrystallization has a slightly distorted CuS₆ octahedral coordination sphere.⁶⁷ The Cu-S distances range from a low of 2.419 Å to a high of 2.459 Å. However, in the copper complex of TTCN with nitromethane as the solvent of recrystallization the distortion is more pronounced. The minimum Cu-S distance is 2.343 Å and the maximum distance is 2.504 Å. A search of the Cambridge Crystallographic Index for thioether copper complexes found 258 structures with reported Cu-S distances. The mean Cu-S distance was 2.324 Å with a standard deviation of 0.123. The CdS₆

coordination sphere in the cadmium complex is a slightly distorted octahedron. The mixed crystals were prepared in order to do detailed EPR studies on isolated $\text{Cu}(\text{TTCN})_2^{2+}$ sites.

Experimental

Synthesis of $\text{Cd}(\text{TTCN})_2(\text{BF}_4) \cdot 2\text{CH}_3\text{NO}_2$

A sample of 2.01 (63.8 mg, 0.35 mmol, Aldrich Chem. Co.) was dissolved in ethanol (10 mL) by gentle heating. Cadmium (II) tetrafluoroborate (60 mg, 0.18 mmol, Alfa Chemical Co.) was added to the warm ethanol solution. A white precipitate formed as the ethanol cooled. The precipitate was filtered and washed with diethyl ether ($\approx 3\text{mL}$) and allowed to dry to give a white solid (120 mg, 95% yield): IR (KBr) 2988, 1649, 1424, 1289, 1053 (s, BF_4^-), 929, 889, 824, 521 cm^{-1} . Recrystallization by vapor diffusion of diethyl ether into a nitromethane solution of this complex yielded small translucent white crystals suitable for X-ray structure analysis. One crystal was mounted in a sealed capillary tube with a drop of the recrystallization solvent and submitted for X-ray analysis. The structure was solved using the Patterson heavy-atom method which revealed the position of the Cd atom. The remaining atoms were found in succeeding difference Fourier syntheses. Hydrogens atoms

were included at idealized positions ($C-H = 0.95 \text{ \AA}$). In subsequent refinements the hydrogens were restrained to ride on the atom to which they are bonded, with fixed isotropic thermal parameters. The experimental details and results are presented in Table II.1. Figure II.1 shows an ORTEP⁷³ drawing of the structure.

Synthesis of $Cu(TTCN)_2(BF_4)_2 \cdot 2CH_3NO_2$ and $Cu(TTCN)_2(BF_4)_2 \cdot 2CH_3CN$

A solution of copper (II) tetrafluoroborate hydrate (0.72 g, 2.6 mmol, Alfa Chemical Co.) in absolute ethanol (20 mL) was added to a solution of 2.01 (0.93g, 5.2 mmol) in absolute ethanol (20 mL). A brown solution formed immediately followed by precipitation of a brown solid. The precipitate was filtered off and washed with absolute ethanol to yield 1.24g of a fine brown powder. This procedure is the same as reported by Glass⁶⁷ et al. and was used to make several batches of the complex which were recrystallized in the following ways.

Recrystallization of the crude product by vapor diffusion of diethyl ether into a nitromethane solution yielded small translucent brown crystals of $Cu(II)(TTCN)_2(BF_4)_2 \cdot 2CH_3NO_2$ as shown by X-ray diffraction analysis. The structure was solved in a manner identical to that used for the cadmium complex. The experimental details

and results are presented in Table II.2. Figure II.2 shows an ORTEP drawing of the structure. IR (KBr) 2975, 1555, 1445, 1422, 1287, 1056 (s, BF_4^-), 932, 893, 820, 669, 520 cm^{-1} .

Recrystallization of the crude product by vapor diffusion of diethyl ether into an acetonitrile solution of the crude complex yielded brown crystals whose IR was identical with those reported for the copper complex with acetonitrile as the solvent of recrystallization⁶⁷.

Synthesis of Cu doped $\text{Cd}(\text{TTCN})_2(\text{BF}_4)_2 \cdot \text{CH}_3\text{NO}_2$.

A sample of $\text{Cd}(\text{II})(\text{TTCN})_2(\text{BF}_4)_2 \cdot 2\text{CH}_3\text{NO}_2$ (79 mg, 0.1 mmol) and $\text{Cu}(\text{II})(\text{TTCN})_2(\text{BF}_4)_2 \cdot 2\text{CH}_3\text{NO}_2$ (5.2 mg, 0.008 mmol) was dissolved in nitromethane (3 mL) and diethyl ether was allowed to diffuse in overnight. Pale brown crystals were obtained. (no weight was obtained) An EPR spectrum, shown in Figure II.1, of the crystals indicated that there was indeed some paramagnetic $\text{Cu}(\text{II})$ in the crystals (Cadmium (II) is diamagnetic). Also, ICP analysis of this sample showed 0.61% by weight copper.⁷⁴

Figure II.1

ORTEP of Cd(II) (TTCN)₂(BF₄)₂•2CH₃NO₂

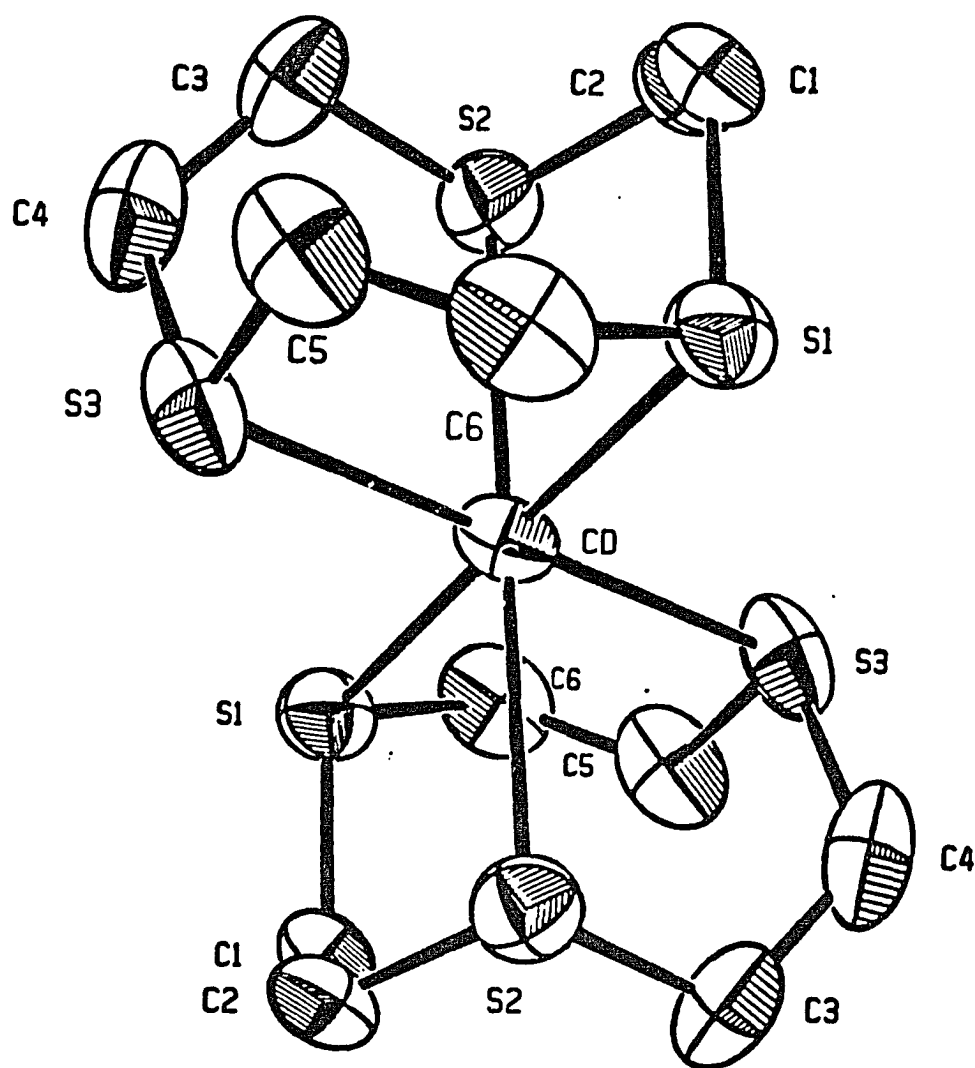
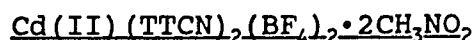
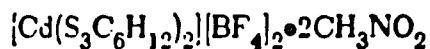


Table II.1X-Ray Data for**Crystal Data**

F.W. 768.80

 $F(000) = 772$

crystal dimensions: 0.55 x 0.18 x 0.28 mm

peak width at half-height = 0.21°

Nb-filtered Mo K α radiation ($\lambda = 0.71073 \text{ \AA}$)

temperature = 23° ± 1

monoclinic space group $P2_1/c$ $a = 10.31 \text{ \AA}$ $b = 15.138(2) \text{ \AA}$ $c = 9.461(2) \text{ \AA}$ $\beta = 99.39(1)^\circ$ $V = 1457.3 \text{ \AA}^3$ $Z = 2$ $\rho(\text{calc}) = 1.75 \text{ g/cm}^3$ $\mu = 12.3 \text{ cm}^{-1}$ **Intensity Measurements**Instrument: Nicolet P2₁Scan type: $2\theta/\theta$

Scan rate: 2-10°/min

Scan range, deg: $2.0 + (2\theta_{K_{\alpha_2}} - 2\theta_{K_{\alpha_1}})$ Maximum 2θ : 50.0°

No. of refl. measured: 4650 total, 4273 unique

Corrections: Lorentz-polarization

reflection averaging (agreement on I=2.2%)

analytical absorption (30.74 to 56.31 on I)

TABLE II.1 CONTINUED

Structure Solution and Refinement

Solution: Patterson method
Minimization function: $\sum w(|F_o| - |F_c|)^2$
Least-squares weights: $4 F_o^2 / \sigma^2(F_o^2)$
Anomalous dispersion: All non-hydrogen atoms
Reflections included: 2870 with $F_o^2 > 3.0\sigma(F_o^2)$
Parameters refined: 169
Unweighted agreement factor: 0.053
Weighted agreement factor: 0.068
Std of obs. of unit weight: 3.19
Convergence, largest shift: 0.30
High peak in final diff. map: 0.91 (13) e/Å³
Computer hardware: PDP-11
Computer software: SDP-PLUS (Enraf-Nonius & B.A. Frenz & Associates, Inc.)^{*}

^{*} B. A. Frenz, "The Enraf-Nonius CAD 4 SDP - A Real-time System for Concurrent X-Ray Data Collection and Crystal Structure Determination," in Computing in Crystallography, H. Schenk, R. Olthof-Hazelkamp, H. vanKoningsveld, and C. C. Bassi, Eds, Delft University Press, Delft, Holland, 1978, pp 64-71.

Table II.1 CONTINUED

Table of Positional and Thermal Parameters

Atom	x	y	z	B(Å ²)
Cd	0.000	0.000	0.000	3.617(8)
S1	-0.0050(1)	-0.03821(9)	0.2739(1)	4.14(2)
S2	0.1274(1)	-0.15236(8)	0.0060(1)	4.09(2)
S3	0.2362(1)	0.06248(9)	0.1044(1)	4.80(3)
C1	0.0834(5)	-0.1420(3)	0.2957(5)	4.5(1)
C2	0.0684(6)	-0.1985(3)	0.1590(6)	4.8(1)
C3	0.2950(5)	-0.1208(4)	0.0770(7)	5.4(1)
C4	0.3318(5)	-0.0272(5)	0.0464(7)	5.7(1)
C5	0.2471(6)	0.0433(4)	0.2951(5)	5.4(1)
O6	0.1166(6)	0.0418(4)	0.3495(5)	5.3(1)
B	0.3514(6)	-0.1061(5)	0.6534(7)	4.7(1)
F1	0.3705(6)	-0.1382(6)	0.5309(6)	13.5(2)
F2	0.2271(5)	-0.1066(5)	0.6650(8)	13.4(2)
F3	0.3900(9)	-0.0263(5)	0.674(1)	18.0(3)
F4	0.4173(9)	-0.1466(7)	0.7524(9)	24.0(3)
O1	0.1855(6)	0.2054(6)	0.587(1)	14.6(3)
O2	0.2785(9)	0.1983(7)	0.7980(7)	23.3(3)
N	0.2815(6)	0.1999(4)	0.6823(7)	8.1(2)
C	0.4028(7)	0.1927(6)	0.6333(9)	7.8(2)

Anisotropically refined atoms are given in the form of the isotropic equivalent thermal parameter defined as:

$$8\pi^2(U_{11}+U_{22}+U_{33})/3$$

Table II.1 CONTINUED

Table of Atomic Distances

Atom	Atom	Distance(Å)	Atom	Atom	Distance(Å)
Cd	S1	2.663(1)	F2	B	1.305(5)
Cd	S2	2.650(1)	F3	B	1.276(6)
Cd	S3	2.649(1)	F4	B	1.228(5)
S1	C1	1.811(3)	O1	N	1.228(7)
S1	O6	1.806(4)	O2	N	1.100(6)
S2	C2	1.800(3)	N	C	1.408(6)
S2	C3	1.814(3)	C1	C2	1.538(5)
S3	C4	1.814(4)	C3	C4	1.507(6)
S3	C5	1.814(3)	C5	O6	1.517(5)
F1	B	1.301(5)			

Table II.1 CONTINUED

Table of Atomic Angles

Atom	Atom	Atom	Angle(deg)	Atom	Atom	Atom	Angle(deg)
S1	Cd	S1	i180.00(0)	C4	S3	C5	103.4(2)
S1	Cd	S2	83.01(2)	O1	N	O2	125.6(7)
S1	Cd	S2	96.99(2)	O1	N	C	114.6(5)
S1	Cd	S3	82.96(2)	O2	N	C	119.8(7)
S1	Cd	S3	97.04(2)	S1	C1	C2	114.0(2)
S2	Cd	S2	i180.00(0)	S2	C2	C1	117.4(2)
S2	Cd	S3	83.13(3)	S2	C3	C4	115.5(3)
S2	Cd	S3	96.87(3)	S3	C4	C3	118.6(2)
S3	Cd	S3	i180.00(0)	S3	C5	O6	115.2(2)
Cd	S1	C1	102.1(1)	S1	O6	C5	118.2(2)
Cd	S1	O6	96.8(1)	F1	B	F2	111.5(4)
C1	S1	O6	103.4(2)	F1	B	F3	113.8(5)
Cd	S2	C2	97.1(1)	F1	B	F4	110.3(5)
Cd	S2	C3	102.6(1)	F2	B	F3	106.1(4)
C2	S2	C3	103.3(2)	F2	B	F4	111.3(6)
Cd	S3	C4	97.6(1)	F3	B	F4	103.5(6)
Cd	S3	C5	102.6(1)				

Table II.1 CONTINUED

Table of General Temperature Factor Expressions, U's

Atom	$U_{1,1}$	$U_{2,2}$	$U_{3,3}$	$U_{1,2}$	$U_{1,3}$	$U_{2,3}$
Cd	0.0569(2)	0.0392(2)	0.0391(2)	0.0035(2)	0.0014(2)	0.0057(2)
S1	0.0621(6)	0.0546(6)	0.0443(5)	0.0108(6)	0.0203(4)	0.0090(5)
S2	0.0583(6)	0.0411(5)	0.0561(6)	0.0039(5)	0.0102(5)	-0.0095(5)
S3	0.0731(7)	0.0583(6)	0.0505(6)	-0.0275(6)	0.0084(5)	0.0023(5)
F1	0.152(4)	0.245(6)	0.126(3)	-0.005(4)	0.046(3)	-0.082(3)
F2	0.109(3)	0.159(5)	0.255(6)	-0.026(3)	0.077(3)	-0.049(5)
F3	0.277(7)	0.123(4)	0.31(1)	-0.098(4)	0.114(6)	-0.047(5)
F4	0.397(8)	0.347(7)	0.140(5)	0.238(5)	-0.036(5)	0.060(5)
O1	0.079(4)	0.156(6)	0.31(1)	-0.010(4)	0.022(5)	0.056(6)
O2	0.380(7)	0.39(1)	0.160(4)	-0.240(7)	0.184(4)	-0.159(5)
N	0.106(4)	0.094(4)	0.114(4)	-0.040(3)	0.035(3)	-0.026(3)
C	0.075(4)	0.106(6)	0.110(5)	0.003(4)	0.002(4)	-0.010(5)
C1	0.064(3)	0.051(2)	0.058(2)	0.002(2)	0.013(2)	0.022(2)
C2	0.067(3)	0.034(2)	0.080(3)	0.001(2)	0.009(3)	0.012(2)
C3	0.045(2)	0.082(4)	0.081(3)	0.006(3)	0.017(2)	-0.012(3)
C4	0.050(2)	0.105(4)	0.067(3)	-0.016(3)	0.021(2)	-0.008(3)
C5	0.088(4)	0.068(3)	0.044(2)	-0.026(3)	-0.006(3)	-0.006(2)
O6	0.098(4)	0.064(3)	0.038(2)	-0.002(3)	0.012(2)	-0.011(2)
B	0.057(3)	0.064(3)	0.057(3)	-0.003(3)	0.007(3)	-0.000(3)

The form of the anisotropic thermal parameter is:

$$\exp[-2\pi^2(h^2a^2U_{1,1}+k^2b^2U_{2,2}+l^2c^2U_{3,3}+2hkabU_{1,2}+2hlacU_{1,3}+2klbcU_{2,3})]$$

where a, b, and c are reciprocal lattice constants.

Figure II.2

ORTEP of Cu(II)(TTCN)₂(BF₄)₂·2CH₃NO₂

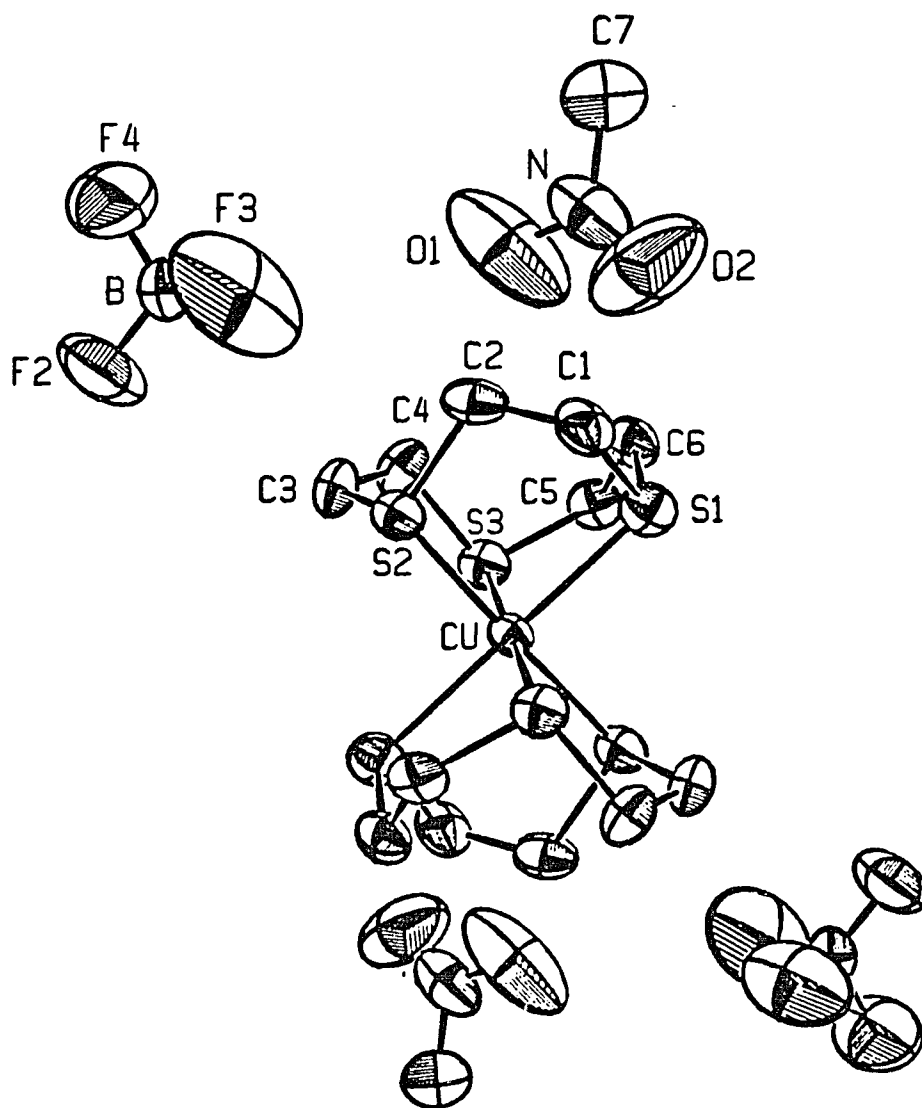


Table II.2
X-Ray Data for
Cu(II)(TTCN)₂(BF₄)₂·2CH₃NO₂

A. Crystal Data

[Cu(S₈C₁₂H₂₄)](BF₄)₂(CH₃NO₂)₂
 F.W. 709.13 F(000) = 1448
 crystal dimensions: 0.55x 0.05x 0.20 mm
 peak width at half-height = 0.20°
 Mo K α radiation (λ = 0.71073 Å)
 temperature = 23 \pm 1°
 orthorhombic space group Pbca
 a = 19.746 (2) Å b = 15.422 (2) Å c = 9.227 (1) Å
 V = 2810.0 Å³
 Z = 4 ρ = 1.68 g/cm³
 μ = 12.8 cm⁻¹

Table of Experimental Details

B. Intensity Measurements

Instrument:	Syntex-Nicolet P2 ₁ diffractometer
Monochromator:	Graphite crystal, incident beam
Scan type:	θ -2 θ
Scan rate:	2 - 8°/min
Scan width, deg:	2.0 + (2 θ K α_2 - 2 θ K α_1)
Maximum 2 θ :	50.0°
No. of refl. measured:	2846 total, 2486 unique
Corrections:	

Lorentz-polarization

Table of Experimental Details

C. Structure Solution and Refinement

Solution:	Patterson method
Refinement:	Full-matrix least-squares
Minimization function:	$\sum w(F_o - F_c)^2$
Least-squares weights:	$4F_o^2 / \sum^2(F_o^2)$
Anomalous dispersion:	All non-hydrogen atoms
Reflections included:	1098 with $F_o^2 > 3.0\sigma(F_o^2)$
Parameters refined:	169
Unweighted agreement factor:	0.053
Weighted agreement factor:	0.061
Std of obs. of unit weight:	2.29
Convergence, largest shift:	0.09 σ
High peak in final diff. map:	0.55 (10) e ⁻¹ /Å ³
Low peak in final diff. map:	-0.34 (0) e ⁻¹ /Å ³
Computer hardware:	VAX
Computer software:	SDP/VAX (Enraf-Nonius)*

B. A. Frenz, "The Enraf-Nonius CAD 4 SDP - A Real-time System for Concurrent X-Ray Data Collection and Crystal Structure Determination," in *Computing in Crystallography*, H. Schenk, R. Olthof-Hazelkamp, H. vanKoningsveld, and G. C. Bassi, Eds, Delft University Press, Delft, Holland, 1978, pp 64-71.

Table II.2 CONTINUEDTable of Positional Parameters and Their Estimated Standard Deviations

Atom	x	y	z	B(Å ²)
----	-	-	-	-----
Cu	0.000	0.000	0.000	2.63(3)
S1	-0.0043(2)	-0.0349(2)	0.2649(3)	4.09(5)
S2	0.1107(1)	0.0508(2)	0.0345(3)	3.42(5)
S3	-0.0483(1)	0.1474(2)	0.0361(3)	3.70(6)
C1	0.0637(6)	0.0397(7)	0.317(1)	4.6(3)
C2	0.1277(5)	0.0356(7)	0.227(1)	4.2(2)
C3	0.1572(5)	-0.0360(6)	-0.054(1)	4.0(2)
C4	-0.1385(4)	0.1271(6)	0.010(1)	4.2(2)
C5	-0.0233(5)	0.1939(6)	-0.134(1)	3.6(2)
C6	0.0360(5)	-0.1421(5)	0.268(1)	3.8(2)
B	0.3199(6)	0.1157(8)	0.062(1)	3.8(3)
F1	0.3090(6)	0.0328(6)	0.085(1)	13.3(3)
F2	0.3115(4)	0.1352(6)	-0.0742(7)	9.8(2)
F3	0.2810(6)	0.1528(8)	0.150(1)	20.0(4)
F4	0.3836(5)	0.1256(7)	0.106(1)	11.7(3)
C7	0.1975(6)	0.1754(7)	0.717(1)	6.0(3)
N	0.1524(6)	0.1969(6)	0.602(1)	7.1(3)
O1	0.1744(9)	0.1801(6)	0.482(1)	14.4(5)
O2	0.1029(5)	0.2380(8)	0.623(2)	14.4(4)

 Anisotropically refined atoms are given in the form of the
 isotropic equivalent displacement parameter defined as:
 $(4/3) * [a^2*B(1,1) + b^2*B(2,2) + c^2*B(3,3) + ab(\cos \gamma)*B(1,2)$
 $+ ac(\cos \beta)*B(1,3) + bc(\cos \alpha)*B(2,3)]$

Table II.2 CONTINUED

Table of General Displacement Parameter Expressions - U's

Name	U(1,1)	U(2,2)	U(3,3)	U(1,2)	U(1,3)	U(2,3)
Cu	0.0391(7)	0.0300(6)	0.0307(6)	-0.0012(8)	-0.002(1)	0.0011(8)
S1	0.057(1)	0.046(1)	0.053(1)	0.006(2)	-0.001(2)	0.001(1)
S2	0.051(1)	0.038(1)	0.041(1)	-0.008(1)	-0.007(1)	0.002(1)
S3	0.051(1)	0.041(1)	0.049(2)	-0.005(1)	-0.006(1)	-0.001(1)
C1	0.073(8)	0.070(7)	0.033(5)	-0.006(7)	-0.006(6)	-0.011(5)
C2	0.061(7)	0.051(6)	0.048(6)	-0.004(6)	-0.024(6)	-0.005(5)
C3	0.039(6)	0.057(6)	0.056(6)	0.000(5)	0.013(5)	-0.004(5)
C4	0.036(5)	0.054(6)	0.070(7)	0.005(5)	0.006(6)	-0.006(7)
C5	0.056(6)	0.021(5)	0.062(6)	0.006(5)	-0.006(6)	0.009(5)
C6	0.059(6)	0.038(5)	0.047(6)	-0.002(5)	-0.003(6)	0.012(5)
B	0.056(7)	0.036(6)	0.053(7)	0.000(6)	0.009(7)	0.001(6)
F1	0.196(9)	0.144(7)	0.164(8)	-0.069(7)	-0.069(7)	0.038(7)
F2	0.139(7)	0.179(7)	0.055(4)	0.056(6)	0.001(5)	0.028(5)
F3	0.33(1)	0.32(1)	0.113(7)	0.216(8)	0.065(7)	-0.031(7)
F4	0.116(6)	0.181(7)	0.148(7)	-0.067(6)	-0.044(6)	0.045(7)
C7	0.084(9)	0.058(7)	0.088(9)	0.009(7)	-0.016(8)	-0.012(7)
N	0.136(9)	0.076(6)	0.059(6)	-0.052(6)	-0.025(7)	0.013(5)
O1	0.37(2)	0.095(7)	0.080(7)	-0.077(9)	-0.03(1)	-0.007(6)
O2	0.091(7)	0.146(8)	0.31(1)	-0.009(7)	-0.03(1)	0.114(9)

The form of the anisotropic displacement parameter is:

$$\exp[-2\pi^2(h^2a^2U(1,1)+k^2b^2U(2,2)+l^2c^2U(3,3)+2hkabU(1,2)+2hlacU(1,3)+2klbcU(2,3))]$$

where a, b, and c are reciprocal lattice constants.

Table II.2 CONTINUED

Table of Bond Distances in Angstroms

Atom 1	Atom 2	Distance	Atom 1	Atom 2	Distance
C1	H1	0.950(8)	C5	H9	0.950(7)
C1	H2	0.950(8)	C5	H10	0.950(7)
C2	H3	0.950(7)	C6	H11	0.950(7)
C2	H4	0.950(7)	C6	H12	0.950(8)
C3	H5	0.950(7)	C7	H13	0.950(9)
C3	H6	0.950(8)	C7	H14	0.950(8)
C4	H7	0.950(8)	C7	H15	0.950(9)
C4	H8	0.950(7)			

Numbers in parentheses are estimated standard deviations in the least significant digits.

Table II.2 CONTINUEDTable of Bond Angles in Degrees

Atom 1	Atom 2	Atom 3	Angle	Atom 1	Atom 2	Atom 3	Angle
S1	C1	H1	108.1(6)	C3	C4	H8	109.9(7)
S1	C1	H2	107.1(6)	H7	C4	H8	109.5(7)
C2	C1	H1	109.4(7)	S3	C5	H9	107.8(5)
C2	C1	H2	106.7(7)	S3	C5	H10	107.1(5)
H1	C1	H2	109.5(7)	C6	C5	H9	107.4(7)
S2	C2	H3	108.7(6)	C6	C5	H10	107.2(6)
S2	C2	H4	109.0(5)	H9	C5	H10	109.5(7)
C1	C2	H3	109.4(7)	S1	C6	H11	108.7(6)
C1	C2	H4	108.0(7)	S1	C6	H12	107.5(5)
H3	C2	H4	109.5(7)	C5	C6	H11	110.0(6)
S2	C3	H5	107.7(6)	C5	C6	H12	107.8(7)
S2	C3	H6	108.2(6)	H11	C6	H12	109.5(7)
C4	C3	H5	108.2(7)	N	C7	H13	106.9(9)
C4	C3	H6	107.1(7)	N	C7	H14	111.0(8)
H5	C3	H6	109.5(7)	N	C7	H15	110.4(9)
S3	C4	H7	108.9(5)	H13	C7	H14	109.5(9)
S3	C4	H8	109.2(6)	H13	C7	H15	109.5(8)
C3	C4	H7	108.3(7)	H14	C7	H15	109.5(9)

Numbers in parentheses are estimated standard deviations in the least significant digits.

REFERENCES

1. Tollin, G.; Hanson, L. K.; Caffrey, M.; Meyer, T. E.; Cusanovich, M. A. Proc. Natl. Acad. Sci. USA, **1986**, 83, 3693.
2. Lardy, H. A.; Ferguson, S. M. Ann. Rev. Biochem., **1969**, 38, 991.
3. Capon, B.; McManus, S. A. "Neighboring Group Participation"; Plenum Press: New York, **1976**; Vol. 1.
4. Glass, R. S.; Hojjatie, M.; Petsom, A.; Wilson, G. S.; Göbl, M.; Mahling, S.; Asmus, K.-D. Phosphorus and Sulfur, **1985**, 23, 143.
5. Wilson, G. S.; Swanson, D. D.; Klug, J. T.; Glass, R. S.; Ryan, M. D.; Musker, W. K. J. Am Chem. Soc., **1979**, 101, 1040.
6. see for example: Eliel, E.; Knox, D. E.; J. Am. Chem. Soc., **1985**, 107, 2946 (and references therein).
7. Asmus, K.-D, Acc. Chem. Res., **1979**, 12, 436.
8. Setzer, W. N.; Coleman, B. R.; Wilson, G. S.; Glass, R. S. Tetrahedron, **1981**, 37, 2743.

9. Clark, T. J. Comput. Chem., **1982**, 3, 112;
Clark, T. J. Am. Chem. Soc., **1988**, 110, 1672;
Gill, P. M. W.; Radom, L. J. Am. Chem. Soc.,
1988, 110, 4931.
10. Perkins, C. W.; Martin, J. C.; Arduengo, A. J.; Lau,
W.; Algeria, A.; Kochi, J. K. J. Am Chem. Soc., **1980**,
102, 7753.
11. Bard, A. J.; Faulkner, L. R. "Electrochemical Methods",
John Wiley and Sons: New York, **1980**, chps. 2,3.
12. Bard, A. J.; Faulkner, L. R. ibid., chp. 6.
13. Fukuzumi, S.; Wong, C. L.; Kochi, J. K. J. Am. Chem.
Soc., **1980**, 102, 2928.
14. "The Study of Fast Processes and Transient Species
by Electron Pulse Radiolysis", Baxendale, J. H.;
Bushi, F. (Editors), D. Reidel: Boston, **1981**.
15. Asmus, K.-D. in "Fast Processes in Radiation Chemistry
and Biology", Adams, G. E.; Fielden, E. M.; Michael, B.
D. Eds., Wiley: New York, **1973**. pp 40 - 59.
16. Dorfman, L. M.; Adams, G. E. Natl. Stand. Ref. Data
Ser. (U. S. Natl. Bur. Stand.), **1973**, NSRDS-NBS, 46.
17. Bonifacic, M.; Möckel, H.; Bahnemann, D.; Asmus, K.-D.
J. Chem. Soc. Perkin Trans. 2, **1975**, 675.
18. Nelsen, S. F.; Parmelee, W. P.; Göbl, M.; Asmus, K.-D.
J. Am. Chem. Soc., **1980**, 102, 5606.

19. Asmus, K.-D.; Bahnemann, D.; Fischer, Ch.-H.; Veltwisch, D. J. Am. Chem. Soc., **1979**, 101, 5322.
20. Musker, W. K.; Roush, P. B. J. Am. Chem. Soc., **1976**, 98, 6745.
21. Broeker, J. L.; Glass, R. S. unpublished results.
22. Ryan, M. D.; Swanson, D. D.; Glass, R. S.; Wilson, G. S. J. Phys. Chem., **1981**, 1069.
23. Glass, R. S.; Andruski, S. W.; Broeker, J. L.; Firouzabadi, H.; Steffen, L. K.; Wilson, G. S. J. Am. Chem. Soc., **1989**, 111, 4036.
24. Broeker, J. L. Ph.D. Dissertation, The University of Arizona, **1988**.
25. ibid. Chp. 1.
26. ibid. p 148.
27. Asmus, K.-D., in Methods in Enzymology; L. Packer, Ed.; Academic Press, New York, **1984**, 105, 167.
28. Asmus, K.-D. Radiat. Phys. Chem., **1972**, 4, 417.
29. Glass, R. S.; Petsom, A.; Hojjatie, M.; Coleman, B. R.; Duchek, J. R.; Klug, J.; Wilson, G. S. J. Am. Chem. Soc. **1988**, 110, 4772.
30. Petsom, A. Ph.D. Dissertation, The University of Arizona, Tucson, **1987**.

31. Glass, R. S.; Petsom, A.; Wilson, G. S. J. Org. Chem., 1987, 52, 3537.
32. Glass, R. S.; Hojjatie, M.; Sabahi, M.; Steffen, L. K. Submitted.
33. Bard and Faulkner
34. Hardin, J. A. Undergraduate Honors Thesis, The University of Arizona, Tucson, 1986. See also reference 29.
35. University of Arizona Research Reactor Facility.
36. Glass, R. S.; Hojjatie, M.; Wilson, G. S.; Mahling, S.; Göbl, M.; Asmus, K.-D. J. Am. Chem. Soc. 1984, 106, 5382.
37. Coleman, B. R.; Glass, R. S.; Setzer, W. N.; Prabhu, U. D. G.; Wilson, G. S. Adv. Chem., 1982, 201, 18, 417.
38. Glass, R. S.; Petsom, A.; Wilson, G. S. J. Org. Chem., 1987, 52, 3537.
39. Bonifacic, M.; Möckel, H.; Bahnemann, D.; Asmus, K.-D. J. Chem. Soc. Perkin Trans. 2, 1975, 2, 675.
40. Glass, R. S.; Hojjatie, M.; Wilson, G. S.; Mahling, S.; Asmus, K.-D. J. Org. Chem., 1987, 52, 3717; Perkins, C. W.; Martin, J. C.; Arduengo, A. J.; Lau, W.; Alegria, A.; Kochi, J. J. Am. Chem. Soc., 1980, 102, 7753; Chatgililoglu, C.; Castelhana, A. L.; Griller, D. J. Org. Chem., 1985, 50, 2516; Davies, M. J.; Gilbert, B. C.; Norman, R. O. C. J. Chem. Soc. Perkin Trans. 2, 1983, 731; Perkins,

C. W.; Clarkson, R. B.; Martin, J. C. J. Am. Chem. Soc., **1986**, 108, 3206.

41. Mönig, J.; Göbl, M.; Asmus, K.-D. J. Chem. Soc. Perkin Trans. 2, **1983**, 731; Musker, W. K.; Surdhar, P. S.; Ahmad, R.; Armstrong, D. A. Can. J. Chem., **1984**, 62, 1874; Musker, K. K.; Hirshon, A. S.; Doi, J. T. J. Am. Chem. Soc., **1978**, 100, 7754.
42. Asmus, K.-D.; Bahnemann, D.; Bonifacic, M.; gillis, H. A. Discuss. Faraday Soc., **1977**, 63, 213; Musker, W. K.; Hirshon, A. S.; Doi, J. T. J. Am. Chem. Soc., **1978**, 100, 7754.
43. Bonifacic, M.; Asmus, K.-D. J. Chem. Soc. Perkin Trans. 2, **1980**, 758; Clark, T. J. Am. Chem. Soc., **1988**, 110, 1672; Gill, P. M. W.; Radom, L. J. Am. Chem. Soc., **1988**, 110, 4931.
44. Perkins, C. W.; Martin, J. C.; Arduengo, A. J.; Lau, W.; Alegria, A.; Kochi, J. K. J. Am. Chem. Soc., **1980**, 102, 26, 7753.
45. Mahling, S.; Asmus, K.-D.; Glass, R. S.; Hojjatie, M.; Wilson, G. S. J. Org. Chem., **1987**, 52, 3717.
46. Hiller, K.-O.; Asmus, K.-D. Int. J. Radiat. Biol., **1981**, 40, 583.
47. Mahling, S.; Asmus, K.-D.; Glass, R.S.; Hojjatie, M.; Wilson, G.S. J. Org. Chem. **1987**, 52, 3717.
48. Glass, R.S.; Hojjatie, M.; Wilson, G.S.; Mahling, S.; Göbl, M.; Asmus, K.-D. J. Am. Chem. Soc. **1984**, 106, 5382.
49. Asmus, K.-D. Acc. Chem. Res. **1979**, 12, 436.

50. Schonheich, C. unpublished results
51. Bonifacic, M.; Möckel, H.; Bahnemann, D.; Asmus, K.D. J. Chem. Soc. Perkin Trans. 2, 1975, 675.
52. Janata, E.; Veltwisch, D.; Asmus, K.-D. Radiat. Phys. Chem., 1980, 16, 43.
53. Pseudo-Kolbe reactions involve oxidation of a site remote from the carboxylate followed by electron transfer and decarboxylation. See: Gassman, P. G.; Fox, B. L. Chem. Comm., 1967, 32, 480; Organic Electrochemistry 2nd Ed., Baizer and Lund Ed.; Marcel Dekker: New York, 1983, pp 443, 455, 574.
54. Mönig, J.; Goslich, R.; Asmus, K.-D. Ber. Bunsenges. Phys. Chem., 1986, 90, 115.
55. Hiller, K.-O.; Asmus, K.-D. J. Phys. Chem., 1983, 89, 19, 3682.
56. Hiller, K.-O.; Masloch, B.; Göbl, M.; Asmus, K.-D. J. Am. Chem. Soc., 1981, 103, 2734.
57. Asmus, K.-D.; Göbl, M.; Hiller, K.-O.; Mahling, S.; Mönig, J. J. Chem. Soc. Perkin Trans. 2, 1985, 641.
58. Asmus, K.-D., in Methods in Enzymology; L. Packer, Ed.; Academic Press, New York, 1984, 105, 167.
59. Asmus, K.-D. Radiat. Phys. Chem., 1972, 4, 417
60. Monig, J.; Chapman, R.; Asmus, K.-D. J. Phys. Chem., 1985, 86, 3139.

61. Glass, R. S.; Duchek, J. R.; Klug, J. T.; Wilson G. S. J. Am. Chem. Soc., 1977, 99, 7349.
62. Glass, R. S.; Petsom, A.; Hojjatie, M.; Coleman, B. R.; Duchek, J. R.; Klug, J.; Wilson, G. S. J. Am. Chem. Soc., 1988, 110, 4772.
63. Asmus, K.-D.; Bahnemann, D.; Fischer, Ch.-H.; Veltwisch, D. J. Am Chem. Soc., 1979, 101, 5322.
64. Glass, R. S.; Sabahi, M.; Singh, V. P. unpublished data.
65. Zuika, I. V.; Bankovskii, Yu. A. Russ. Chem. Rev. 1973, 42, 24.
66. See: Mertes, M. P. J. Org. Chem. 1961, 26, 5236; Szmant, H. H.; Rigau, J. J. J. Org. Chem., 1966, 31, 2288.
67. Glass, R. S.; Hojjatie, M.; Setzer, W. N.; Wilson, G. S. J. Org. Chem., 1986, 51, 1817.
68. Hammerich, O.; Parker, V. D. J. Am. Chem. Soc., 1974, 93, 13, 4289.
69. Setzer, W. N.; Ogle, C. A.; Wilson, G. S.; Glass, R. S. Inorg. Chem. 1981, 22, 266.
70. Blake, A. J.; Holder, A. J.; Hyde, T. I.; Schröder, M. J. J. Chem. Soc. Chem. Commun. 1987, 987.
71. Kuppers, H.-J.; Wieghardt, K.; Nuber, B.; Weiss, J.; Bill, E. Inorg. Chem. 1987, 26, 3762.

72. Setzer, W. N.; Coleman, B. R.; Wilson, G. S.; Glass, R. S. Tetrahedron **1981**, 37, 2743.
73. Johnson, C. K. "ORTEP"; Oak Ridge National Laboratory: Oak Ridge, TN.
74. Analysis performed by the Strategic Metals Recovery Research Facility at the University of Arizona.